

AIR ENTRAINMENT IN VERTICAL DROPSHAFTS

by

STEPHEN WILLIAM TIBKE B.Sc.

A thesis submitted in partial fulfilment
of the requirements for the degree of

DOCTOR OF PHILOSOPHY

of the

COUNCIL FOR NATIONAL ACADEMIC AWARDS

Dept. of Building and Civil Engineering
Liverpool Polytechnic
Clarence Street
Liverpool

July 1982

ACKNOWLEDGEMENTS

I should like to thank sincerely, Mr. C. Dyson, under whose supervision this work was carried out. His advice, suggestions, criticisms and encouragement were invaluable in the completion of this study.

I would also like to acknowledge the assistance received from the Technicians of the Department in the construction of the test apparatus required for the model studies. May I also extend my gratitude to Dr. J. Bland for his guidance in the use of computer techniques.

Finally, I wish to express my thanks to Mrs. D. Fernihough for the careful typing of this thesis.

ABSTRACT

AIR ENTRAINMENT IN VERTICAL DROPSHAFTS

S.W. TIBKE

This thesis describes an investigation into the phenomenon of air entrainment in vertical dropshafts conveying water from a high level to a lower level. The study initially commenced with hydraulic tests on scale models of a vortex-entry dropshaft arrangement. This subsequently expanded into a more detailed analysis of the mechanisms involved in the air entrainment, rejection and transport processes evident in the early stages of the work.

An attempt has been made to define the criteria controlling these three modes of operation in air/water systems. The physical process of initial entrainment by the plunging water film was researched extensively. The inability to accurately reproduce the bubble sizes in scale models conclusively shows that this aspect is fundamental to the understanding of the problem.

A dimensional analysis of the parameters controlling the rate of entrainment in the system was undertaken in the investigations. A number of dimensionless groups were obtained to describe the relationships between the parameters involved in the process. This enables the rate of air entrainment to be predicted in any system of dropshafts under certain flow and geometrical conditions.

The downward passage of air bubbles in water (just one mode of operation in two-phase flow systems) was investigated to establish the air transport capabilities of various flows and hence the air rejection process. An empirical relationship was derived which describes the air void ratio at various discharges and hence enables many aspects of the transport of air bubbles to be studied. A series of values defining the limits of operation of the phases involved in air entrainment were also identified, e.g. onset of air entrainment and air transport.

CONTENTS

CHAPTER ONE

INTRODUCTION		Page No.
1.1	Air Entrainment	1
1.2	Reasons for present research and a summary of the work presented in this thesis	7

CHAPTER TWO

LITERATURE SURVEY

2.1	The general problem	16
2.2	Model tests to predict air entrainment	18
2.3	Froudian models	27
2.4	Motion of air bubbles in two-phase flow	29
2.5	The surface air entrainment phenomena	30

CHAPTER THREE

EXPERIMENTAL PROCEDURES AND APPARATUS

3.1	Apparatus	34
3.1.1	General layout of apparatus	34
3.1.2	The vortex chamber models	37
3.1.3	The dropshaft	38
3.1.4	The separator tank	38
3.1.5	Performance of separator tank	42
3.1.6	8.8m dropshaft length	43
3.1.7	Rectangular column dropshaft	44
3.2	Experimental procedures	47
3.2.1	Vortex-entry dropshafts	47
3.2.2	Rectangular column dropshafts	47
3.3	Gamma ray absorption technique for measuring void fraction	49

CONTENTS

CHAPTER FOUR

THEORETICAL CONSIDERATIONS		Page No.
4.1	Air entrainment	53
4.1.1	Dimensional analysis	53
4.1.2	Determination of the relevant variables	57
4.2	Air transport	65
4.2.1	Velocity of air bubbles in two-phase flow	69
4.2.1.1	Zero liquid flow	69
4.2.1.2	Finite liquid upflow	71
4.2.1.3	Downward liquid flow with rising bubbles	73
4.2.1.4	Downward liquid flow and downward bubble motion	74
4.2.2	Determination of void fraction by gamma ray absorption	79

CHAPTER FIVE

ANALYSIS OF EXPERIMENTAL RESULTS

5.1	Classification of flow regimes	81
5.2	Vortex-entry dropshafts - Model results	84
5.3	Rectangular column dropshafts - Model results	91
5.4	Dimensional analysis of vortex-entry dropshaft results	114
5.4.1	Determination of relevant parameters	114
5.4.2	Dimensional analysis	118
5.5	Void fraction determination	136
5.6	Review of previous investigations	147

CONTENTS

CHAPTER SIX

CONCLUSIONS		Page No.
6.1	General	154
6.2	Conditions for air entrainment	156
6.3	Dimensional Relationships	160
LIST OF REFERENCES		162
APPENDICES		
Appendix A	Calibration of meters	A1
Appendix B	Determination of velocities in vortex chamber	A4
Appendix C	Solution of Equation 4.1.18	A11
Appendix D	Data for Non-Dimensional Groups	A13

LIST OF FIGURES

Figure No.		Page No.
CHAPTER ONE		
1	Definition sketch for dropshaft	9
CHAPTER TWO		
2.1	Relationship between spillway air demand and discharge for model and prototype	19
2.2	Air entrained by spiral flow (Laushey and Mavis)	21
2.3	Air entrained by modified apparatus (Laushey and Mavis)	23
2.4	Viparelli's curve	23
CHAPTER THREE		
3.1	General layout of apparatus	36
3.2	Details of vortex-entry chamber	39
3.3	Arrangement of vortex-chamber, drop-pipe and separator tank	41
3.4	Rectangular column dropshaft	46
3.5	Arrangement for measurement of void fraction	51
3.6	Calibration apparatus for measurement of void fraction	52
CHAPTER FOUR		
4.1	Identification of control parameters	54
4.1.1	Definition sketch for boundary layer growth	62
4.2.1	Shape and terminal rise velocity of air bubbles	67
4.2.9	Relationship between air/water ratio and void ratio - Theoretical	78

LIST OF FIGURES

Figure No. Page No.

CHAPTER FIVE

5.1	Typical flow patterns in dropshaft Airflow rates in vortex dropshaft:-	83
5.2	1:10.9 model	85
5.3	1:21.6 model Air/water ratio in vortex dropshaft:-	86
5.4	1:10.9 scale model	88
5.5	1:21.6 scale model Air/water ratio in rectangular column:-	89
5.6	Shaft width D = 38mm	95
5.7	Shaft width D = 45mm	96
5.8	Shaft width D = 50mm	97
5.9	Relationship between limiting air/water ratio and n.w.v. - rectangular column	100
	Air/water ratio at increasing droplength at constant n.w.v. - rectangular column:-	
5.10	Nominal water velocity = 0.237 m/s	102
5.11	Nominal water velocity = 0.315 m/s	103
5.12	Nominal water velocity = 0.412 m/s	104
	Air/water ratio at increasing droplength at constant entry velocity - rectangular column:-	
5.13	Flow rate = 6.596 m ³ /s	106
5.14	Flow rate = 5.713 m ³ /s	107
5.15	Flow rate = 4.399 m ³ /s	108
5.16	Flow rate = 3.341 m ³ /s	109
5.17	Flow rate = 2.507 m ³ /s	110

LIST OF FIGURES

Figure No.			Page No.
	Air/water ratio at increasing drop-length at constant entry velocity - rectangular column:-		
5.18	Flow rate = 4.418 m ³ /s		111
5.19	Flow rate = 3.373 m ³ /s		112
5.20	Flow rate = 2.519 m ³ /s		113
5.21	Variation of β with Non-Dimensional Group $\left[\frac{Q_w}{(D^3 g)^{0.5}} \right]$ - Circular Shafts		120
5.22	Relationship between j_w and j_w/u_c		122
5.23	Variation of β with Non-Dimensional Group $\left[\frac{Q_w}{(d^3 g)^{0.5}} \right]$ - Rectangular Shaft		125
5.24	Variation of β with N.D.G. $\left[\frac{L - z_t}{D} \right]$ Circular Shafts		126
5.25	Variation of β with N.D.G. $\left[\frac{L - z_t}{d} \right]$	d=38	127
5.26	Variation of β with N.D.G. $\left[\frac{L - z_t}{d} \right]$	d=45	128
5.27	Variation of β with N.D.G. $\left[\frac{L - z_t}{d} \right]$	d=50	129
5.28	Relationship between β/β_{max} and N.D.G.'s Circular Shafts - Liverpool Poly.		132
5.29	Relationship between β/β_{max} and N.D.G.'s Circular Shafts - Liverpool Poly		133
5.30	Relationship between β/β_{max} and N.D.G.'s Circular Shafts - H.R.S.		134
5.31	Relationship between β/β_{max} and N.D.G.'s Rectangular Shafts		135
5.32	Calibration curves for determination of void fraction by gamma ray absorption technique		138
5.33	Relationship between absolute air and water velocities		140

Figure No.		Page No.
5.34	Relationship between relative velocity and nominal water velocity	141
5.35	Relationship between air/water ratio and void ratio - Experimental	145
5.36	Proposed mechanism for air entrainment and rejection	149

LIST OF NOTATIONS

A	cross-sectional area
B	breadth of wall - rectangular column
b	bubble diameter
D	pipe diameter
d	column width
Fr	Froude number
g	acceleration due to gravity
h	head on inlet gate
I	radiation intensity
j _w	nominal water velocity
L	free fall droplength
p	pressure intensity
q	flow per unit width
Q _w	volumetric water discharge
Q _a	volumetric air discharge
r	pipe radius
R	Reynolds number
s	width of inlet gate opening
t	time
u _B	bubble rise velocity
u _C	relative rise velocity
U	mean velocity
U _m	maximum velocity along pipe axis
v _i	inlet velocity
v _a	absolute air velocity
v _w	absolute water velocity
v	instantaneous velocity
V	volume
W	velocity of boundary layer
W _C	velocity at transition from laminar to turbulent
W _O	velocity at leading edge of film
We	Weber number
z	length of boundary layer
z _C	length of boundary layer at transition
z _t	critical length of boundary layer
α	air void ratio (concentration)
β	air/water flow ratio
δ	boundary layer thickness
δ	film thickness
ν	coefficient of kinematic viscosity
μ	coefficient of dynamic viscosity
ρ	specific mass (density)
σ	coefficient of surface tension
τ	shear stress

CHAPTER ONE
INTRODUCTION

The introduction to this thesis has been divided into two sections. Firstly, the development of the air entrainment problem is identified, with a brief historical outline of the practicalities involved when air is entrained in a system. This is followed by an outline of the reasons for this research investigation and a summary of the work presented in this thesis.

1.1 Air Entrainment

The air entrainment problem in water transport systems is imperfectly understood and in many instances completely overlooked. This entrainment of air in water, characterised by the appearance of white water, generally occurs in two main processes;

- i) when a high velocity flow produces surface aeration for example, fast flow in steep chutes.
- ii) when fast and slow moving bodies of water meet, entrainment of discrete air bubbles occurring at the point of interaction.

It is the latter form of air entrainment which is of concern in this investigation and is commonly found occurring in hydraulic structures such as spillways, siphon and stepped spillways, overflow weirs, aerators, drop-shafts and other devices used on dams and in hydro-

electric engineering practice. When a dropshaft is used to convey water from a high level to a lower level, the falling mass of water entrains large quantities of air within the shaft and this can produce adverse side effects unless the system is suitably designed to minimise or eliminate these effects.

The ability to predict the air demands of vertical dropshafts is necessary to adequately design the system. Since air entrainment cannot be eliminated, then a de-aeration system must be incorporated into the overall arrangement to maintain the operational safety of the structure. Allowances must be made for supplying the air demand of the shaft as well as releasing the entrained air. If these requirements are not met, severe disruptions in the operating efficiency of the dropshaft may result. This point is well illustrated by considering the example of the San Pablo Dam near Oakland, California.⁽¹⁾

This dam was constructed in 1917-1920 and was provided with both an open-channel spillway and an auxillary vertical shaft spillway. The horizontal leg of the shaft spillway was so arranged that a water cushion would always be provided by a twenty-four foot column of water impounded at the bottom of the vertical shaft. The problem of disposal of air carried by the falling water into the horizontal leg, if considered, was dismissed as not being of serious importance.

In operation, it was found that air entrained in the vertical shaft was transported into the horizontal leg where it accumulated in large air pockets along the roof. These air pockets moved through the tunnel toward the outlet and discharged periodically with explosive violence, throwing water as spray to a height of forty to fifty feet in the air. The vibration caused in the tunnel following each of these air discharges was also a serious problem.

To investigate these occurrences, a model of the shaft arrangement was built to a 1 to 14 scale. In the model test, air bubbles discharging freely at the tunnel outlet through the horizontal leg threw spray to a height of about one foot. This would be equivalent to fourteen feet in the prototype but as previously stated, this was forty to fifty feet in the actual prototype operation. Likewise the mild vibrations in the model would be difficult to translate into the violent tremblors of the prototype. Thus it would appear that strict conformity between model and prototype cannot be easily obtained under conditions of air entrainment in closed conduits.

In 1965 a report was published by the Hydraulics Research Station, detailing model studies of a dropshaft and de-aeration chamber performance carried out in connection with the Plover Cove Water Supply Scheme,

(2)
Hong Kong. To meet the increased water demand for Hong Kong, several reservoirs were created and interconnected by a network of tunnels, pipelines and open channels. Along the length of the system a number of dropshafts were constructed and water from the larger mountain streams dropped down these shafts into the tunnels and passed to the reservoirs.

Hydraulic model studies were undertaken to assist in the design of the dropshafts, with particular attention given to the problem of de-aeration at their lower ends. The design adopted was to provide a short length of cross-tunnel between the end of the dropshaft and the feeder tunnel to act as a de-aeration chamber. The air which collected in the roof of the de-aeration chamber, escaped to the surface up a vent pipe built alongside the dropshaft.

There were fifty-three dropshafts in the scheme, each having a diameter of ten feet, with a vortex chamber entry arrangement. The maximum discharge down any one ten feet diameter dropshaft was initially fixed at 800 cusecs for model test work, but was later increased to 900 cusecs. However, many dropshafts sited in small catchment areas, had smaller maximum flows, the lowest being less than 100 cusecs. The depth of each dropshaft depended on the elevation of the stream above the feeder tunnel and varied from 230 ft. to 350 ft.

The model studies were carried out at three different scales. Although the models showed similar qualitative air demand characteristics, there was no systematic quantitative relationship with scale, and the performance of any one of the models could not be predicted from the other two. It was proposed to carry out prototype measurements for comparison with the model results but this was never achieved.

The fundamental problem in predicting air entrainment rates from model studies appears to be associated with the size of the air bubbles. When modelling situations in which bubbles of air are transported by water, these bubbles should also be modified in size, so that the drag force exerted upon them by the water is such that they behave in a similar manner to the bubble motion in the prototype.

However, the mechanism for entraining air bubbles is independent of scale, so bubbles of equivalent diameter 3-5 mm. are generated in all cases. The rate at which air is initially entrained by a film of water running down the wall of a pipe will depend on the penetration of the film into the standing water, and the degree of disturbance of the surface. If a thin film discharges into a large pool, the buoyant air bubbles will come to the surface and return to the atmosphere. However, if a relatively thick film discharges

into a small diameter vertical shaft, the downward drag force on the bubbles will be greater than the buoyancy force, so some proportion will be carried down with the water. The drag and buoyancy forces are related to the bubble diameter.

The phenomena of air entrainment appears to be a question of understanding the initial entrainment of air at the point of interaction of the fast and slow moving bodies of water and of the subsequent transport of the air bubbles by the water in the lower part of the shaft.

Various forms of entry arrangements have been used for dropshafts in an attempt to minimise the air demand. For example, a vortex-entry arrangement, a radial entry or a vertical plunge entry. It has been shown that for short droplengths, a vertical plunge entry can yield up to ten times greater air demand than vortex entry for similar water flow rates.⁽³⁾ The air/water flow ratios of the two shafts converge as the droplength increases, probably due to the decrease in swirl of the vortex.

It is thought that the vortex action induces a pressure gradient below the standing water level, causing entrained air bubbles to migrate towards the centre of the shaft where they are more readily released back up into the air core within the shaft. In the upper regions of the shaft, above the ambient water level, the vortex action forces the water against

the shaft walls giving smoother entry conditions and decreasing the tendency of the water film to break away from the walls.

Within this thesis, no attempts have been made to verify these propositions or to investigate the various forms of entry arrangements. Furthermore, the current investigation does not include studies on the release of entrained air, by mechanical devices or other means, either within the dropshaft or at the outlet. Cotillon⁽⁴⁾ has presented a report aimed at providing solutions to the problem of reducing or eliminating the air entrained in vertical and inclined shafts.

1.2 Reasons for present research and a summary of the work presented in this thesis.

The present investigation was initiated by an opportunity to carry out tests on a prototype dropshaft. A vortex-entry vertical dropshaft had been constructed by Liverpool City Engineers to connect a high level drainage system to a trunk sewer running at a lower level. Permission was obtained to use the structure for the purpose of obtaining large-scale measurements. The construction of the chamber was slightly modified to accommodate equipment necessary for this purpose. The original aim of this research was therefore to perform

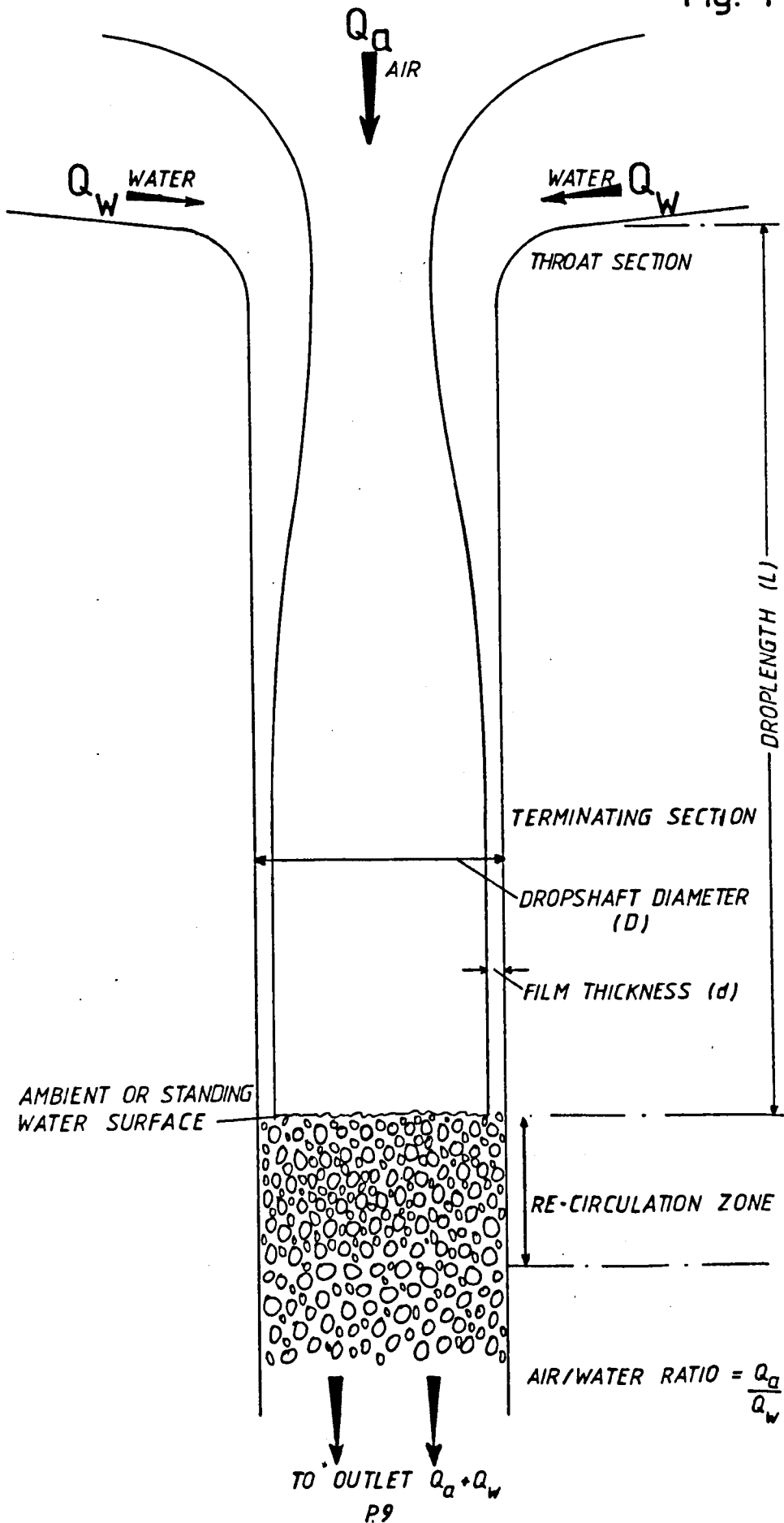
field trials on the prototype and to compare the results with those from two geometrically similar scale models of the vortex entry dropshaft. From this, it was hoped to achieve some scaling relationships for use in air entrainment situations. However, due to innumerable practical difficulties with the prototype operation, these measurements have still to be obtained and consequently the original aim has had to be re-assessed.

The work presented in this thesis reports on both model and theoretical analyses of the air entrainment phenomenon in a vortex-entry circular dropshaft and a vertical plunge rectangular column model. The study divides into consideration of two separate, yet inter-related, aspects of the entrainment of air by falling water. Initially, the rate at which air is entrapped at the ambient water surface was studied. Secondly, the investigation was extended to include the subsequent air transport process in an attempt to ascertain the carry-down characteristics in an air/water emulsion and in the re-circulation zone after the initial entrainment process. Reference to Fig (1) will provide a clearer understanding of the physical processes involved.

From Fig (1), it can be seen that the major parameters in the air entrainment system are as follows;

Definition Sketch for Dropshaft

Fig. 1



- a) Water discharge, the volume of water per second passed into the shaft, i.e. water flow rate.
- b) Air demand, the net volume of air per second drawn through the system as entrained air bubbles i.e. air flow rate.
- c) Droplength, the length of free fall of the water on the sides of the shaft from the inlet arrangement to the standing water level.
- d) Standing or ambient water level, a downstream gate valve controls this level which serves to simulate changes of head in downstream conditions in the prototype and hence varies the droplength.
- e) Film thickness, the thickness of the water film on the sides of the shaft.
- f) Re-circulation zone, the section directly below the standing water level where the initial entrainment and rejection processes occur.
- g) Air/Water Ratio , a quantitative air to water ratio based on the measured volumetric discharges.

The initial problem envisaged was to find a relationship between the water flow rate, the droplength, and the air entrained in the vortex entry dropshaft. For example at the same flow rate, the droplength was varied and the air demand investigated, and at the same droplength, the air demand was measured for different flow rates. This was done initially with a short droplength, but it

was found desirable to increase the length of dropshaft available to investigate further.

Observation of the entrainment process at the ambient surface proved extremely difficult within the circular dropshafts. The flow regimes present within the falling water film was also difficult to ascertain, e.g. the measurement of surface roughness and film thickness. In order to study the influence of these factors, and the effect of the annular jet striking the standing water surface, a change in the geometry of the system was undertaken. It was decided to 'open-out' the circumference of the shaft to a flat plate and run the water film down one side of a rectangular column.

A similar exercise had been carried out previously by Whillock and Thorn.⁽³⁾ For this reason, the column was constructed with an adjustable wall to vary the effective column cross-section and hence the downward nominal water velocity. This enabled a study to be made of the effect of nominal water velocity on the transport of air bubbles. Further to this aspect, the rectangular column dropshaft had a moveable gate to control the opening from the header tank which enabled the inlet velocity to be varied for the same flow rates and droplengths.

An extensive search of the literature was made to try to find information regarding the bubble transport mechanism. The ability to predict the void fraction or percentage air content of a mixture, in connection with the operating parameters, is of considerable importance to nuclear technology and also to the chemical process industry. Consequently, numerous publications dealing with both the theoretical and the experimental aspects of the problem have been produced. However, these papers have tended to be directed towards solving a particular design problem and have paid little attention to other measurements and information which were outside the designer's immediate need. The majority of researchers have investigated the upward co-current flow of air and water relevant in the aforementioned industries, thus it was necessary to conduct an investigation into the downward co-current flow of air and water operating at atmospheric pressure.

A gamma-ray absorption technique to determine the air void fraction of a two-phase mixture has previously been employed by several investigators.^(5,6) The aim in this investigation was to enable absolute air and water velocities to be determined by having established a relationship between the air void ratio and the air/water discharge ratio. These ratios may appear at first to be equal, but on closer examination, it is apparent

that they are not. Simply explained, the air bubbles have a natural rise velocity and are carried down by the drag force exerted on them by the falling water; this force varies according to the absolute velocity of the water. Hence, at any section, the air content is evident, but air will only be carried downwards if the drag force is sufficient to do so. A more detailed analysis of the phenomena is presented in Chapter Four.

Following this chapter, the literature survey covers the development of the research into the air entrainment phenomena up to the present investigation. It is evident that there are several variances to date in the research associated with air entrainment. However, there is no attempt to discuss the reasons for these discrepancies within the scope of this chapter.

Chapter Three details the experimental methods adopted and covers the construction and operation of the hydraulic scale models for both the vortex-entry dropshafts and the rectangular column vertical plunge model. Methods of measurement of the various parameters are also specified.

A theoretical analysis is presented in Chapter Four covering the two aspects of the phenomena under investigation. The initial air entrainment is considered to be due to the effects of the falling nappe on the pipe wall impinging on the ambient water surface in the dropshaft. This process is distinct from the second area of investigation which is the transport of the entrained air bubbles in

the downward flow of water in the lower shaft. A study of air bubble motion in water is considered from first principles and developed to give an expression for the transport of air in flowing water.

Chapter Five presents the results of the investigations. The general trends in the study of initial air entrainment for the vortex-entry models are developed and the relevant parameters are produced from the theoretical and semi-empirical relationships. A statistical analysis to determine a functional relationship between the operating parameters is also presented in this chapter. The results of the air transport investigation are shown in general terms for the rectangular column at different transport velocities. Utilising the methods of the radio-isotope investigation to determine the void fraction of the two-phase flow, an empirical relationship is derived relating the relative bubble rise velocity to the nominal water velocity.

The thesis terminates with conclusions and recommendations arrived at from the current investigation.

CHAPTER TWO

LITERATURE SURVEY

The literature survey covers the major published works dealing with the phenomenon of air entrainment over the past fifty years. The scope of this chapter is limited to publications directly relevant to the case of air entrainment of the dropshaft variety; and not to air entraining mechanisms such as the bulking of high-speed, free-surface flows.

Attention is also given to the problem of modelling air/water mixtures and to the general behaviour of air bubbles in a fluid medium. Throughout this section, the terminology used and comments made are those of the original author concerned. Opinions on these publications, thought appropriate by the present author, have been reserved and will be discussed in connection with the results of the present investigation in the concluding sections of this thesis.

2.1 The general problem

This is discussed in detail in Chapter One, and is well reported by Hall⁽¹⁾ and H.R.S.⁽²⁾. Peterka⁽⁷⁾ reports on the model and prototype performance of the Hearte Butte Dam spillway constructed around 1950. Hydraulic model tests were conducted on a 1 to 21.5 scale model of the dam and tests were carried out on several aspects of the operating features of the design. The flood-control spillway consisted of a morning-glory spillway, discharging into a vertical shaft, this was then connected to a 90° vertical bend and nearly horizontal tunnel under the dam crest, which discharged into a hydraulic jump stilling basin.

Water discharge and air demand were measured in the model over the complete range of discharges for the spillway. At a very early date after its completion, the overflow discharge in the prototype reached 68% of its maximum design flow and enabled a large range of prototype data to be accumulated. At the time of the model tests, it was known that air flow in small hydraulic models was uncertain and that a greater percentage of air could be expected to enter a similar prototype structure. A design was adopted, after the model tests but allowing for an increase in air demand, and the facility to measure air flow was built in to the prototype.

For all practical purposes, there was good agreement between the model and prototype discharge characteristics,

however, as expected this was not the case for air demand. The results are shown in Fig 2.1, for the spillway air demand. The prototype curve also takes into account the pressure measurements made in the horizontal air vent which were considered more accurate. Thus the prototype curve follows a trend similar to that for the model. The percentage of air entrained in the spillway discharge for both model and prototype shows a decrease as the discharge increases. In this respect, the model predicted the performance of the prototype. The prototype, however, entrained approximately four times as much air as was predicted by the model. When the model showed an air entrainment of 5.5% of the water discharge for 1,000 cu.ft. per sec. of spillway discharge, the prototype showed 20.5%. For 3,600 cu.ft. per sec., the model showed 1.9% air entrainment and the prototype 7.7%. Thus accurate predictions could not be made from the model tests to determine how much more air the prototype would entrain.

Cotillon⁽⁴⁾ presents a paper discussing the general problems associated with air entrainment in dropshafts supplying pressure tunnels. The paper is limited to the description of twenty prototype dropshaft installations constructed by L'Electricité de France, and to how the problems of air entrainment have been overcome. This has been achieved by adopting a design to ensure one of the following results;

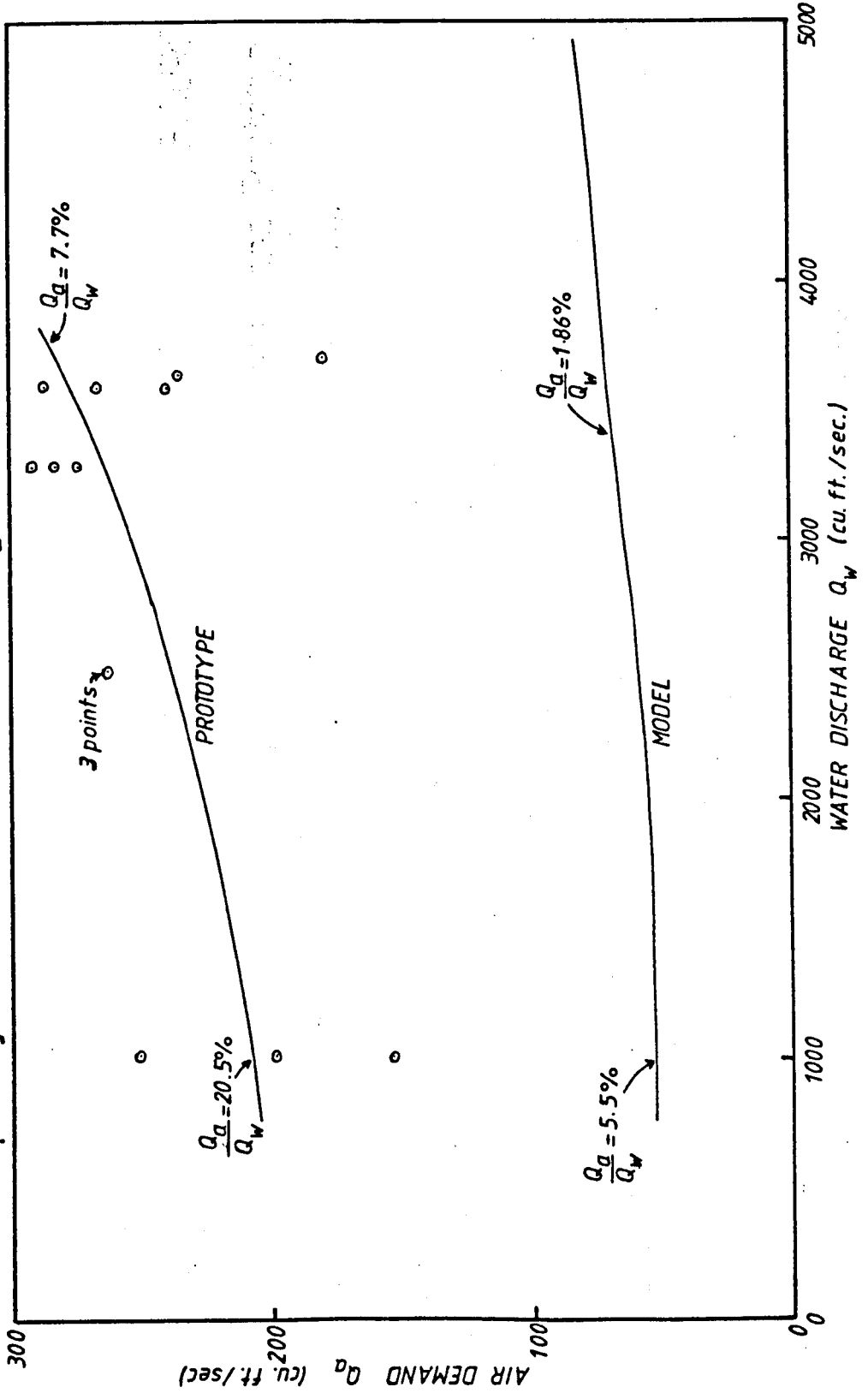
- a) Natural de-aeration, eg. a large diameter shaft so that any air initially entrained will rise upwards and not be carried down.
- b) De-aeration under pressure, air is entrained but discharged at a given point in the shaft or tunnel.
- c) Suppression of air entrainment, by preventing the water from falling in air, eg. fall in a vacuum tube, or supply shaft kept under pressure.

2.2 Model tests to predict air entrainment

Dawson and Kalinske⁽⁸⁾ investigated the pneumatic disturbances in water flowing down partly full vertical pipes in a plumbing system. As water entered a vertical pipe from a horizontal drain, air was entrained by the falling water. The air was compressed near the bottom of the stack to a degree depending on the ease with which the air could escape at the bottom. To prevent the formation of excessive pressure differentials in the drains, air had to be supplied or removed at definite rates. The determination of these rates of air flow formed part of their investigation. They used Manning's equation and open channel flow theories to establish a relationship between the velocity at any point below the entrance and the initial velocity and length of fall. The assumption had to be made that the whole perimeter of the vertical pipe was wetted, and the maximum velocity was attained when the acceleration was zero. Thus the length of fall

FIGURE 2.1

Relationship between Spillway Air Demand and Discharge for Model and Prototype



can be calculated for maximum velocity to be achieved. This variable was then related to the experimental results to establish a relationship to predict the theoretical maximum rate of air flow as follows;

$$Q_a = \left[\frac{\pi D^2}{4} - \frac{Q_w}{v_m} \right] v_m$$

where Q_a = theoretical maximum rate of air flow (cu.ft./sec)

Q_w = rate of water flow (cu.ft./sec)

D = diameter of stack (ft.)

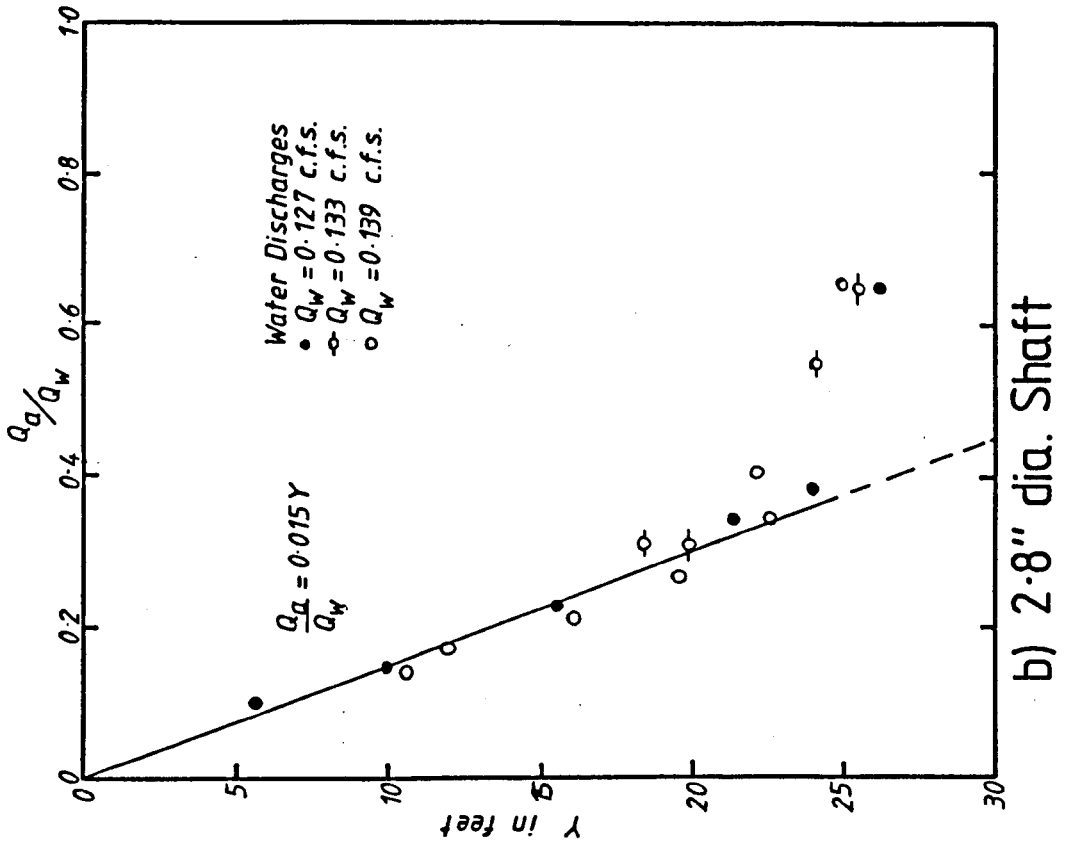
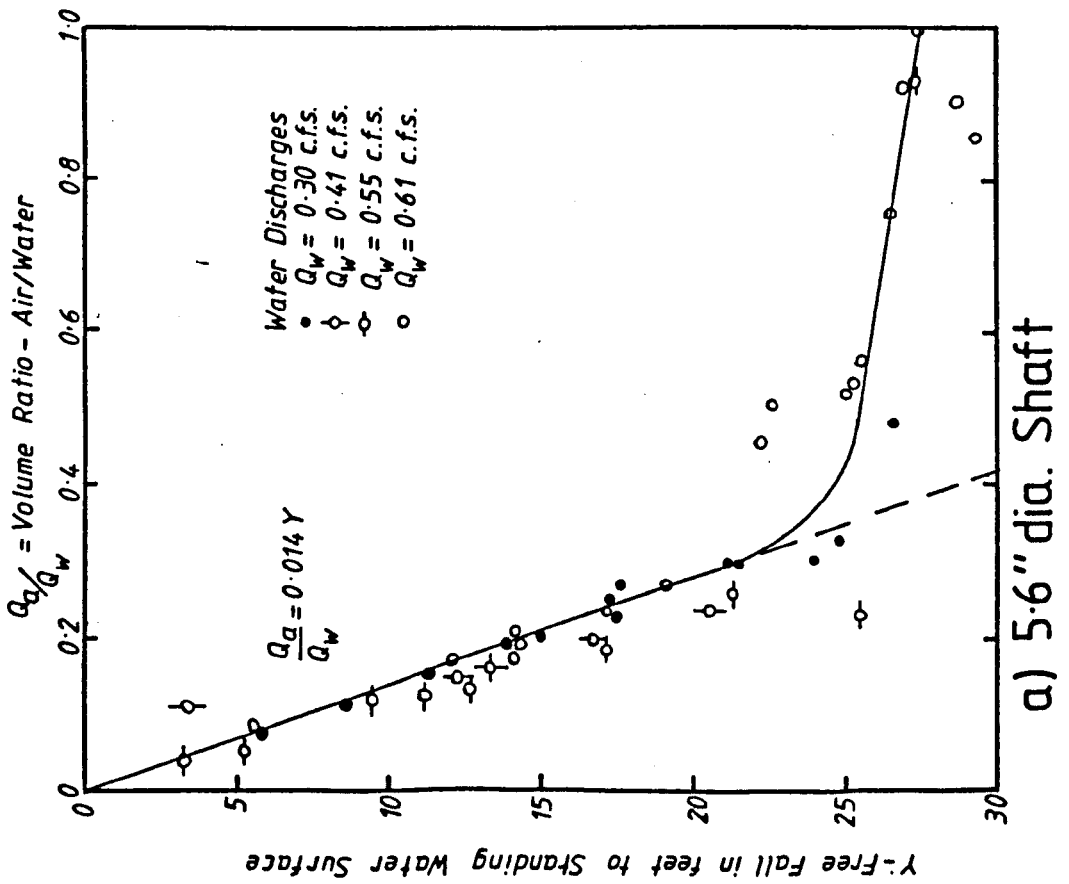
$$v_m = \left[\frac{Q_w \cdot g}{k \cdot \pi \cdot D} \right]^{1/3}$$

k = frictional resistance constant

In 1953, Laushey and Mavis⁽⁹⁾ conducted experiments to determine entrainment in dropshafts with different entry arrangements. Measurements were made of the quantities of air entrained by water falling down 30 feet long shafts of 2.8in. and 5.6in. diameter. They proposed that the degree of air entrainment depended on the following variables; the type of entrance at the shaft inlet; the distance from the inlet to the standing water surface in the shaft; the rate of flow of water; the shaft diameter; and the amount of sub-atmospheric pressure, if any, in the top of the shaft.

Their results are presented in Figures 2.2 and 2.3. Figure 2.2a shows the variation of the air entrained in spiral flow in the larger shaft with Y , the length of free fall. The air/water ratio is directly proportional to Y if Y is less than about 20 feet and it is independent of Q_w . Similar results are shown in Figure 2.2b for tests

FIGURE 2.2 Air Entrained by Spiral Flow



using a smaller diameter shaft. The explanation for the knee in the curves was given as being due to the air core extending almost the full length of the shaft. By modifying the apparatus to ensure that the shaft was always submerged in a stilling pond arrangement, it was possible to produce a straight line relationship for the full shaft length. For spiral flow, for geometrically similar entrances, the air flow can be approximated by the formula;

$$\frac{Q_a}{Q_w} = 0.015Y \quad \text{where } Y \text{ is in feet}$$

Consideration was given to the ability of the water to transport the air bubbles but was limited to visual observations and it was thought that all the air entrained at the standing water level was actually carried down. Thus since a specified water discharge entrained amounts of air in proportion to the distance of free fall, the amount of air entrained must be principally proportional to the square of the velocity of the water film.

Viparelli ⁽¹⁰⁾ investigated along similar lines, using a 96mm shaft with spiral entry, but measured the air demand at the shaft inlet just above the throat section. Two situations were considered, one with a freely discharging shaft and secondly with a standing water column in the shaft. The case of the free exit was of little relevant interest. The occurrence of an air/water mixture developing in the shaft was attributed

Viparelli's Curve of h/D & Q_a/Q_w

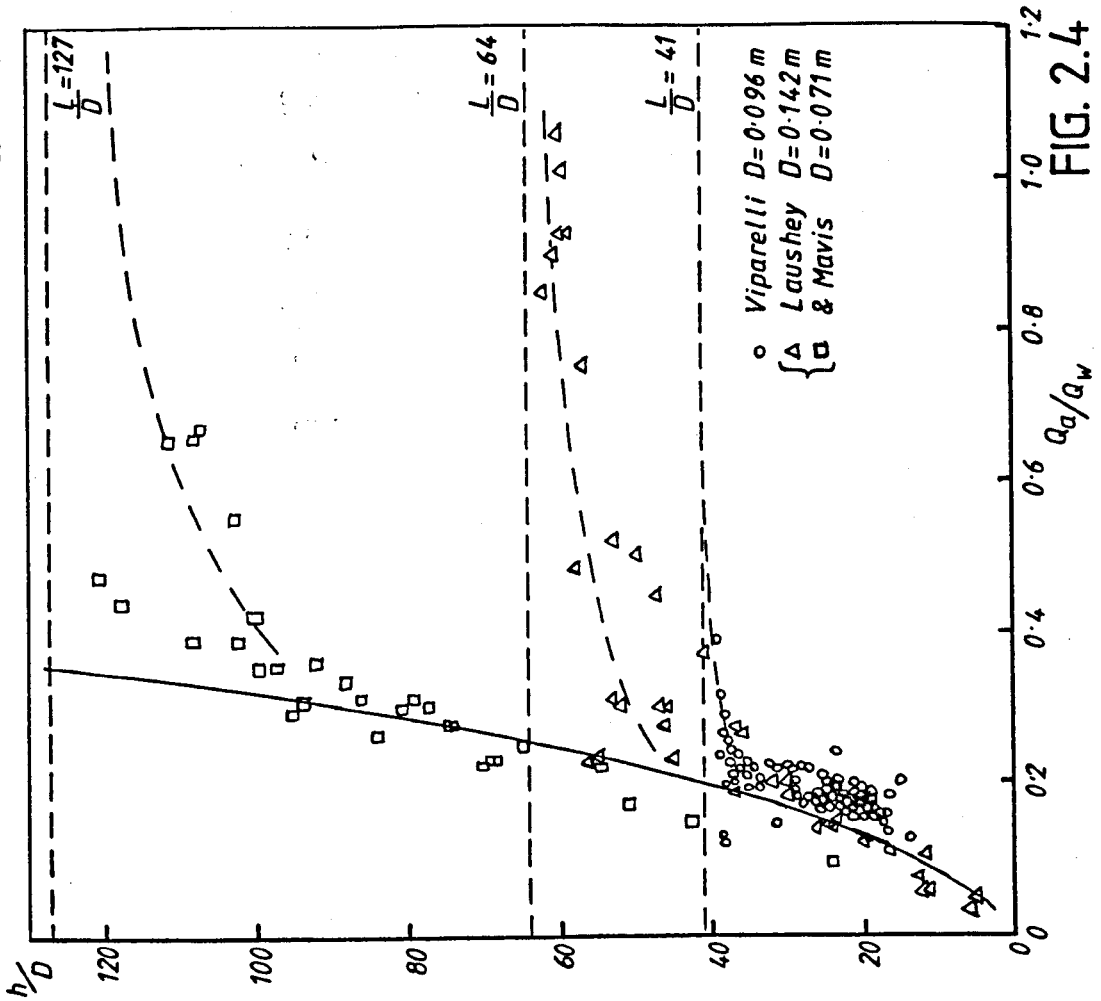


FIG. 2.4

Air Entrained by Modified Apparatus

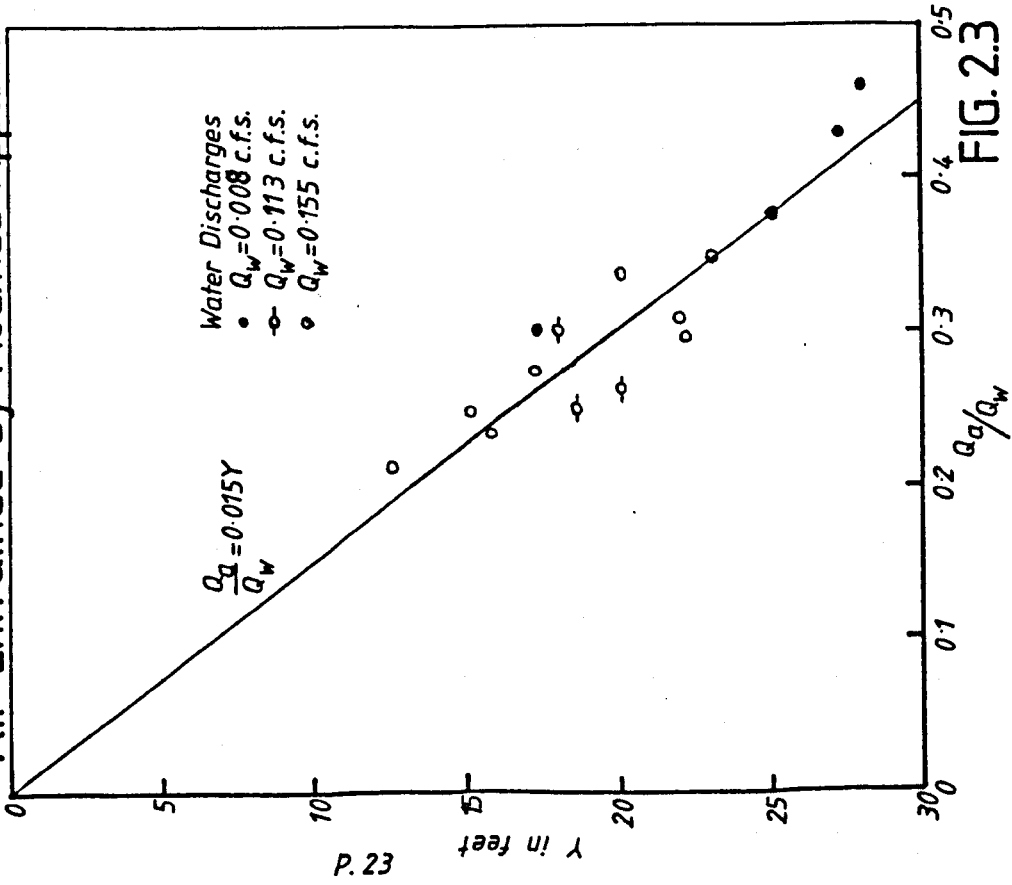


FIG. 2.3

to the presence of a hydraulic jump in the shaft due to a difference in pressure between the shaft inlet and outlet. Viparelli argues that whenever a complete jump develops in the shaft (i.e. the water column contains the jump), the air entrainment depends on the flows both upstream of the jump and downstream of the shaft.

In the upper shaft, the velocity of the air in the centre of the shaft can be considered to approach that of the free falling water along the walls of the shaft. Using Kalinske and Dawson's⁽⁸⁾ approach to determining the terminal velocity of the falling water, then the air volume passed into the shaft is equal to the product of the air core area and the water velocity. The air entrainment chiefly depends on the height over which the water falls freely, and on the proportion of air in the mixture. If the lower part of the shaft, beyond the hydraulic jump, is sufficiently long, then the air flow can be evaluated from;

$$\frac{Q_a}{Q_w} = 0.022 \left[\frac{h}{D} \right]^{3/5} \quad \text{where } h = \text{free fall height}$$

$$D = \text{pipe diameter}$$

Fig 2.4 is a reproduction of Viparelli's analysis of his own work and that of Laushey & Mavis⁽⁹⁾. The explanation forwarded for the deviations from the general curve is that the velocity is not sufficiently attenuated at the longer droplengths since the standing water level is very close to the shaft outlet. Hence a large increase in air passed through can be expected. (i.e. the situation approaches that present for a free exit).

The Hydraulics Research Station, Plover Cove⁽²⁾ experiments involved measuring similar quantities to Viparelli, i.e. discharge, air demand, and droplength, at three different model scales of a prototype vortex dropshaft. The models were all designed to Froudian scaling. The results are plotted in the form air/water ratio versus droplength/pipe diameter. A consistent pattern within each model emerges which shows an increase of air/water ratio at a given droplength with increase in discharge, up to a certain value of discharge. Above this value, the experimental results fall around a unique line. However, there was no similar or consistent behaviour between the three hydraulically similar models. This is at variance with the findings of both Laushey and Mavis and Viparelli.

Whillock and Thorn⁽³⁾ investigated air entrainment in a rectangular dropshaft model. They used two models, 0.15m x 0.15m square and 0.3m x 0.3m square, the maximum practicable shaft length was about 3.8m. For the smaller model, the length was originally scaled, but later extended to full length. The discharges were modelled to Froudian scaling and were varied from 7 l/s to 74 l/s for the larger model, and 2 l/s to 17 l/s in the smaller one. The entry conditions were simply a vertical plunge arrangement directly from a header tank.

Their results indicated that air entrainment increased with droplength and with increasing nappe

thickness (and flow). A stage was reached when any further increase in nappe thickness at inlet did not produce any further increase in the air/water ratio. This limiting characteristic for which the air/water ratio depends on droplength alone, was achieved when the discharge produced a nominal shaft water velocity greater than 0.5 m/s. If a model dropshaft were constructed to Froudian scale proportions, but with droplength varied to permit the jet to attain prototype velocity, then the authors considered a reasonable prediction of prototype air demand could be made if the surface roughness characteristics were similar.

The paper also presents the observation that all the air entrained was not necessarily transported by the water flow. A proportion of the initial volume of air entrained was re-circulated above the ambient water surface. However, no definitive measurements were taken of this phenomena. Various flow regimes were also identified by Whillock and Thorn. They observed the effect of the position of the ambient water surface and hence the recirculation region on the net air demand. For example at short droplengths, the recirculation zone was wholly contained in the shaft and air bubbles were carried down by the flow. For a long droplength, the recirculation region passed beyond the end of the shaft, thus the net air demand increased considerably.

Ervin and Kolkman⁽¹¹⁾ utilised the results of Whillock and Thorn to present a report on air entrainment

and transport in conduits. They proposed a relationship for predicting air entrainment of the following form:

$$\beta = K \cdot Fr^2 \left(1 - \frac{v_c}{v_b}\right) \left(1 - \frac{v_{br}}{v_o}\right)$$

where β = nett air transport ratio
 v_c = minimum entraining velocity
 v_b = velocity of flow
 v_{br} = bubble rise velocity
 v_o = outlet velocity
 $Fr = v_b / \sqrt{g \cdot d_b}$
 d_b = upstream jet thickness
 $K = (3 - 3.5 \times 10^{-3})$

Attention was given also to the determination of the minimum velocity to entrain air, reported at 0.8 to 1.0 m/s for the dropshaft; and the minimum velocity to transport air, given between 0.15 to 0.2 m/s. They emphasised that the minimum transport velocity gave rise to larger scale effects than the minimum entrainment velocity for most hydraulic structures, and further work is required on the exact nature of the transport velocity.

2.3 Froudian Models

By discarding direct Froude similarity, Kenn^{(12),(13)} and Zanker⁽¹³⁾ have proposed new approaches which favour utilising factors of similarity that give a better reproduction of the major full scale influences.

A model using the same working fluids as the prototype is feasible when the system operates predominantly under only two sets of forces. If other forces

operate, then this becomes impossible and either different fluids must be used or the model results must be adjusted to allow for the scale effects. It is possible in some instances to separate the scale effects in a model and compute accurate numerical predictions for the prototype from the model results. In other cases, the working fluid can be changed to compensate for scale effects.

Wisner⁽¹⁴⁾ presents a paper which discusses the relevance of Froudian models in air entraining situations. He proposed the following relationship for the transport of air bubbles;

$$\bar{c} = f \left[\left(\frac{v}{\sqrt{gR}} \right), \left(\frac{u}{\sqrt{g d_b}} \right), \left(\frac{d_b}{R} \right) \right]$$

where \bar{c} = mean concentration
 v = mean flow velocity
 u = bubble rise velocity
 d_b = bubble diameter
 R = hydraulic radius
 g = acceleration due to gravity

The bubble size, and hence the bubble rise velocity, is independent of scale. Therefore the value of $(u/\sqrt{g d_b})$ is essentially constant, and for (d_b/R) to remain constant, the hydraulic radius must assume a fixed value and hence a reduced scale model is impossible to construct, unless the scale effects can be compensated for by suitable scaling factors.

2.4 Motion of air bubbles in two-phase flows

Many investigators have attempted to study the motion of gases in a liquid medium and there are several books on the subject now available.

Curtet and Djonin⁽⁵⁾ considered the emulsion formed by a jet impinging upon a free water surface in an upright cylindrical pipe. The system is thus not comparable with the present study from the aspect of air entrainment. However, they also utilised a gamma ray technique to measure the air concentration within the pipe at one level. An analysis was undertaken by measuring the air concentration at chords across the pipe section. The peak concentration occurred on the pipe diameter, the intensity decreasing towards the edges of the pipe section.

Having determined the air concentration, or void fraction, they were able to predict the true water velocity at about 0.24 m/s at which air begins to be transported. Thorn⁽⁶⁾, using a gamma ray absorption technique on the shafts previously mentioned in the research of Whillock and Thorn⁽³⁾, also determined the air flow threshold. It is reported as being between 0.21 - 0.31 m/s in the 0.3m square shaft and between 0.24 - 0.29 m/s in the 0.15m square shaft. He also estimated the true water velocity at the beginning of the limiting air demand condition as being between 0.77 - 0.82 m/s in the 0.15m square shaft and 0.81 - 0.86 m/s in the 0.3m square shaft.

Curtet and Djonin related their findings to the results of Zuber and Findlay⁽¹⁵⁾ and Wallis⁽¹⁶⁾, and obtained a relationship between the average concentration and the air and water flows.

Nicklin⁽¹⁷⁾ discusses the various factors contributing to the motion of the bubbles in two-phase flow. He presents a theory which shows that the velocity of the bubbles consists of a component equal to the superficial liquid velocity, a component equal to the superficial gas velocity and a component due to buoyancy. Simple experimental work in support of the theory is described. This involved direct measurement of the buoyancy component of velocity by suddenly stopping the gas flow and timing the rise of a bubble swarm. Energy losses associated with two-phase gas-liquid flow are discussed and the author shows that in bubble flow, "the energy loss due to slip" is closely related to the buoyancy component of bubble motion.

2.5 The surface air entrainment phenomena

As previously discussed, the entrainment phenomena present on steep chutes is considered to be a distinctly separate process of air entrainment from that under consideration within the scope of this investigation. However, the assessment of the mechanism for initial air entrainment incorporates the concept of depth of flow becoming wholly turbulent as a parameter controlling the degree of entrainment.

Hall⁽³⁴⁾ suggested that on steep chutes, the initial entrainment of air depends to a great extent on the entrance conditions. Water accelerates uniformly down the slipway gradually drawing air into the water; this insufflation develops first along the side-walls and spreads gradually into the section until the admixture of air and water covers the entire wetted area.

It has been reasonably well established by several observers^(35,36) that for flow down steep chutes, aeration does not occur until a point is reached at which the boundary layer thickness is equal to the depth of flow. The characteristic roughening of the water surface immediately upstream of the appearance of white water can be readily observed. With increasing initial water depths, the positions where the surface roughening and the white water occur move downstream along with the intersection of the boundary layer with the water surface. The surface aeration is enhanced by entrainment of air from the sides of the chute. At a further distance downstream, when the air/water mixture is present throughout the full depth of flow, the flow continues with uniform velocity, depth and air concentration.

Hickox⁽³⁶⁾ developed a relationship on the basis of observations on models and prototypes of concrete chutes and overflow dam spillways between the distance l (m) of the critical point from the spillway crest and

the specific discharge q ($\text{m}^3/\text{s}/\text{m}$). The empirical equation may be expressed as follows:

$$l = 14.7q^{0.53}$$

the critical point being that position at which the film becomes wholly turbulent (i.e. $\text{depth} = h_{cr}$). Novak⁽³⁷⁾ proposes an approximation from Hickox's measurements as follows:

$$\frac{l}{h_{cr}} = 100$$

relating the length to critical point and the turbulent depth of flow.

In recent years, several investigators have reported that the turbulence of the fluid body is fundamental to the prediction of air entrainment rates. Elsayy and McKeogh⁽³⁸⁾ investigated the volume of air entrained by a circular jet impinging on a stilling pool. It was found that in turbulent entrainment, the volume of air entrained increased with the increase in height of free fall up to a certain limit, beyond which, no further increase in volume of air entrapped occurred. The turbulence level of the jet at the point of impact was found to have a significant effect on the penetration depth and volume of air entrained.

Hack⁽³⁹⁾ investigated air entrainment in dropshafts with annular flow condition and free central air core. By special model design of the flow regimes in a dropshaft, Hack reported that the entire air entrainment

could be shown to be dependent on the wall roughness and the Froude number in the dropshaft under the assumption of undisturbed turbulent diffusion between the air and water.

The air entrainment phenomena occurring in dropshafts or shaft spillways was considered by Hack to be due to three different origins. He defined the three flow regimes in the dropshaft as follows:

- a) annular flow; air entrained by turbulent diffusion in the boundary layer between air and water
- b) bubbly and slug flow; air entrained by forced local turbulence, i.e. the hydraulic jump
- c) closed conduit flow after transmission to submerged inlet; air entrainment by vortex action.

Previously, investigators have treated these different origins simultaneously and consequently have been unable to predict prototype performance. Hack established a relationship for predicting air entrainment for the annular flow regime in shaft spillways by turbulent diffusion in the mixing layer between air and water.

CHAPTER THREE

EXPERIMENTAL PROCEDURES AND APPARATUS

3.1 Apparatus

3.1.1 General layout of apparatus

Figure 3.1 shows a general layout of the laboratory apparatus. The water was raised from the main sump to the vortex chamber by means of a variable speed centrifugal pump. A gate valve, situated just downstream of the pump, was used to control the flow to the model in conjunction with the operating speed of the pump.

The water was conveyed from the pump through rigid 101 mm diameter P.V.C. pipe to the base of the vertical leg at which point the pipe was reduced to 51 mm diameter for the rising leg. An orifice plate was located on the rising leg to measure the inflow water rate to the vortex chamber.

The orifice plate was made in accordance with B.S.1042; Part I:1964, and consisted of a 31mm diameter square-edged orifice plate with corner tappings located in a 51 mm diameter pipe. The pressure tapping points were connected to a differential manometer to measure the pressure difference. Initially the manometer was water filled but when higher flow rates were required,

a mercury manometer was introduced. The orifice plate was calibrated before use and the calibration curve is shown in Appendix A.

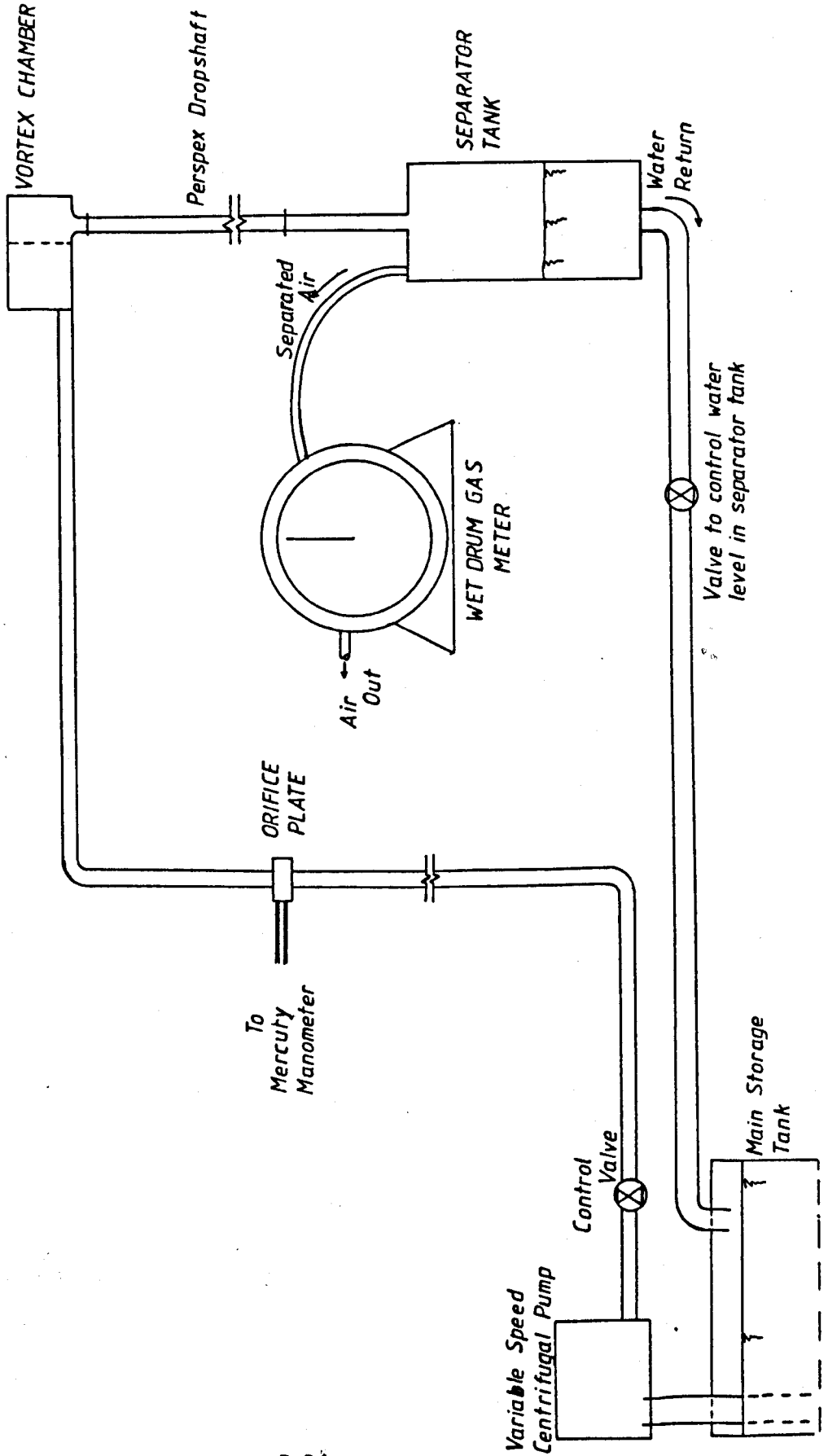
A 2m length of rigid P.V.C. pipe, 51mm diameter but flared to 56mm diameter on entry to the vortex chamber, was used to convey the water into the vortex chamber inlet. The flow was returned to the sump from the separator tank via a 76mm diameter P.V.C. pipe. The water level in the separator tank was maintained at a constant level by means of a valve located on the return pipe to the sump.

The air demanded by the system was drawn into the vortex chamber from the atmosphere, and separated in the separator tank. An outlet in the top of this tank was connected by a 19mm diameter flexible polythene pipe to a wet-drum gas meter manufactured by Alexander Wright of Westminster. This gas meter was used to measure the volume of air in cubic feet passed through it over a timed period to give the volumetric air flow rate. The meter was calibrated using a positive displacement method. A known volume of water in an airtight container was displaced by air fed into the container after passing through the wet-drum meter. Hence a direct comparison was possible; the accuracy of the gauge readings were acceptable within the scope of the experimental procedure for measuring air flow.

The overall arrangement was designed to allow the

General Layout of Apparatus

FIGURE 3.1



1:21.6 scale model to be replaced by the larger 1:10.9 scale model without too many changes in the feeder arrangement and separation part of the system.

3.1.2 The Vortex Chamber models

The vortex chamber models were constructed on the basis of the prototype design. The two scales for the models were chosen based on the availability of commercial pipe sizes. They were 51mm and 101mm diameter perspex pipes for the dropshaft; the prototype dropshaft being 1100mm diameter pipe.

The vortex chambers were built from fibreglass moulded around a short length of P.V.C. pipe which served as the top of the dropshaft. The throat section and chamber invert were carefully formed to the correct radius and slope as shown in Fig 3.2. The spiral geometry for the vortex was set out and the inner face formed by bending flexible fibreglass sheet to provide a smooth surface. The wall thickness of the chamber was increased using fibreglass mat and resin moulded over steel bars and wire mesh which provided some reinforcement.

In the case of the 1:21.6 model, a perspex cover was fitted to seal the top of the vortex chamber. Air was fed in through a 19mm diameter hole in the cover located above the centre of the dropshaft. This permitted air demand to be measured and compared with air ejected from the separator tank.

The inlet channel in the vortex chamber was shaped to form a smooth transition from the circular feed pipe to a rectangular section in the inlet. In the 1:10.9 scale model, a baffle was fitted across the outlet of the circular pipe in order to decrease the turbulence of the flow at high flow rates, and thus maintain a spiral vortex flow pattern into the dropshaft.

3.1.3 The dropshaft

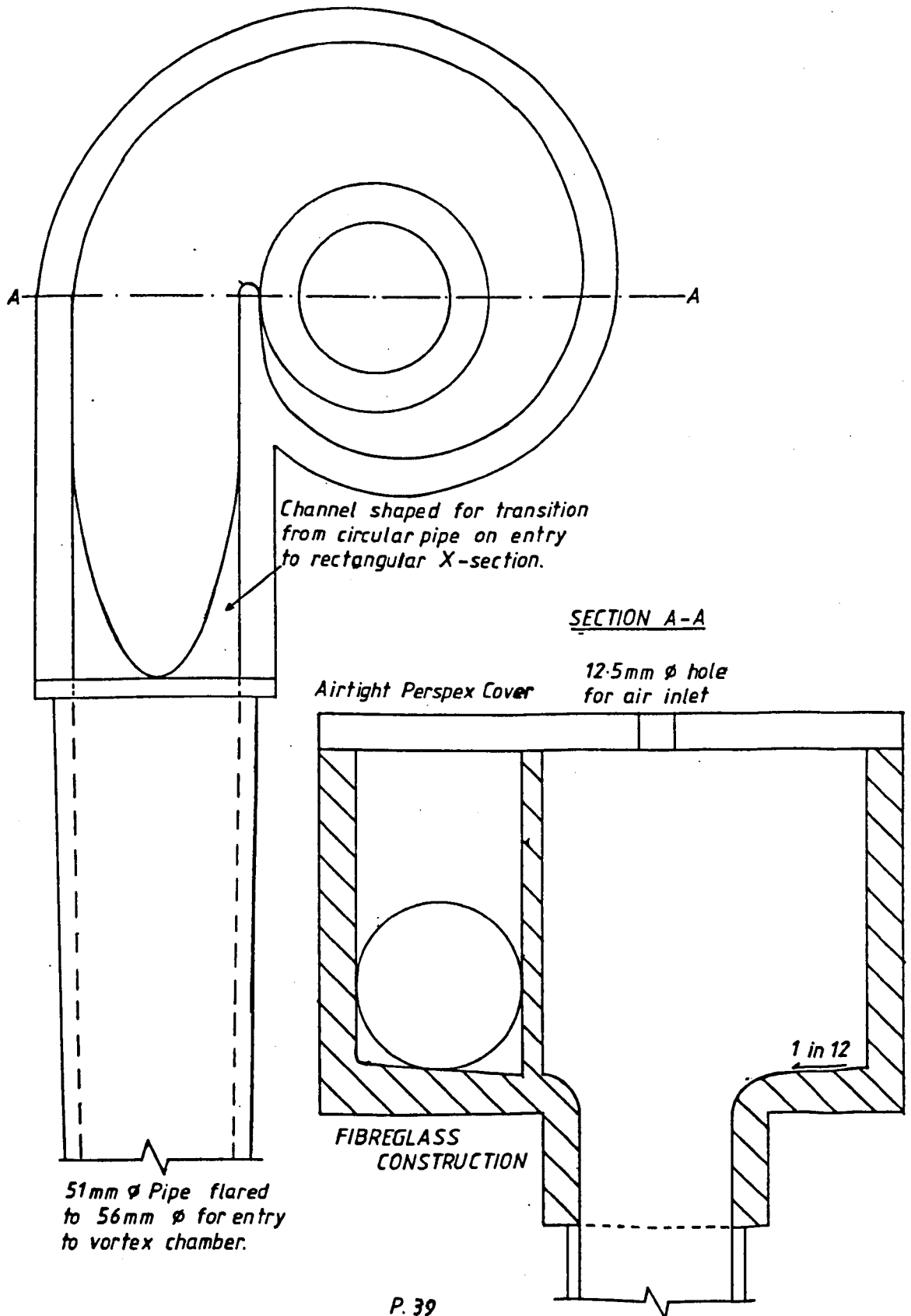
The dropshaft consisted of 2.0m long sections of perspex pipe of either 51mm or 101mm diameter. The only requirements for the dropshaft was that the joints had to be smooth and airtight, and the shaft had to be vertical. For the 51mm pipes, perspex flanges were glued to the ends of the perspex pipes and they were butt-jointed together with a flat rubber gasket between the flanges. This arrangement was improved for the 101 mm diameter pipes by using a spigot and socket type arrangement for the flanges to try to achieve a smoother flow past the joints. In each model, a short length of perspex pipe was connected to the P.V.C. pipe protruding from beneath the vortex chamber, it was critical to ensure a smooth transition at this joint especially.

3.1.4 The separator tank

It was thought desirable to separate the air/water

Details of Vortex Chamber Geometry

FIGURE 3.2



mixture into its individual components in order to measure the quantity of air actually transported through the system by the water. The separator was designed to achieve this and a series of tests were carried out to determine its efficiency.

For the 1:21.6 scale model, a 380mm diameter P.V.C. pipe was used for the tank and end plates were fitted, see Fig 3.3. The dropshaft was connected to a 51mm diameter perspex pipe fitted to a perspex cover plate which served as the tank top. The water return pipe was connected to the bottom of the tank and a shelf fitted above the outlet to prevent excessive draw-down through the outlet.

A conical plug was devised and fitted to a mechanism on the cover plate which allowed movement of the conical plug in a vertical direction. This permitted the annular gap between the plug and the end of the drop-pipe to be varied and consequently was used to control the level of the standing water in the dropshaft. By adjusting the standing water level in the shaft, the length of free fall of the water from the vortex chamber before onset of air entrainment, was varied accordingly.

In order to maintain a constant water level in the separator tank, a valve was fitted on the return pipe to the sump and a piezometer was connected to the tank to measure the water level. Air was ejected from the tank through a 19mm diameter pipe fixed to the cover

Arrangement of Vortex Chamber, Drop-pipe and Separator Tank

FIGURE 3.3

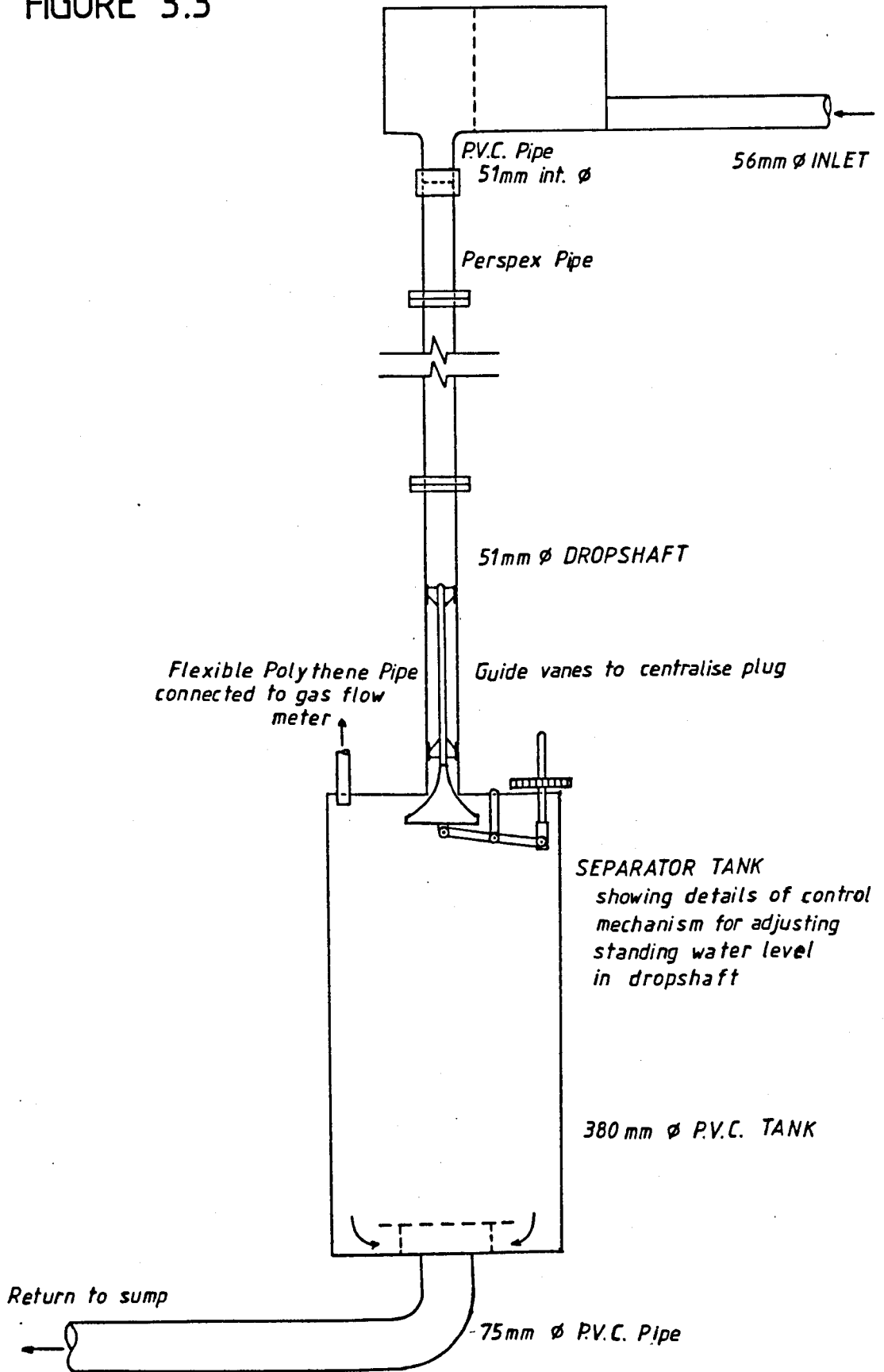


plate and the separated air was passed through a wet-drum gas meter.

For the 1:10.9 scale model, the separator tank had to be modified to accommodate the higher flow rates of air and water. This was achieved by fixing a 600mm square box, 300mm deep, constructed from 6mm thick P.V.C. sheet, to the top of the 380mm diameter tank. The air outlet from the separator tank was increased to 28mm diameter, and the inlet to the tank was changed to a 101mm diameter perspex pipe. The conical plug and operating mechanism was utilised in its original form for the larger model.

3.1.5 Performance of separator tank

The air/water mixture passed down the dropshaft and was observed to pass through the annular ring created between the conical plug and the pipe wall in a thin film and be deflected against the side walls of the tank. The water fell to the reservoir in the tank, maintained at a constant level, and the air collected in the upper section of the tank was passed to atmosphere via the gas meter.

A series of tests were carried out to determine the efficiency of the separation process. This was achieved by taking measurements of the air demanded through the vortex chamber and comparing them with measurements of the air ejected from the separator tank

under the same dropshaft conditions, (i.e. flow rate and droplength). The mean efficiency of the separator was 97%.

3.1.6 8.8m Dropshaft length

The apparatus described has been for the laboratory arrangement, the length of the dropshaft being 2.8m from the vortex chamber to separator tank. However, subsequent to the laboratory tests, the system was moved to another location outside the laboratory to enable a dropshaft of 8.8m to be constructed. This involved adding three further sections of perspex pipe into the dropshaft length, the joints being made as for the laboratory arrangement. It was also necessary to alter the feed pipe arrangement to the appropriate lengths and geometry.

For the 1:21.6 scale model, a Grundfoss, 1.5kW, 4 stage centrifugal pump was used to lift the water to the vortex chamber. The system had to be arranged in a closed loop which necessitated changing the water at frequent intervals due to heating of the water in the system. For the 1:10.9 scale model, a 3-phase, 5.5kW, Flyght submersible pump was employed to deliver the required flow to the vortex chamber, again heating effects had to be carefully monitored. The air temperature and water temperature were measured and the system only operated within a range of water temperatures that

were considered acceptable and did not affect the degree of entrainment.

3.1.7. Rectangular Column Dropshaft

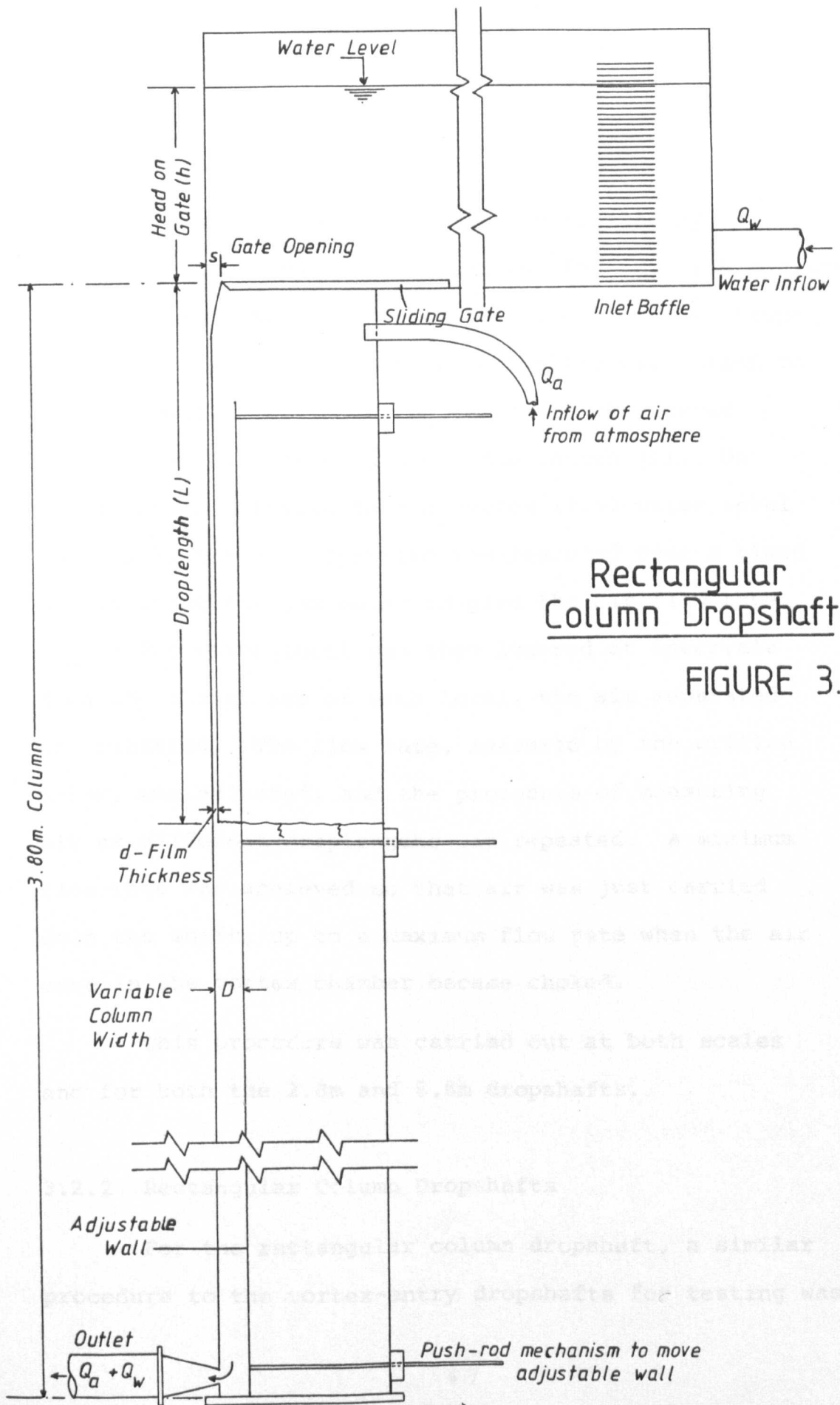
The rectangular column dropshaft was supplied by the same layout as for the vortex-entry dropshafts. However, no attempt was made to separate the air/water mixtures, the flow was returned to the main sump in a two-phase condition. The net air demand was measured through the gas meter via a 28mm diameter flexible P.V.C. pipe fitted into the wall of the column opposite the face carrying the water film.

A rectangular column, 304mm square was fabricated in 12mm thick perspex sheet, flow occurred down one internal face, 280mm wide between side walls. The overall length of the column from inlet slot to the base was 3.8m. Above the column, an open rectangular tank (1370mm x 304mm x 460mm deep) was fitted to feed the water into the column across the width of the 280mm face, see Fig 3.4. The rising leg of the arrangement for the vortex-entry dropshafts was connected to convey the water into this rectangular tank. The orifice plate located on this pipe was used to measure flow rate. A baffle was placed across the top tank near the inlet to settle the flow conditions.

A sliding gate was arranged on the floor of the tank over the column, to vary the opening in the tank floor, thus allowing variation in head on the gate

and permitting different inlet velocities to be created. An adjustable wall of 6mm thick perspex sheet, 280mm wide, extending 3.60m in length was fitted internally in the column parallel with the face intended to carry the water flow. Rubber strips located longitudinally on the edges of this adjustable wall prevented air bubbles escaping into the still water behind the wall. This adjustable wall was moved laterally by a set of push-rods, located in pairs at intervals through the back face of the column and locked in position against the supporting framework. Each push-rod passed through an 'O' ring seal and perspex boss fastened to the perspex wall to maintain an airtight column. Strips of 'dexion' angle also had to be attached to the thin adjustable wall to act as extra vertical stiffeners due to the internal forces created by the process of air entrainment. The column had to be tied to the supporting framework to prevent movement due to these forces.

The standing water level in the column and hence the droplength, was controlled by a gate valve on the 76mm diameter P.V.C. pipe returning the flow to a sump. A special transition section was made for the outlet from the column. A 200mm wide x 25mm deep slot near the base of the column was connected by the transition section, constructed of 12mm thick P.V.C. sheet to the 76mm diameter return pipe. This proved a better arrangement than having the 76mm pipe directly connected to the centre of the wall, the flow pattern was smoothed



Rectangular Column Dropshaft

FIGURE 3.4

considerably.

3.2 Experimental Procedure

3.2.1 Vortex-entry dropshafts

For a set flow rate, (Q_w), controlled by the gate valve and pump speed, water was fed into the elevated vortex chamber and allowed to fall freely in the dropshaft. The water level in the dropshaft was raised to a high level, just below the throat of the vortex chamber outlet, giving a short droplength (L). On attaining equilibrium in the system (i.e. water level constant), the air separated was measured over a timed period using the gas meter to give the air flow rate, (Q_a). The water level was then lowered at intervals down the shaft, and at each level, the air separated was measured. The flow rate, measured by the orifice meter, was adjusted, and the procedure of measuring air at different droplengths was repeated. A minimum flow rate was achieved so that air was just carried down the shaft, up to a maximum flow rate when the air core in the vortex chamber became choked.

This procedure was carried out at both scales and for both the 2.8m and 8.8m dropshafts.

3.2.2 Rectangular Column Dropshafts

For the rectangular column dropshaft, a similar procedure to the vortex-entry dropshafts for testing was

used. However, this model was also designed to vary the inlet velocities of the free falling jet and to vary the nominal downward water velocity of the air/water mixture.

The adjustable wall was arranged so that it effectively narrowed the depth of the column using the positions 25mm, 38mm, 45mm, 50mm and 55mm. This varied the cross-sectional area for the flow of air and water and hence the nominal downward water velocity. Rubber strip had to be glued to the vertical edges of the adjustable wall to prevent the passage of air bubbles around the edge and into the still water behind this wall.

For a fixed position of the adjustable wall, the sliding gate in the header tank was positioned to give a parallel slot width of 5mm. A flow rate was obtained such that the water level in the header tank was a maximum and steady. The air demand, measured through the gas meter, was determined for different lengths of free falls of the water film. The standing water level was controlled by the gate valve on the return pipe to the sump. Before each reading was taken, it was necessary to allow the standing water level to equalise to avoid measuring the air drawn in to replace the water displaced on opening the valve.

The sliding gate was then opened a further 2.5mm thus reducing the head at the same flow rate and hence

the inlet velocity. The procedure of measuring the air demand at different droplengths was repeated. The flow rate was then increased to obtain the inlet velocity achieved for the first slot width and the procedure repeated. This operation of increasing the slot width in 2.5mm increments was repeated up to a 15.0mm opening. The flow rate was adjusted to give similar inlet velocities in each case to provide a basis for comparison. For one position of the adjustable wall, 15 test runs were carried out in the column, measuring air demand at different droplengths and flow rates.

The adjustable wall was then moved and the whole procedure repeated. In the case of the adjustable wall being only 25mm from the column face, three runs only were carried out due to coalescence of the bubbles into slug formations, which were then ejected upwards from the mixture.

3.3 Gamma ray absorption technique for measuring void fraction

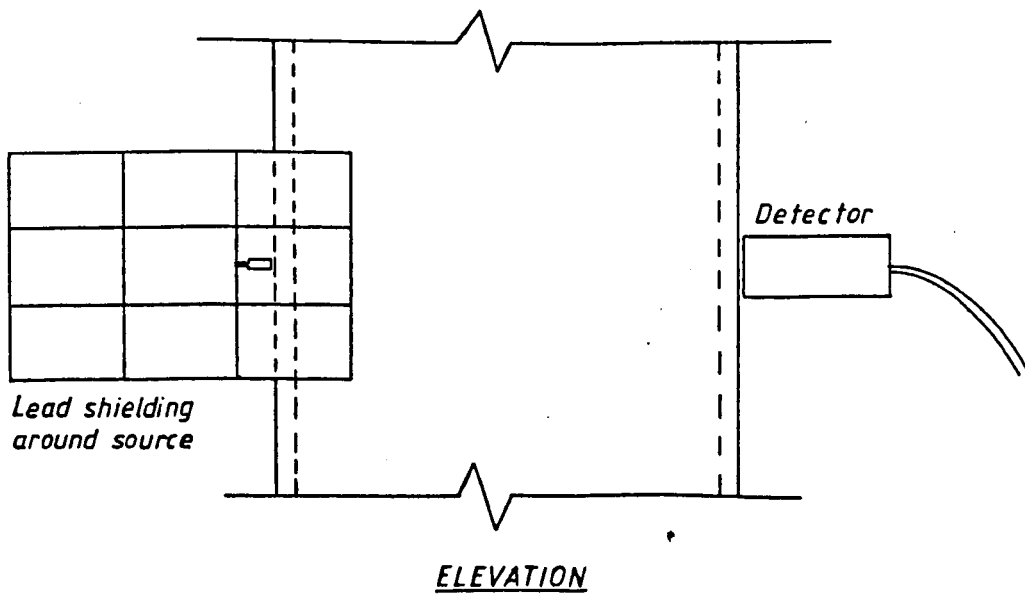
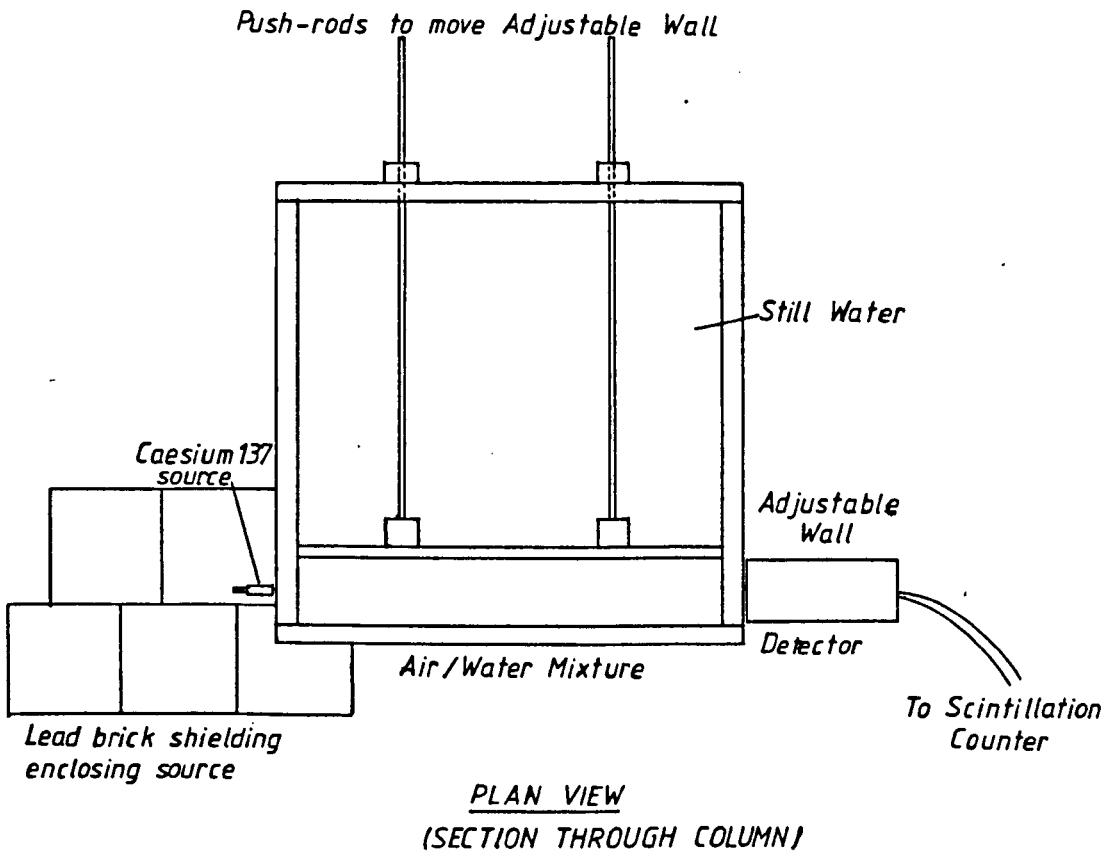
A caesium-137 radio isotope was used to emit a collimated beam of gamma rays which were measured by a detector connected to an E.G. & G. scintillation counter. The operation was carried out on the rectangular column with the adjustable wall set at two different positions.

The source was mounted in a lead block with the collimation of the radio-active rays provided by a 6mm

diameter hole drilled in the lead block. This was shielded by an arrangement of standard lead bricks. On the opposite side of the column (see Fig 3.5), the detector was mounted horizontally, in line with the emitted beam of gamma-rays, and connected to the scintillation counter.

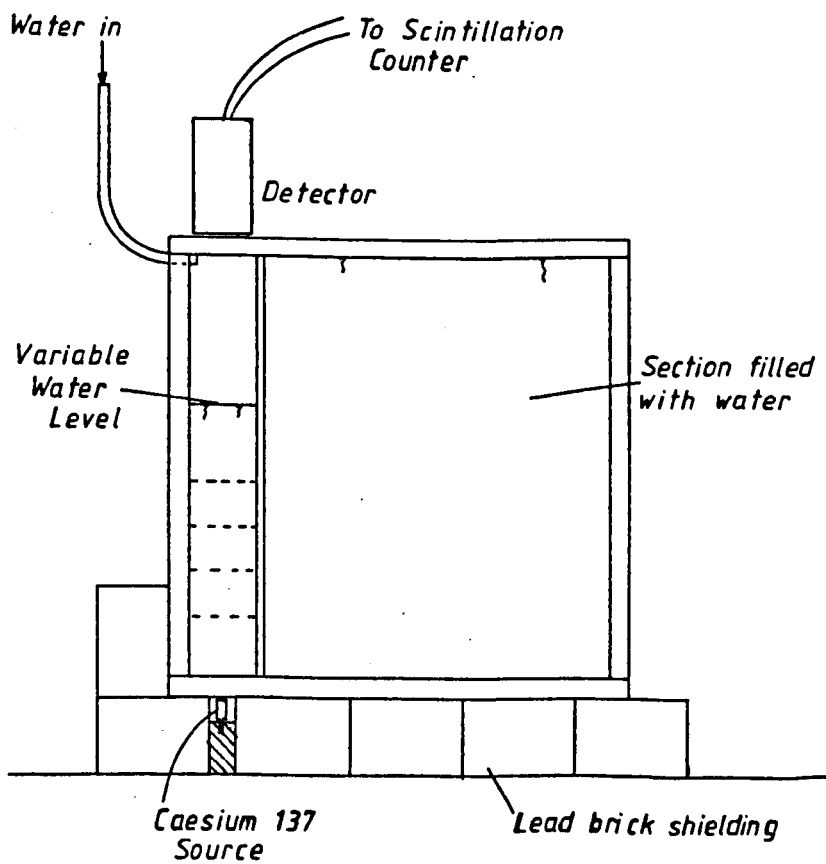
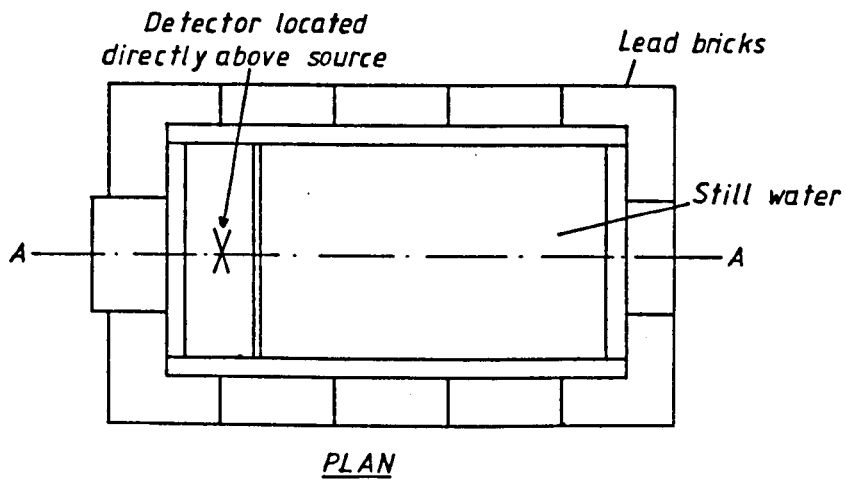
The method previously described for determining the air entrainment rates in the column dropshaft was repeated. For each flow rate and at each droplength at that flow rate, the intensity of the gamma-rays were measured by recording the count rate displayed for 100 second time period on the scintillation counter.

A section of the column was constructed using the same materials and with the same dimensions to provide a device to enable a calibration to be carried out. Fig 3.6 shows the arrangement of the source and detector located around the column section. The narrow section, through which the gamma-ray beam was directed, was filled with an increasing volume of water in increments so that at each interval, the intensity of the radiation was measured. This process was repeated for two positions of the adjustable wall in the rectangular column dropshaft. This calibration provided a relationship between intensity of radiation and the void fraction or density of the mixture. The theory is presented in Chapter Four.



Arrangement for Measurement of Void Fraction

FIGURE 3.5



SECTION A-A

Calibration Apparatus for Void Fraction Measurement

FIGURE 3.6

CHAPTER FOUR

THEORETICAL CONSIDERATIONS

This chapter considers the theoretical aspects of the air entrainment phenomenon. The second section of the chapter deals with the transport of air bubbles in two-phase flow. The first section covers the prediction of air entrainment rates from model studies, and the determination of the relevant parameters involved in the entrainment process.

4.1 Air Entrainment

4.1.1 Dimensional Analysis

Hydraulic model analysis requires very careful consideration of the operating parameters. The fundamental scale for any hydraulic modelling is the geometric scale and is dependent on the construction of the model. The requirements for dynamic similarity may be used to determine other model scales. However, fluid systems are subject to a number of force systems and it is not always possible to simultaneously meet all the criteria for full physical similarity.

When the variables in a system are inter-related, it is not possible to change two parameters at a time, maintaining the other variables temporarily constant, to allow the effect of each parameter to be studied separately.

Using the Method of Dimensions or Dimensional Analysis it becomes possible to present the experimental data so that the effect of each variable can be seen.

Consider the dropshaft arrangement in Fig. 4.1, the principal variables in the system are;

Q_w = volumetric water flow rate

Q_a = volumetric air flow rate

g = gravitational constant

b = bubble diameter

D = pipe diameter

δ = terminal film thickness

L = free fall droplength

$\beta = \frac{Q_a}{Q_w}$ = air/water flow ratio

ρ = specific mass (density)

μ = coefficient of dynamic viscosity

σ = coefficient of surface tension

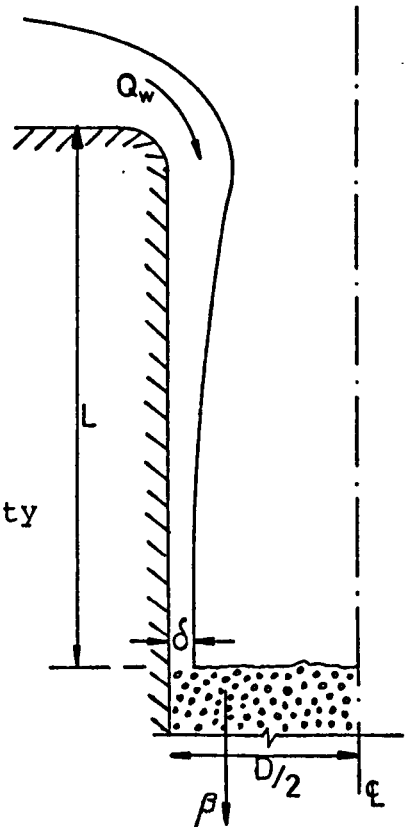


Figure 4.1

Using Rayleigh's Method of Dimensional Analysis, the air entrainment ratio can be expressed as a function of the other parameters;

$$Q_a = \phi [Q_w, L, D, b, g, \delta, \rho, \mu, \sigma] \quad 4.1.1$$

The dimensions of the dependent variable, β , are equal to the dimensionless constant, k , multiplied by the product of the dimensions of each of the independent variables raised to some undefined power. Thus;

$$Q_a = k Q_w^a, L^c, D^e, g^h, \delta^j, \rho^m, \mu^n, \sigma^p, b^f \quad 4.1.2$$

where $k, a, c, e, f, h, j, m, n$ and p are undefined constants. Rewriting the equation in terms of the dimensions involved gives;

$$\frac{L^3}{T} = k, \frac{L^{3a}}{T^a} \cdot L^c \cdot L^e \cdot L^f \cdot \frac{L^h}{T^{2h}} \cdot L^j \cdot \frac{M^m}{L^{3m}} \cdot \frac{M^n}{L^n T^n} \cdot \frac{M^p}{T^{2p}} \quad 4.1.3$$

Equating indices of M, L and T now provides the following;

$$\text{for M } 0 = m + n + p \quad (\text{i})$$

$$\text{for L } 3 = 3a + c + e + f + h + j - 3m - n \quad (\text{ii})$$

$$\text{for T } -1 = -a - 2h - n - 2p \quad (\text{iii})$$

Selecting $Q_w, D,$ and $\rho,$ as reference variables to establish the dimensionless groups, the equations can be re-arranged.

$$\text{from eq. (i)} \quad m = -n - p$$

$$\text{from eq. (iii)} \quad a = 1 - 2h - n - 2p$$

$$\text{from eq. (ii)} \quad e = -3a - c - f - h - j + 3m + n$$

$$\text{hence} \quad e = 5h + 3p - c - f - j + n$$

Substituting in Equation 4.1.2

$$Q_a = k Q_w^{1-2h-n-2p}, L^c, D^{5h+3p-c-f-j+n}, b^f, g^h, \delta^j, \rho^{-n-p}, \mu^n, \sigma^p$$

Hence

$$Q_a = k Q_w \left[\frac{L}{D} \right]^c \left[\frac{D^5 g}{Q_w^2} \right]^h \left[\frac{D \mu}{Q_w \rho} \right]^n \left[\frac{b}{D} \right]^f \left[\frac{\delta}{D} \right]^j \left[\frac{\sigma D^3}{Q_w^2 \rho} \right]^p$$

In general terms any parameters in a functional, dimensionless equation can be multiplied by any constant or raised

to any power without destroying the validity of the equation. The equation can thus be written;

$$\frac{Q_a}{Q_w} = \beta = \phi \left[\frac{Q_w^2}{D^5 g}, \frac{L}{D}, \frac{b}{D}, \frac{\delta}{D}, \frac{Q_w \rho}{D \mu}, \frac{Q_w^2 \rho}{D^3 \sigma} \right] \quad 4.1.4$$

Equation 4.1.4 is the general equation for the rate of air entrainment in a vertical dropshaft in prototype and in the model. For geometrical similarity between model and prototype and between models of differing scales, the ratios $\frac{b}{D}$, $\frac{L}{D}$, and $\frac{\delta}{D}$ must be in the same scale ratio. For tests carried out at equal pressures, with the same fluid, the bubble diameter, b , is the same irrespective of scale. Hence the ratio, $\frac{b}{D}$, cannot be maintained constant. L and δ are geometrical properties of the film prior to impinging into the standing liquid, and can be varied to satisfy the requirement of similarity at different scales.

Further dimensionless groups occurring in Equation 4.1.4, containing, separately, g , μ , and σ , are forms of Froude, Reynolds and Weber numbers respectively. Using the same fluid at all scales, the fundamental relationships between Q_w and D are;

$$\left[\frac{Q_w}{D^{2.5}} \right]_M = \left[\frac{Q_w}{D^{2.5}} \right]_P \quad \text{to satisfy Froude}$$

$$\left[\frac{Q_w}{D} \right]_M = \left[\frac{Q_w}{D} \right]_P \quad \text{to satisfy Reynolds}$$

$$\left[\frac{Q_w}{D^{1.5}} \right]_M = \left[\frac{Q_w}{D^{1.5}} \right]_P \quad \text{to satisfy Weber}$$

Clearly it is not possible to comply with these conditions

simultaneously in modelling air entrainment systems. In the very highly agitated flow regimes necessary for air to be entrained, the influence of the forces due to the viscous and surface tension properties of the fluid are very minor when compared with the gravitational forces acting upon the system. It is thus proposed that the equality of Reynolds and Weber numbers are not a necessary requirement when comparing results from systems of differing scale.

In the rectangular dropshaft system, one further variable is involved in the analysis, i.e., the breadth of wall down which the water film flows, B . The diameter of the circular shaft, D , is replaced by the variable width, d , of the rectangular shaft. Hence the dimensionless groups become;

$$\frac{Q_a}{Q_w}, \frac{Q_w^2}{gd^5}, \frac{b}{d}, \frac{L}{d}, \frac{\delta}{d}, \frac{B}{d}, \frac{\rho Q_w}{\mu \cdot d}, \frac{\rho Q_w^2}{\sigma \cdot d^3} \quad 4.1.4a$$

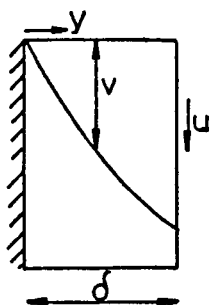
4.1.2 Determination of the relevant variables

Several investigators^(9,10) have suggested that the rate of air entrainment is proportional to the length of free fall of the jet. This result is at variance with the results of recent work⁽³⁾, and of the current investigation. However, the droplength is considered to be one of the variables in the entrainment process.

It is considered that the flow regime is critical to the onset of air entrainment. Air demand does not

occur until a certain droplength is attained irrespective of discharge. For this reason, it is thought that the air demand commences when the falling water film is wholly turbulent across its thickness. This occurs when the film attains the same thickness as the boundary layer, i.e. the turbulent boundary layer projects through the actual physical thickness of the falling water film. From this point, the film thickness is wholly turbulent and air demand commences if the other conditions are appropriate, e.g. the nominal downward water velocity of air/water mixture, etc.

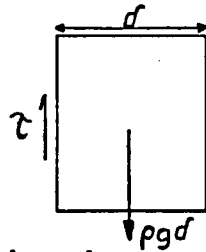
By making several simplifying assumptions and employing the work of Prandtl and Blasius, then it is possible to evaluate the terminal thickness of the boundary layer. Prandtl's $1/7$ th power law is used to determine the velocity distribution.



$$\begin{aligned} \text{Take } \frac{v}{U} &= \left(\frac{y}{\delta}\right)^{1/7} \\ \text{gives } v &= U \cdot \left(\frac{y}{\delta}\right)^{1/7} \\ \text{Flow/unit width } q &= \int_0^{\delta} v \cdot dy \\ &= U \cdot \int_0^{\delta} \left(\frac{y}{\delta}\right)^{1/7} dy \\ q &= \frac{7}{8} \cdot U \cdot \delta \quad 4.1.5 \end{aligned}$$

If the surface is long compared with the extent of the laminar layer near its leading edge, then the laminar layer can be ignored and the turbulent layer is assumed to occupy the whole surface. Thus the shear stress everywhere is that applicable to the turbulent layer.

Considering an element of fluid falling adjacent to the pipe wall, the force diagram is shown thus;



The value of the shear stress, τ , at the wall, cannot be obtained simply by determining $\partial u / \partial y$ from the assumed velocity distribution. An expression for τ may be obtained from the work of Blasius for hydraulically smooth pipes. In a pipe, the thickness, d , of the boundary layer in fully-developed flow equals the radius, r , and the maximum velocity, U_m (along the axis), corresponds to the velocity of the main stream past a flat plate. If these assumptions are made, then for the flat plate

$$\tau = 0.023 \rho U_m^2 R^{-1/4} \quad - \quad \text{Blasius}$$

which becomes

$$\tau = 0.023 \rho U^2 \left(\frac{\nu}{Ud} \right)^{1/4}$$

For flow down a vertical flat plate

$$\tau = \rho g d = 0.023 \rho U^2 \left(\frac{\nu}{Ud} \right)^{1/4}$$

4.1.6

Substituting in 4.1.6 for U from 4.1.5

$$U = \frac{8}{7} \frac{q}{d} \quad \text{and taking } \nu = 1.2 \times 10^{-6}$$

gives
$$\frac{g d^3}{q^2} = \frac{64}{49} \cdot 0.023 \left(\frac{7}{8} \frac{1.2 \times 10^{-6}}{q} \right)^{1/4}$$

$$d^{12} = 9.2334 \times 10^{-17} \cdot q^7 \quad (d \text{ in m.})$$

for d in mm.

$$d^{12} = 9.2334 \times 10^{19} \cdot q^7 \quad 4.1.7$$

This gives an expression for the thickness of the boundary layer at fully developed turbulent flow down a vertical flat plate.

In order to ascertain the distance down the plate at which this maximum thickness occurs, it is necessary to produce an analysis of the growth of boundary layer along a vertical flat plate. This requires an analysis from the fundamental Navier-Stokes equations. For the thickness of the boundary layer, $\delta(z)$ of a fluid, density ρ , falling under gravity g , with velocity $W(z)$, as shown in Fig 4.1.1(a), the appropriate Navier-Stokes equations are;

$$\frac{\partial u}{\partial t} + u \frac{\partial u}{\partial x} + w \frac{\partial u}{\partial z} = -\frac{1}{\rho} \frac{\partial p}{\partial x} + \nu \left(\frac{\partial^2 u}{\partial x^2} + \frac{\partial^2 u}{\partial z^2} \right)$$

$$\frac{\partial w}{\partial t} + u \frac{\partial w}{\partial x} + w \frac{\partial w}{\partial z} = g - \frac{1}{\rho} \frac{\partial p}{\partial z} + \nu \left(\frac{\partial^2 w}{\partial x^2} + \frac{\partial^2 w}{\partial z^2} \right)$$

In the case of steady flow, the above system of equations simplifies to;

$$0 = -\frac{1}{\rho} \frac{\partial p}{\partial x} \quad 4.1.8$$

$$u \frac{\partial w}{\partial x} + w \frac{\partial w}{\partial z} = g - \frac{1}{\rho} \frac{\partial p}{\partial z} + \nu \frac{\partial^2 w}{\partial x^2} \quad 4.1.9$$

Equation 4.1.8 indicates that the pressure, p , is constant throughout the boundary layer and so takes the value in the outer flow where $U = 0$ and $w = W(z)$. Substituting these into 4.1.9 gives

$$W \frac{\partial W}{\partial z} = g - \frac{1}{\rho} \cdot \frac{\partial p}{\partial z}$$

Hence

$$\frac{u \partial w}{\partial x} + w \frac{\partial w}{\partial z} = W \frac{\partial W}{\partial z} + \nu \frac{\partial^2 w}{\partial x^2} \quad 4.1.10$$

This equation is of the same form as that for a horizontal plate but the gravity term 'g' is included.

Integrating 4.1.10 with respect to x and using the continuity equation $\frac{\partial u}{\partial x} + \frac{\partial w}{\partial z} = 0$ leads to the Momentum-Integral equation; (cf. Schlichting 1968).

$$\tau_0 = \rho \frac{\partial}{\partial z} \int_0^{\delta(z)} w (W - w) \delta x + \rho \frac{\partial W}{\partial z} \int_0^{\delta(z)} (W - w) \delta x$$

4.1.11

where τ_0 is the shear stress at $x = 0$. This equation is valid for laminar and turbulent boundary layers.

Bland⁽¹⁸⁾ derives an expression for the thickness of a laminar boundary layer growing on a vertical surface. If δ is the thickness of the boundary layer, W_0 is the initial velocity of fluid at the leading edge and W is the fluid velocity at a distance, z , down the vertical plate measured from the leading edge, then

$$\delta = \left[\frac{168}{29} \frac{\nu}{g} (W - W_0)^{\frac{29}{3}} \cdot W^{-\frac{26}{3}} \right]^{\frac{1}{2}} \quad 4.1.12$$

$$\text{and } W = (W_0^2 + 2gz)^{\frac{1}{2}} \quad 4.1.13$$

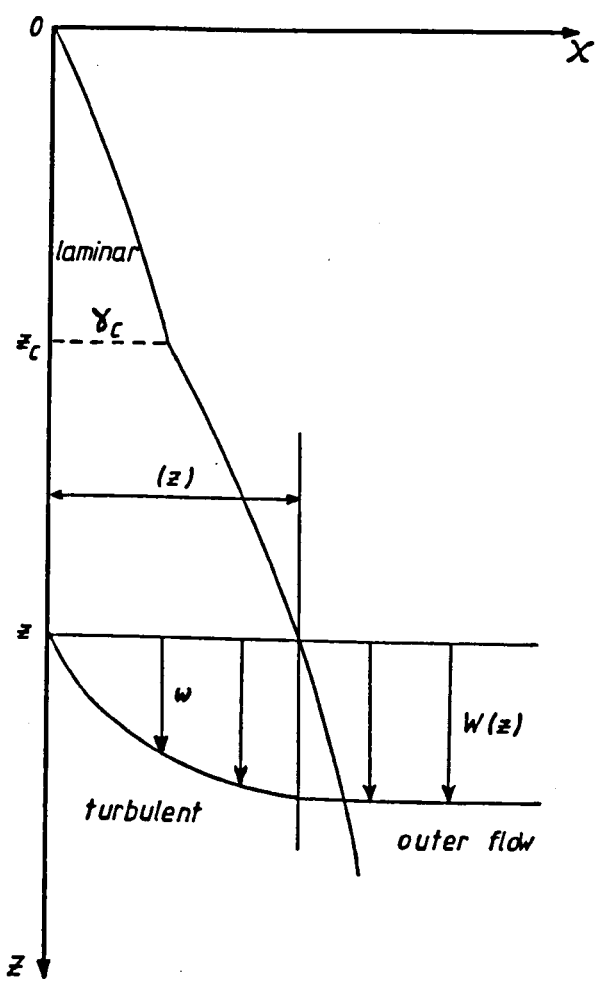


Fig. 4.1.1 (a)

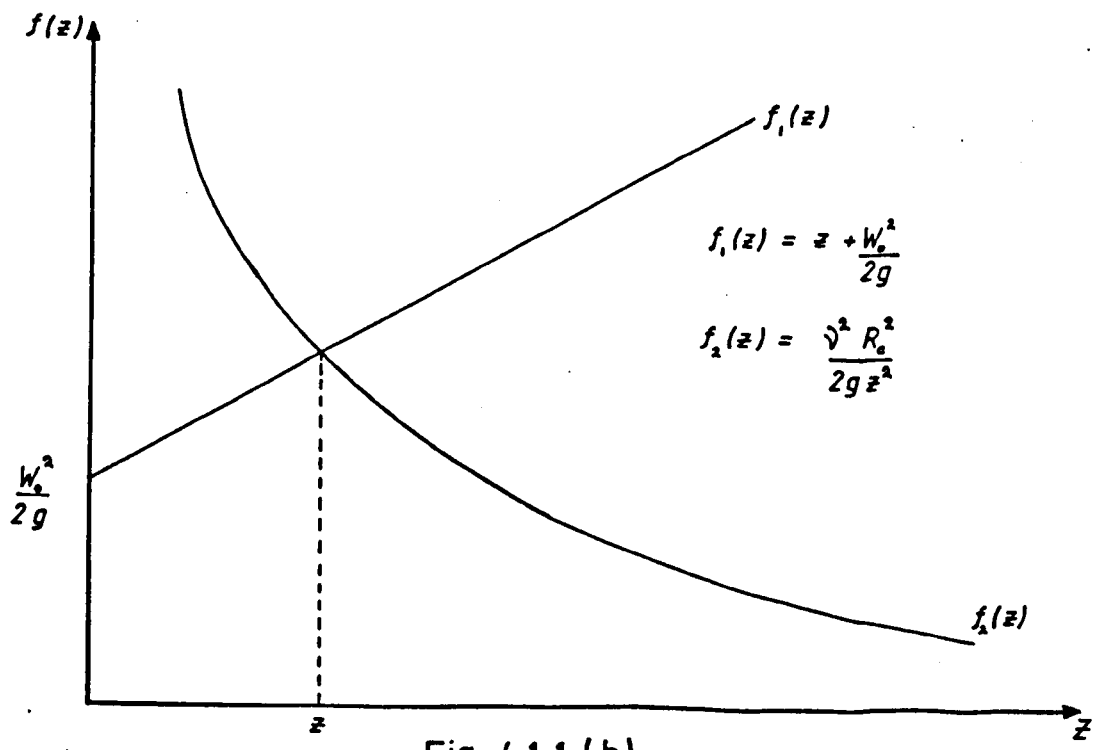


Fig. 4.1.1 (b)

The length of the laminar boundary layer may be calculated by assuming that the transition occurs at a critical value of Reynolds number. Francis⁽²⁶⁾ suggests this transition at $R_c = 5 \times 10^5$ where $R_c = \frac{W_0 z_c}{\nu}$, z_c , being the length of laminary boundary layer.

Using equation 4.1.13 this becomes

$$2g z_c^3 + W_0^2 z_c^2 - \nu^2 R_c^2 = 0$$

Re-writing as

$$\frac{\nu^2 R_c^2}{2g z_c^2} = z_c + \frac{W_0^2}{2g} \quad 4.1.14$$

reveals as shown in Fig 4.1.1(b) that there is only one positive root and hence can be solved for z_c if W_0 is known.

In order to evaluate the thickness of the turbulent boundary layer, a relationship for the shear stress (τ_0) is required. The expression proposed by Blasius for flow over a smooth plate is once again utilised;

$$\tau_0 = 0.023 \rho W^2 \left(\frac{\nu}{W \delta} \right)^{1/4} \quad 4.1.15$$

and the velocity profile is taken to be that due to Prandtl;

$$w = \left(\frac{x}{\delta} \right)^{1/4} W \quad 4.1.16$$

Thus using equations (4.1.15) and (4.1.16), equation (4.1.11) becomes

$$0.023 \rho W^2 \left(\frac{\nu}{W \delta} \right)^{1/4} = \frac{23}{72} \rho W \frac{\partial W \delta}{\partial z} + \frac{7}{72} \rho W^2 \frac{\partial \delta}{\partial z} \quad 4.1.17$$

which using (4.1.13) leads to

$$\frac{\partial (\delta^{5/4})}{\partial z} + \frac{4.107g}{W^2} \delta^{5/4} = 0.296 \delta^{1/4} W^{-1/4}$$

4.1.18

This can be solved by Integrating Factor method (see appendix C) to yield;

$$\delta^{1.25} = \frac{0.0016727}{g} (W^{5.857} - W_0^{5.857}) W^{-4.107}$$

Including the laminar boundary layer thickness, i.e. δ_c when $z = z_c$

$$\delta = \left[\delta_c^{1.25} + \frac{0.0016727}{g} (W^{5.857} - W_c^{5.857}) W^{-4.107} \right]^{0.8}$$

4.1.19

where

$$W_c = (W_0^2 + 2gz_c)^{0.5}$$

It is necessary to calculate the velocity and hence the distance along the plate at which this occurs. Rearranging (4.1.19).

$$0 = W^{1.75} - (W_c^{5.857} W^{-4.107}) - \left[\frac{(\delta^{1.25} - \delta_c^{1.25}) g}{0.0016727} \right]$$

4.1.20

By Newton-Raphson's method a solution for W can be found and the distance z , at which a given thickness of boundary layer is known can be evaluated thus;

$$z = \frac{W^2 - W_0^2}{2g}$$

Hence, the distance down the vertical surface at which the boundary layer thickness projects to the free surface

can be calculated from the boundary layer analysis and equation 4.1.7

The analyses have been simplified by considering the flow conditions at entry to be radial and hence the swirl components of the velocity are not included. The transition zone which occurs between the laminar and wholly turbulent regions of boundary layer growth is also omitted in the above analysis.

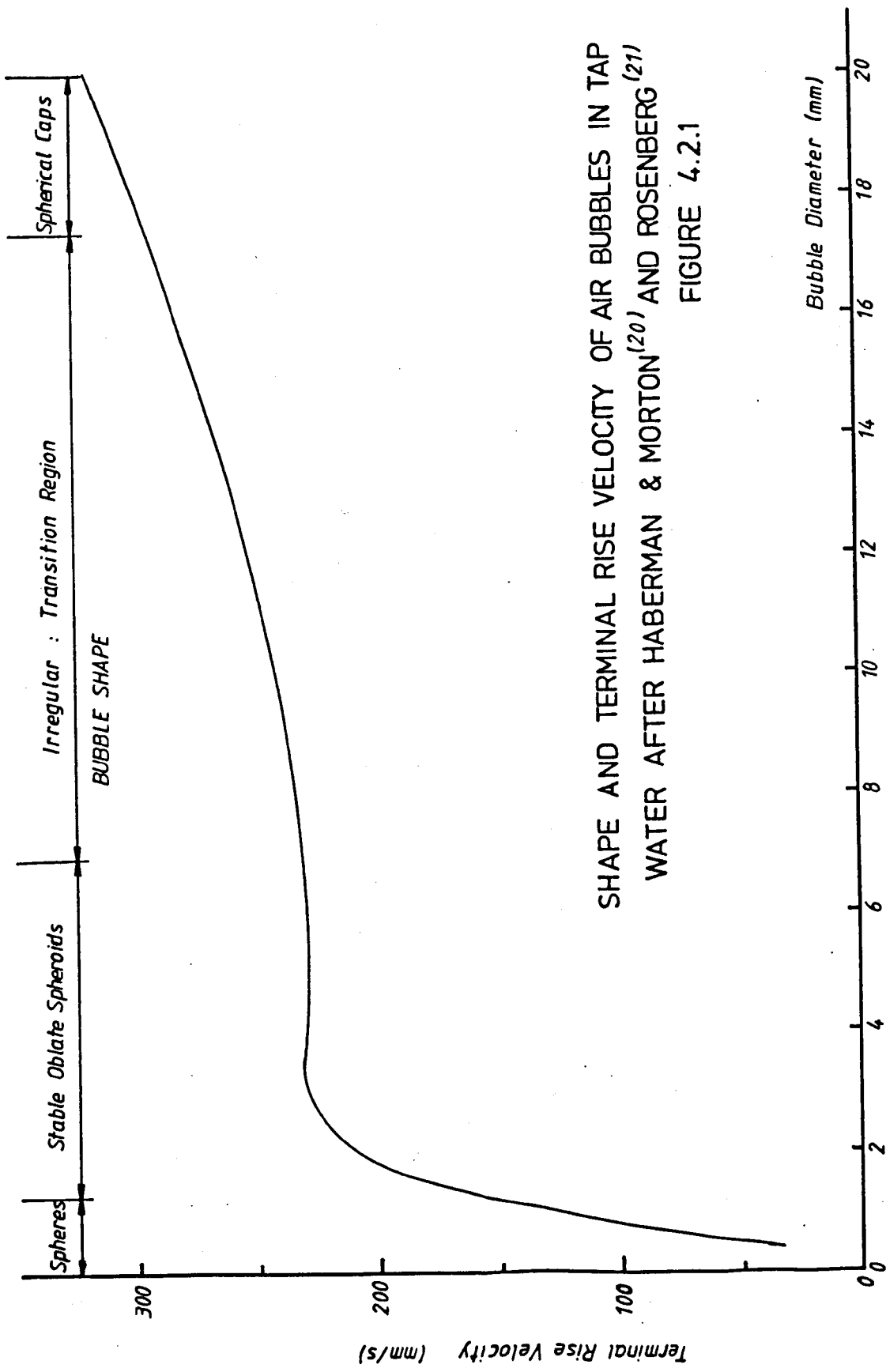
The initial entry velocity, required in the solution of the boundary layer growth problem, is obtained by reference to the work of Ackers and Crump⁽¹⁹⁾ on the vortex-entry dropshaft. The method utilised by Ackers and Crump requires that the discharge and velocity for a particular geometry of vortex-entry dropshaft are calculated at various assumed values of air-core ratio. Hence a programme was formulated and the derived results for each geometric arrangement of the dropshafts are presented in Appendix B.

4.2 Air Transport

In order to assess the behaviour of air/water mixtures, it is necessary to study the action of air bubbles in water under different circumstances. The factors influencing the local conditions of flow in which the bubble characteristics are to be assessed include still water or turbulent flow, single bubbles, bubble swarms continuous emulsion, and confined or unconfined media.

Several investigators have examined the rise velocities of air bubbles in water. Fig 4.2.1 is reproduced from the work of Haberman and Morton⁽²⁰⁾ and Rosenberg⁽²¹⁾ who relate terminal rise velocity of single bubbles in still untreated tap water and in an unconfined medium to size and shape of bubble. The chief feature of the terminal rise velocity curve is the plateau between bubbles of diameter 3.0 to 7.0mm. This indicates an approximately constant terminal rise velocity of about 0.23m/s for the range of the stable oblately spheroidal bubbles which exist in the air entrainment system under investigation. This range of bubble size and shape is confirmed by Wisner,⁽¹⁴⁾ Chanishvili⁽²²⁾ and Cotillon⁽⁴⁾ in model and prototype air entraining structures.

When clouds of bubbles exist instead of single bubbles, it is to be expected that the terminal rise velocity might be modified. This is due to the changes in flow pattern around the bubbles created by the bubble cloud which will affect the drag forces on the following air bubbles and hence the terminal rise velocity, which is a function of drag force. Garner and Hammerton⁽²³⁾ concluded that the terminal rise velocities in still water for streams of bubbles are greater than for a single bubble. Holroyd and Parker⁽²⁴⁾ show that for a continuous cloud of bubbles, in the size range 1 to 5mm diameter, in a nominally unconfined medium (the proportion of the cross-section occupied by the bubbles is considered to be negligible), the terminal rise velocity was



SHAPE AND TERMINAL RISE VELOCITY OF AIR BUBBLES IN TAP WATER AFTER HABERMAN & MORTON⁽²⁰⁾ AND ROSENBERG⁽²¹⁾

FIGURE 4.2.1

0.36 m/s, as compared to 0.23 m/s for single bubbles of similar size.

If the water were flowing, then it would be expected that the relative rise velocity of a bubble would differ from that in still water. Baker and Chao⁽²⁵⁾ and H.R.S.⁽²⁾ have both measured the relative velocity of single bubbles under turbulent flow conditions. Baker and Chao, using de-mineralised water, found that for bubbles of diameter less than 3mm the relative velocity varied non-systematically with various flow rates. For bubbles of diameter 3-4.5mm, the relative velocity increased slightly from 0.23 m/s in still water to 0.26 m/s in turbulent flow. H.R.S., using untreated tap water, observed a relative velocity of 0.30 m/s (as compared to 0.23 m/s) for single bubbles of 3.5mm diameter in smooth turbulent flow. The reason for the difference between Baker and Chao's results and H.R.S.'s results is not obvious, but can perhaps be attributed to the fact that the former used de-mineralised water and the latter used untreated water. Garner and Hammerton⁽²³⁾ have noted that surface films can be formed around the air bubbles by additives in the water.

If the medium is confined, previously the velocities have been discussed for an unconfined medium, then rising bubbles in still water can be expected to induce a downward flow of water between themselves and the walls of the container. The observed rise velocity will be accordingly reduced although the bubble rise velocity

relative to the locally flowing water will be unchanged. Similarly in the case of downward flowing water, the flow velocity is locally increased at the diminished water section around the bubble, and the observed rise velocity is reduced.

The various bubble behaviour patterns in confined flow are discussed by Nicklin⁽¹⁷⁾. The following theories have been evolved to extend Nicklin's arguments for rising bubbles in upward water flow to provide a solution for falling water pulling down air bubbles in the flow.

4.2.1 Velocity of air bubbles in two-phase flow

4.2.1.1 Zero liquid flow

Consider initially the case of stagnant water with air steadily bubbling through it.

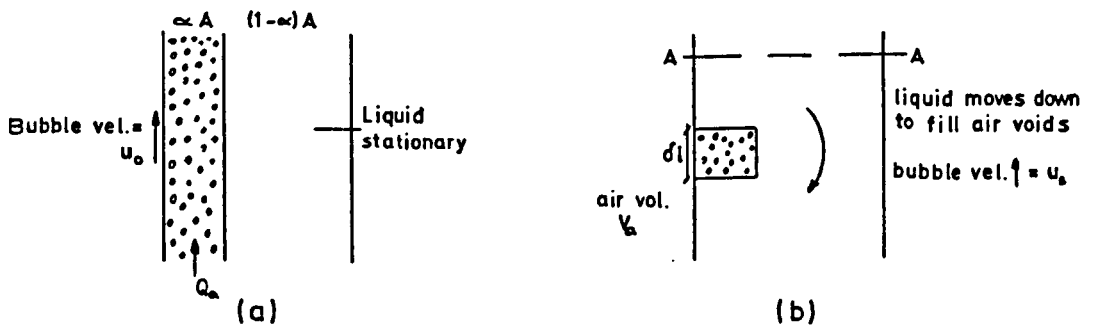


Fig. 4.2.2

let α = air void ratio (air content)

A = cross-sectional area of shaft

From Fig 4.2.2 (a)

$$\text{Absolute velocity of air} = u_0 = \frac{Q_a}{\text{area}} = \frac{Q_a}{\alpha A} = v_a$$

4.2.1

Fig 4.2.2 (b) shows bubbles in the same configuration, but rising in a swarm of finite size (volume, V_a) relative to the stagnant water above.

At section A-A, the fraction of the cross-sectional area occupied by air will be α , and in this case the bubbles rise at a velocity u_B . It is apparent that the two cases are different by considering the flow of water across the section A-A. In Fig 4.2.2 (a) there is no net flow of water, in Fig 4.2.2 (b) there must be a net downward flow of water to cancel the upward flow of gas.

Consider Fig 4.2.2 (b)

For the volume of air, V_a , to pass through the stagnant water, as the cloud passes A-A, the volume of water below A-A must increase by V_a , so there is a downward flow of water past A-A.

$$\text{Downward velocity} = \frac{V_a}{(1-\alpha)A} \cdot \frac{1}{\delta t} \quad 4.2.2$$

assuming δt = time for Volume, V_a , to cross A-A.

Hence absolute water velocity

$$v_w = \frac{Q_w}{(1-\alpha)A} \quad 4.2.2.a$$

$$\text{and } u_B = \frac{V_a}{\alpha A} \cdot \frac{1}{\delta t} \quad 4.2.3$$

If downward velocities u_o and u_B are superimposed on the systems (a) and (b) respectively, the bubbles in each case will be brought to rest. Thus, the two configurations are identical and both sets of bubbles are now stationary. It is apparent that the downward flow of water must be the same in each case, thereby providing a convenient basis for comparison.

From (4.2.2) and (4.2.3)

Downward flow rate of liquid in (a) is $Q_w = (1 - \alpha) A u_0$

Downward flow rate of liquid in (b) is $Q_w = A u_B$

Equating flow rates

$$(1 - \alpha) A u_0 = A u_B$$

$$u_0 = \frac{u_B}{1 - \alpha} \quad 4.2.4$$

Substituting from Equation 4.2.1

$$\frac{Q_a}{\alpha A} = \frac{u_B}{1 - \alpha}$$

gives $\frac{Q_a(1 - \alpha)}{\alpha A} = u_B$

which may be re-written as;

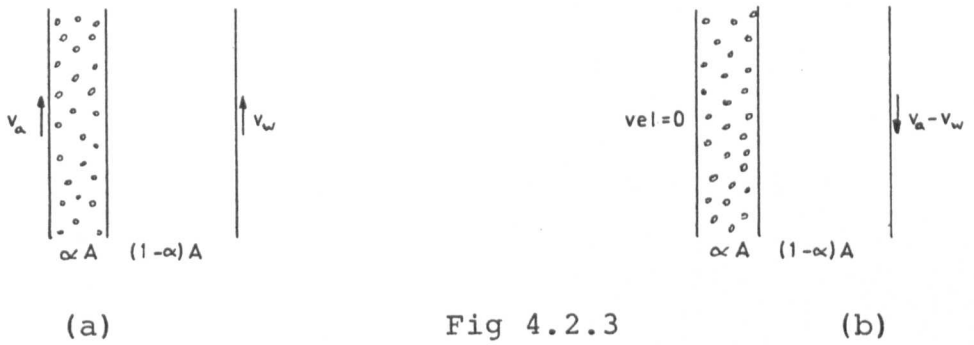
$$\frac{Q_a}{\alpha A} = u_B + \frac{Q_a}{A} \quad 4.2.5$$

This expresses the result that although there is no average flow of liquid in Fig 4.2.2, a factor other than buoyancy contributes to the motion of the bubbles. The buoyancy velocity, u_B , will depend on the properties of the system and the bubble characteristics.

4.2.1.2 Finite liquid upward flow

If there is an upward flow of liquid, the above arguments can be extended.

For a continuous flow of bubbles, see Fig 4.2.3 (a)



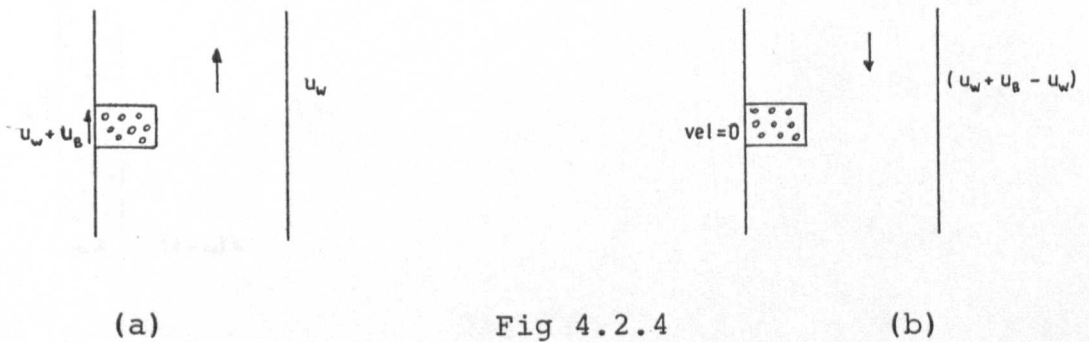
Applying v_a downward to the system to bring the bubbles to rest,

Fig 4.2.3 (b)

$$\text{Downward water velocity} = v_a - v_w$$

$$\text{Downward flow of water } Q_w = (v_a - v_w) A (1 - \alpha)$$

For a bubble swarm rising in rising fluid with velocity u_w , then absolute rise velocity of bubbles = $(u_B + u_w)$ see Fig 4.2.4 (a)



Consider Fig 4.2.4 (b)

Apply $(u_B + u_w)$ downwards to (b) to bring bubbles to rest. \therefore downward flow of water $Q_w = u_B \cdot A$.

Equating flow rates

$$(v_a - v_w)(1 - \alpha)A = u_B \cdot A$$

$$v_a - v_w = \frac{u_B}{1 - \alpha}$$

Substitute for v_a & v_w

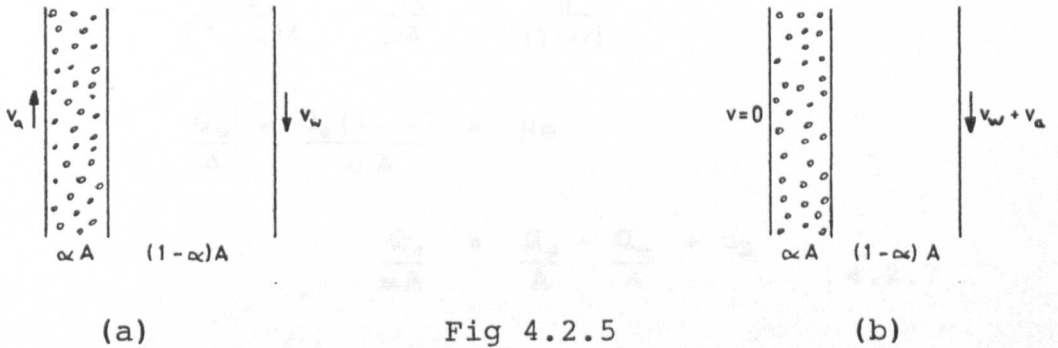
$$\frac{Q_a}{\alpha A} - \frac{Q_w}{(1-\alpha)A} = \frac{u_B}{1 - \alpha}$$

$$(1 - \alpha) \frac{Q_a}{\alpha A} - \frac{Q_w}{A} = u_B$$

$$\frac{Q_a}{\alpha A} = \frac{Q_a}{A} + \frac{Q_w}{A} + u_B \quad 4.2.6$$

4.2.1.3 Downward liquid flow with rising bubbles

Consider now the case of downward liquid flow with rising air bubbles, see Fig 4.2.5 (a)



Applying v_a downwards to system to bring bubbles to rest (Fig 4.2.5 (b))

$$\text{Downward water velocity} = (v_w + v_a)$$

$$Q_w = (v_w + v_a) A (1 - \alpha)$$

For a rising bubble swarm in falling liquid with velocity then absolute rise velocity of bubbles = $(u_B - u_w)$



(a)

Fig 4.2.6

(b)

Applying $(u_B - u_w)$ to system gives

$$Q_w = u_B \cdot A$$

Equating flow rates

$$(v_w + v_a)(1 - \alpha) \cdot A = u_B A$$

$$v_w + v_a = \frac{u_B}{1 - \alpha}$$

Substitute for v_w & v_a

$$\frac{Q_w}{(1 - \alpha)A} + \frac{Q_a}{\alpha A} = \frac{u_B}{(1 - \alpha)}$$

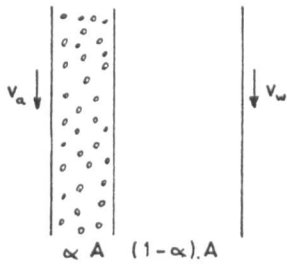
$$\frac{Q_w}{A} + \frac{Q_a(1 - \alpha)}{\alpha A} = u_B$$

$$\frac{Q_a}{\alpha A} = \frac{Q_a}{A} - \frac{Q_w}{A} + u_B \quad 4.2.7$$

4.2.1.4 Downward liquid flow and downward bubble motion

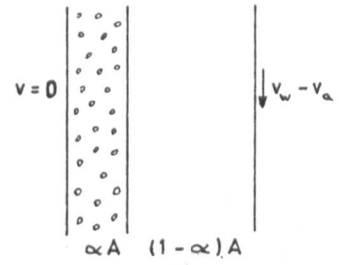
Finally, the case relevant to the investigation under consideration is presented, i.e. falling water flow causing downward air bubble motion, see Fig 4.2.7 (a)

Substituting for



(a)

Fig 4.2.7



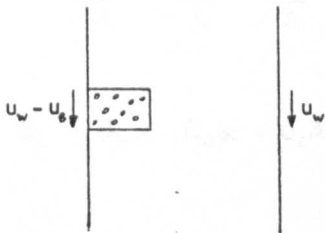
(b)

Applying v_a upwards to bring continuous bubble stream to rest (Fig 4.2.7 (b))

$$\text{Downward water velocity} = v_w - v_a$$

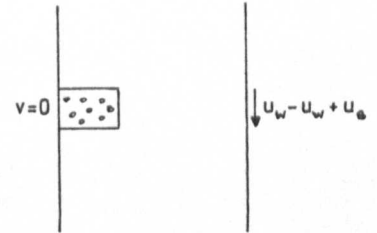
$$Q_w = (v_w - v_a) A (1 - \alpha)$$

For a bubble swarm moving downwards in falling water see Fig 4.2.8 (a)



(a)

Fig 4.2.8



(b)

Applying $(u_w - u_b)$ upwards to system to bring swarm to rest downward water flow $Q_w = u_b \cdot A$

Equating flow rates

$$(v_w - v_a) A (1 - \alpha) = u_b A$$

$$v_w - v_a = \frac{u_b}{1 - \alpha}$$

Substituting for v_a & v_w

$$\frac{Q_w}{A(1-\alpha)} - \frac{Q_a}{\alpha A} = \frac{u_B}{1-\alpha}$$

$$\frac{Q_w}{A} - \frac{Q_a(1-\alpha)}{\alpha A} = u_B$$

$$\frac{Q_a}{\alpha A} = \frac{Q_w}{A} + \frac{Q_a}{A} - u_B$$

4.2.8

This result is similar to one presented by Whillock and Thorn⁽³⁾.

Now $u_B = u_c(1-\alpha)$ where $u_c =$ relative velocity.

hence Equation 4.2.8 becomes

$$\frac{Q_a}{\alpha A} = \frac{Q_w}{A} + \frac{Q_a}{A} - u_c(1-\alpha)$$

$$\frac{Q_a}{\alpha A} - \frac{Q_w}{A} - \frac{Q_a}{A} + u_c(1-\alpha) = 0$$

$$Q_a - Q_w\alpha - Q_a\alpha + u_cA\alpha - u_cA\alpha^2 = 0$$

$$\alpha^2 + \alpha \left[\frac{Q_w}{u_cA} + \frac{Q_a}{u_cA} - 1 \right] - \frac{Q_a}{u_cA} = 0 \quad 4.2.9$$

This can be solved for α thus

$$2.\alpha = \left[1 - \frac{Q_a}{u_cA} - \frac{Q_w}{u_cA} \right] + \sqrt{\left[\frac{Q_w}{u_cA} + \frac{Q_a}{u_cA} - 1 \right]^2 + 4 \frac{Q_a}{u_cA}}$$

In order to evaluate the relationship between the

air content of a water column and the air flow through it given by equation 4.2.9, it is necessary to know the appropriate value of the relative rise velocity of the air bubbles. It was seen earlier in this section that although investigators have attempted to determine the relative rise velocities, the effects of bubble swarms in confined media have not been overcome. The transport of air through the dropshaft mainly involves the continuous flow of a bubble emulsion in a downward direction in turbulent downward water flow.

Equation 4.2.9 can be re-written as follows;

$$\alpha^2 + \alpha \left[\frac{Q_w}{u_c A} + \frac{Q_a}{u_c A} - 1 \right] - \frac{Q_a}{u_c A} = 0$$

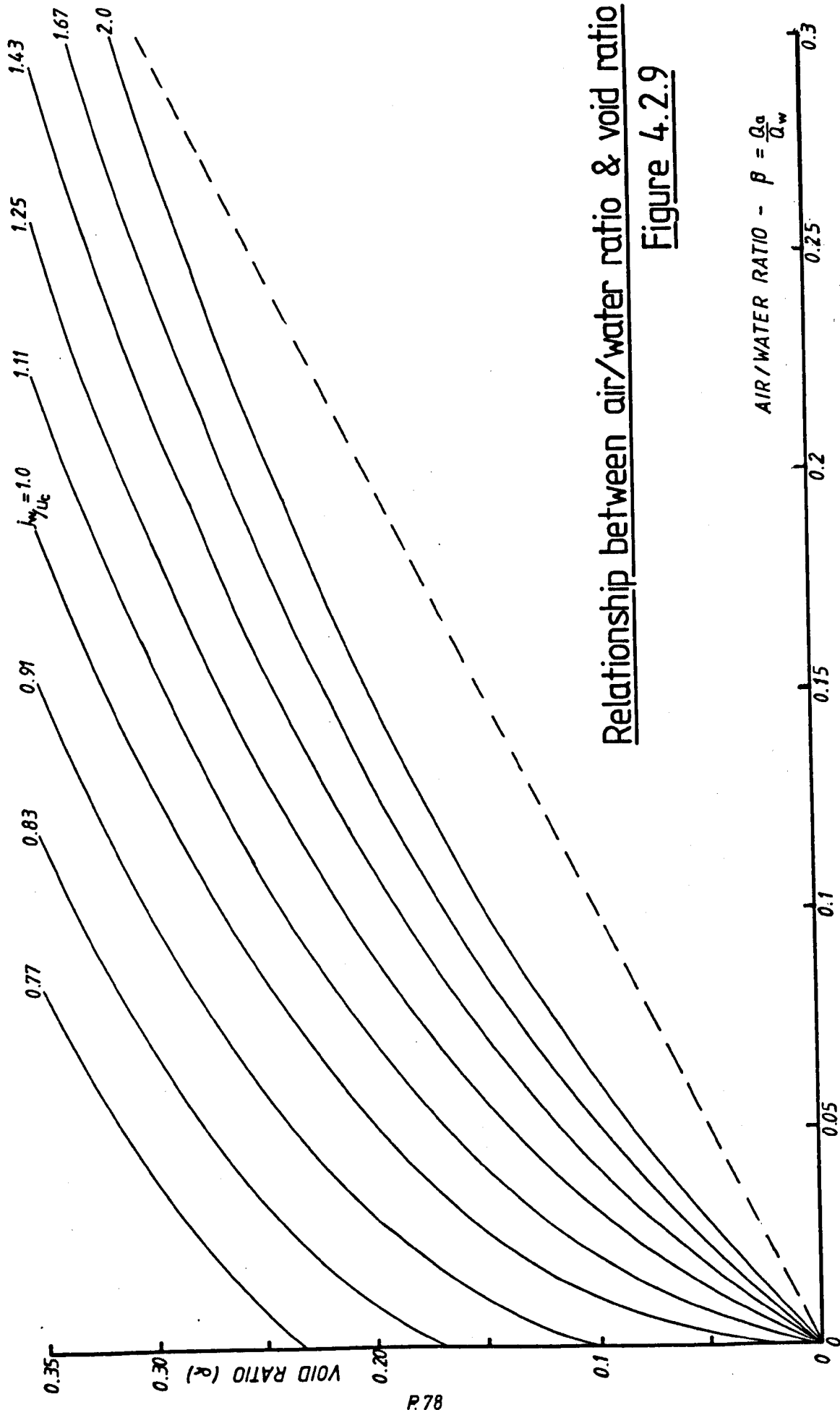
$$\frac{u_c A \alpha^2}{Q_w} + \alpha + \frac{Q_a \alpha}{Q_w} - \alpha \frac{u_c A}{Q_w} - \frac{Q_a}{Q_w} = 0$$

$$\alpha^2 \frac{u_c A}{Q_w} - \alpha \frac{u_c A}{Q_w} + \alpha = \frac{Q_a}{Q_w} - \frac{Q_a}{Q_w} \alpha$$

$$\alpha \frac{u_c A (\alpha - 1)}{Q_w} + \alpha = \frac{Q_a (1 - \alpha)}{Q_w}$$

$$\frac{Q_a}{Q_w} = \frac{\alpha}{1 - \alpha} - \alpha \frac{u_c A}{Q_w} \quad 4.2.10$$

The relationship between α and $\frac{Q_a}{Q_w}$ in Equation 4.2.10 is plotted in Fig 4.2.9 for different values of u_c and Q_w . From this plot it is possible to assess the importance of variations in the value of relative rise velocity, u_c .



Relationship between air/water ratio & void ratio
Figure 4.2.9

It proved impossible to develop a further theoretical analysis to yield a relationship to establish the absolute value of u_c . Consequently this is done utilising the results obtained by the radio-isotope investigation to determine the void fraction of an air/water mixture. An empirical relationship can be established to determine the values of the relative rise velocity.

4.2.2 Determination of void fraction by gamma-ray absorption

Absorption of gamma-rays by matter is dependent on the energy of the impinging radiation and the electron density of the material. The intensity of a narrow beam of gamma-rays passing through an absorber is given by;

$$I = I_0 \cdot e^{-k\rho_m} \quad 4.2.11$$

where I = intensity of radiation at counter
 I_0 = incident intensity of radiation beam
 ρ_m = mean density of the air/water mixture
 (neglecting shaft walls)
 k = constant

When the shaft contains 100% water, density ρ_w

$$I_w = I_0 \cdot e^{-k\rho_w} \quad 4.2.12$$

Divide (4.2.11) by (4.2.12) to give

$$\frac{I}{I_w} = e^{k(\rho_m - \rho_w)}$$

or

$$\log_e \frac{I}{I_w} = K (\rho_w - \rho_m)$$

4.2.13

Where $K = \text{constant}$

If $\alpha = \text{void ratio}$ and $\rho_a = \text{density of air}$

$$\begin{aligned} \rho_w - \rho_m &= \rho_w - [\alpha \rho_a + (1 - \alpha) \rho_w] \\ &= \alpha (\rho_w - \rho_a) \end{aligned}$$

from (4.2.13)

$$\log_e \frac{I}{I_w} = K \cdot \alpha (\rho_w - \rho_a)$$

$$\text{or } \alpha = \frac{1}{K(\rho_w - \rho_a)} \cdot \log_e \frac{I}{I_w}$$

Thus, since $K(\rho_w - \rho_a)$ is a constant, the increase in logarithmic radiation intensity is a linear function of the void ratio of the mixture in the shaft.

CHAPTER FIVE
ANALYSIS OF EXPERIMENTAL RESULTS

The results obtained from the model tests are analysed in a progressive sequence commencing with the preliminary short dropshaft tests carried out in the laboratory.

5.1 Classification of Flow Regimes

The flow regimes are classified by observations made during the operation of the model tests.

- a) Zero airflow - at high to intermediate shaft water levels and low discharges, the re-circulation zone was contained wholly within the shaft. There is no net air demand in the system since the downward water velocity was insufficient to overcome the buoyancy forces of the air bubbles.
- b) Positive airflow - at higher discharges and water levels in the shaft higher than the length of the re-circulation zone. The net air demand of the system was due to the passage of air bubbles of diameters in the 3-5mm range being carried down uniformly within the shaft. There occurs some mixing within the air/water section of the shaft, but over a period of time this can be assumed uniform.
- c) Slug flow - at very high discharges, random air

pockets of varying sizes formed due to coalescence of the air bubbles. The diameter of the pockets were almost up to the full diameter of the shaft but their lengths were estimated to vary from 50mm up to about 0.7m. The buoyancy force of a large air pocket was, at times, greater than the drag force exerted by the increased water velocity hence the rise of the entrained air pockets. However, on other occasions, these air pockets were passed through the shaft to the outlet. During this regime of flow, wide pressure fluctuations were imposed at the shaft exit resulting in gushes of water and air being emitted.

This random occurrence was more prominent in the smaller scale model and was considered to be a 'scale effect'.

d) Free outlet - if the shafts are operated with a free outlet, then the water film extends the full shaft length with the air core present throughout. The air demand was due to the drag of the water film on the air and results in very high airflows. However, this aspect of operation was not considered in this investigation.

The zero airflow and positive airflow regimes are schematised in fig 5.1

The adoption of a particular regime cannot be attributed to one single factor but is a combination of all the parameters existing within the system.

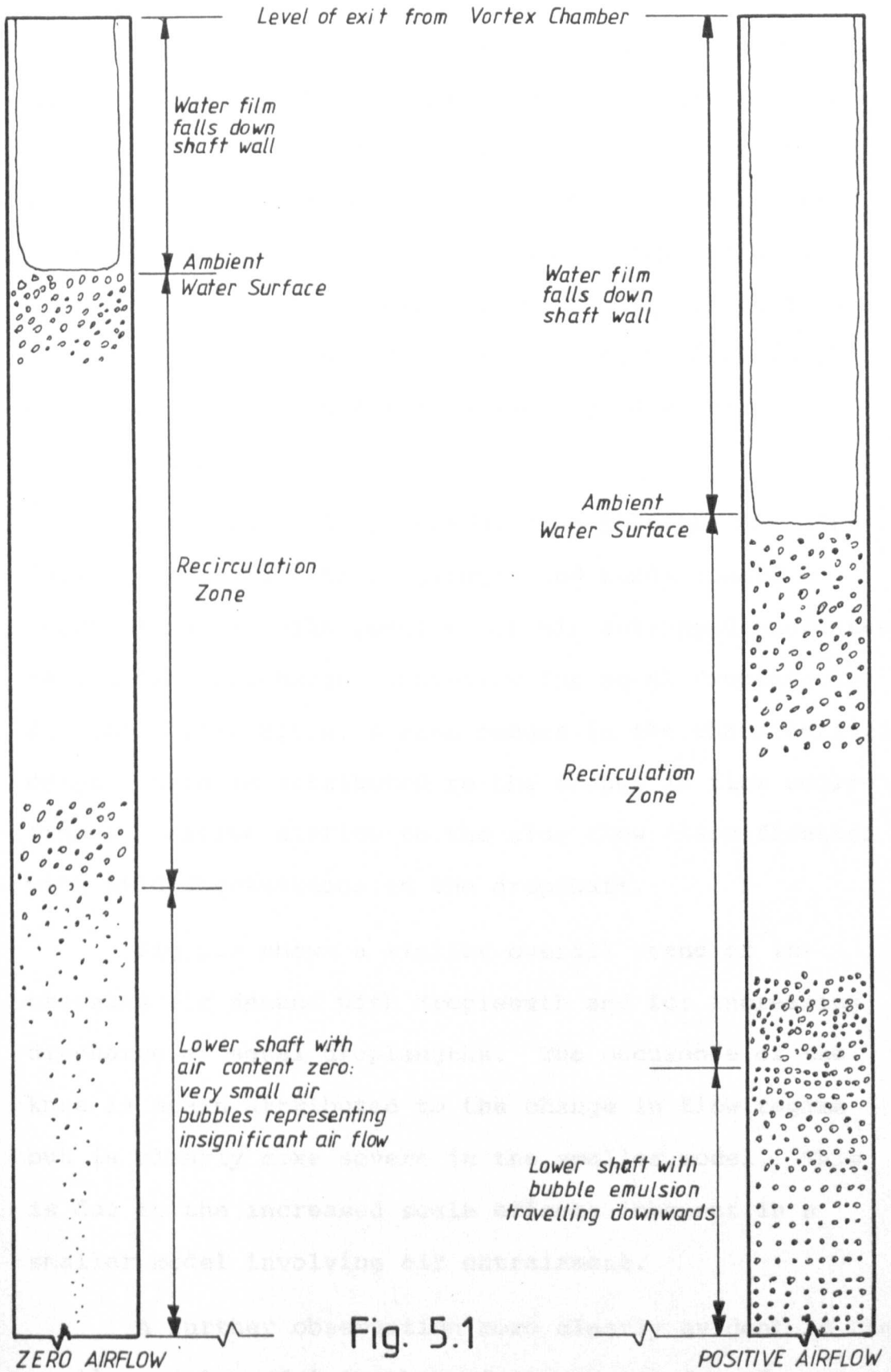


Fig. 5.1

Typical Flow Patterns in Dropshaft

5.2 Vortex-entry dropshafts - Model Results

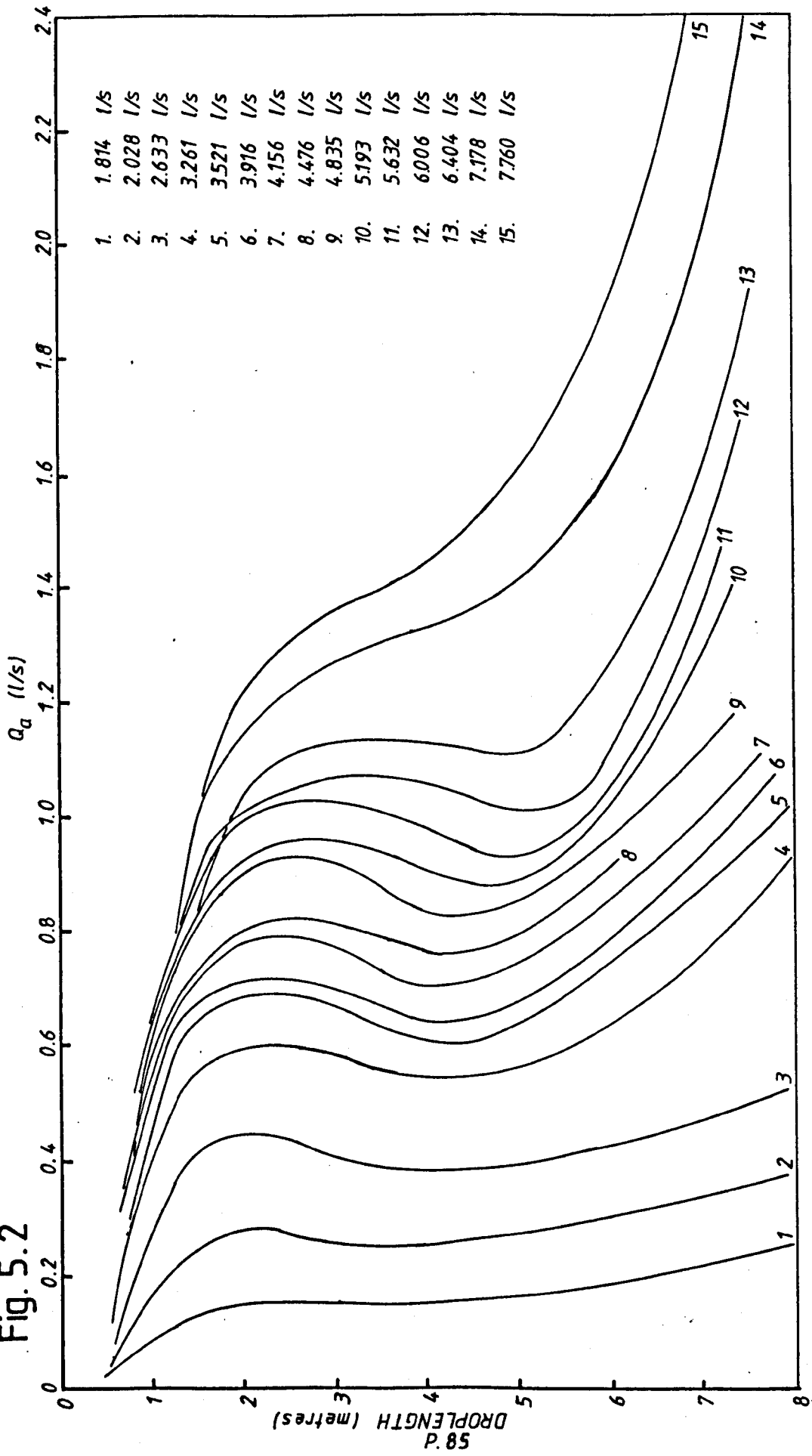
The results of the model tests on the vortex-entry dropshafts of 8.8m shaft length are presented in Figs 5.2 to 5.5. Figs 5.2 and 5.3 show the results for the 1:10.9 and 1:21.6 scale models and are plotted in the form of net air demand against droplength for each flow discharge. Figs 5.4 and 5.5 are plotted on the basis of air/water ratio against droplength for each discharge for the 1:10.9 and 1:21.6 models respectively.

From Fig 5.2, it can be seen that the net air demand increases with droplength and tends toward a terminal value. The quantity of air entrapped increases as the flow discharge increases for equal droplengths. At higher flow rates, a knee occurs in the characteristic demand, this is attributed to the change in flow regime from a positive airflow to the slug flow classification with wild fluctuations in the dropshaft.

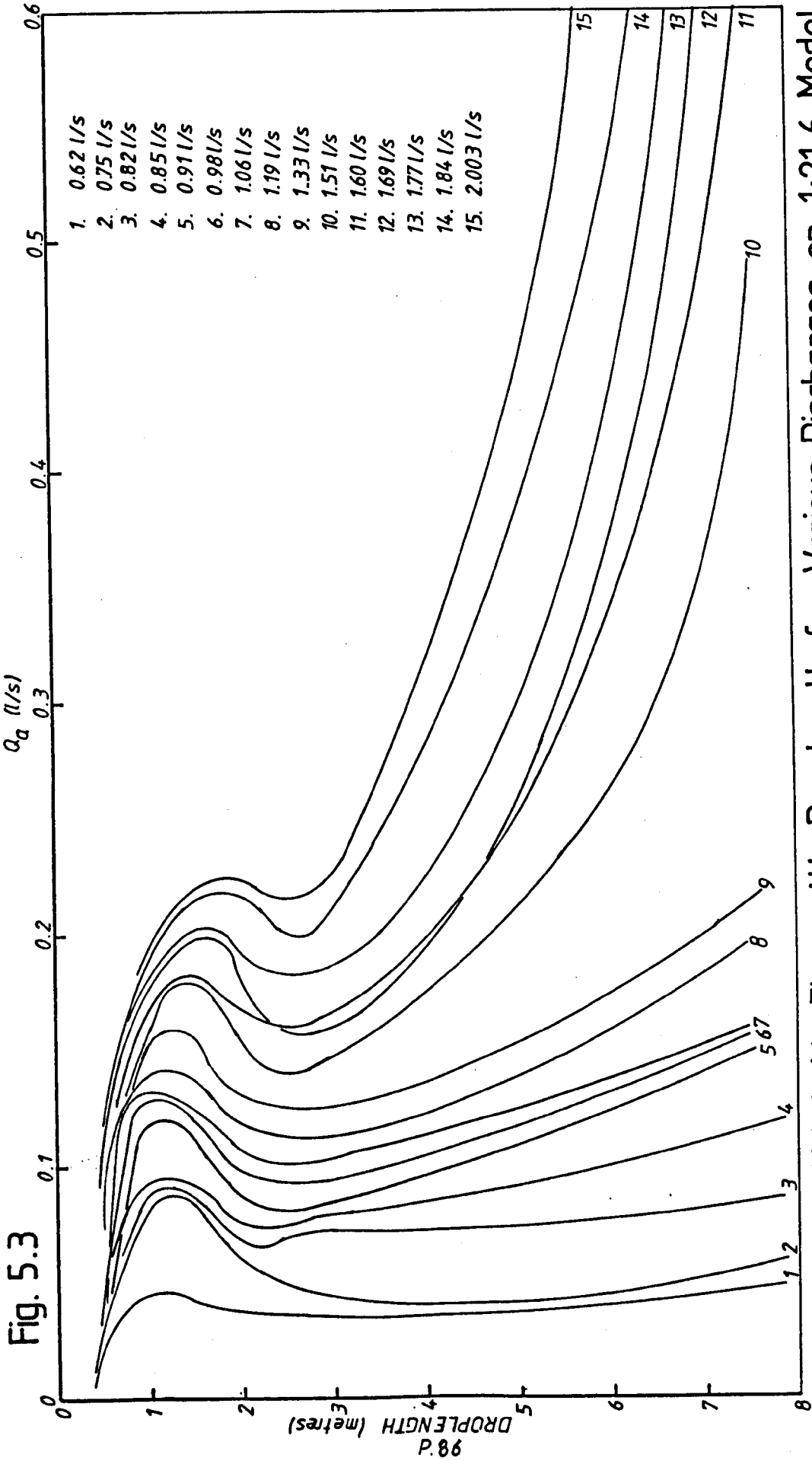
Fig 5.3 shows a similar overall trend of increasing air demand with droplength and for increasing discharge at equal droplengths. The occurrence of the knee is again attributed to the change in flow regime but is clearly more severe in the smaller model. This is due to the increased scale effects inherent in a smaller model involving air entrainment.

A further observation more clearly evident in the smaller scale model is that of a peak air demand occurring at a specific droplength, after which demand

Fig. 5.2



Variation of Total Air Flow with Droplength for Various Discharges on 1:10.9 Model



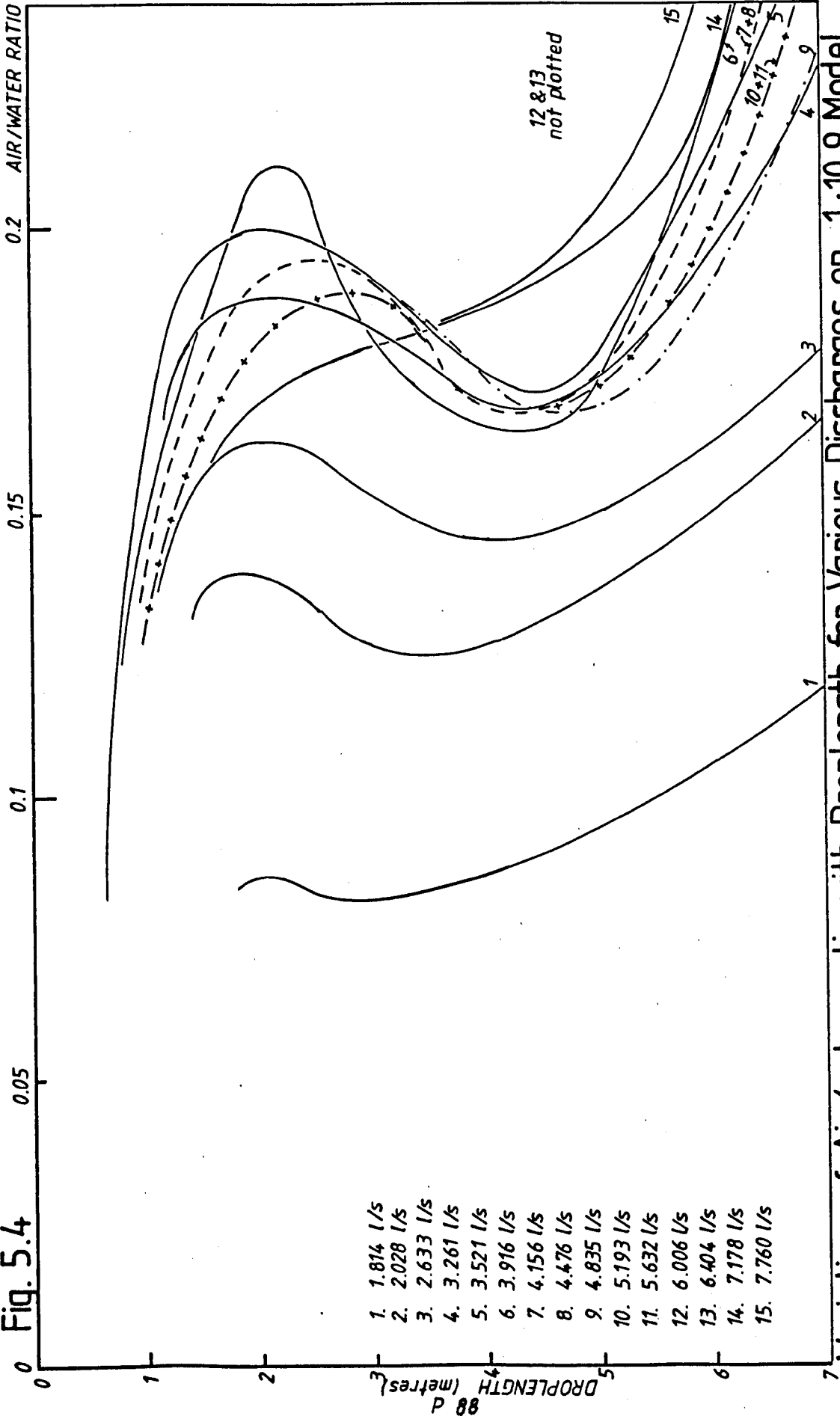
Variation of Total Air Flow with Droplength for Various Discharges on 1:21.6 Model

decreases to terminal conditions at lower flow rates. This peak, however, is defined even at maximum discharges, although the subsequent terminal conditions are not attained.

One explanation for this characteristic is that it is due to the helical motion of the falling water induced by the vortex-entry arrangement to the shaft. At short droplengths, the tangential component of velocity of the water film is still active and hence the jet strikes the ambient water surface with a higher absolute velocity than would be due to gravity alone, and the volume of air entrained is higher. As the droplength increases, the tangential component diminishes until the velocity is due to gravity alone, this velocity possibly being less than the absolute velocity at short droplengths, resulting in a lesser volume of entrained air. This explains the peak and subsequent depression in the general air demand curve until terminal conditions are attained.

In Figs 5.4 and 5.5, it can be seen that the general trend of increasing air demand with droplength and discharge is again evident. In fig 5.4 the curves are distinct for the lowest flow rates. However, as discharge increases, although air demand increases, the ratio of air/water flow rates is banded in a close zone. This is indicative of a maximum value of air/water ratio attainable in any particular model. For the 1:10.9 model, the limiting ratio is approximately 0.19, and beyond this value the regime of flow will change, i.e. the bubbles tend towards coalescence resulting in unsteady surges.

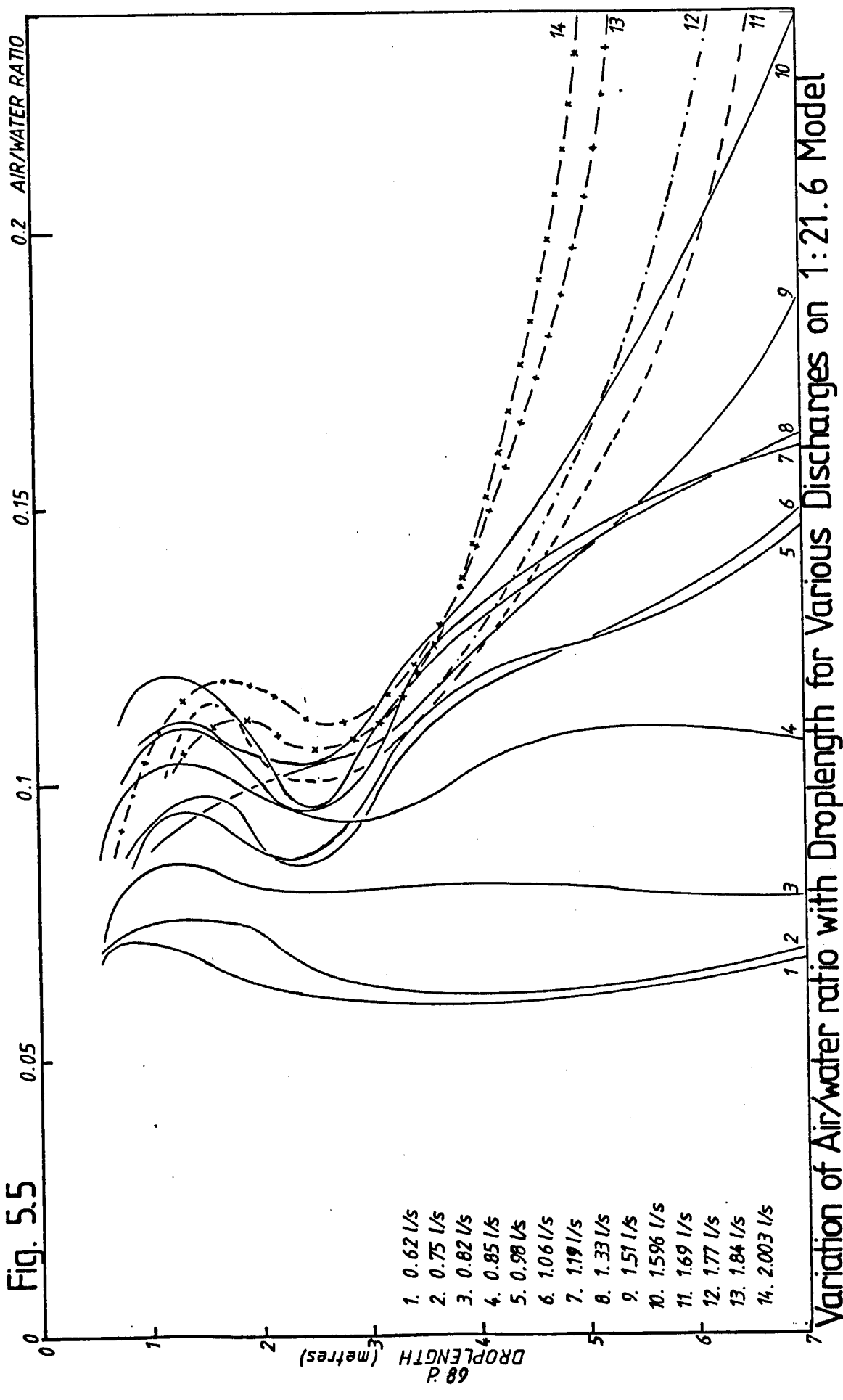
Fig. 5.4



1. 1.814 l/s
2. 2.028 l/s
3. 2.633 l/s
4. 3.261 l/s
5. 3.521 l/s
6. 3.916 l/s
7. 4.156 l/s
8. 4.476 l/s
9. 4.835 l/s
10. 5.193 l/s
11. 5.632 l/s
12. 6.006 l/s
13. 6.404 l/s
14. 7.178 l/s
15. 7.760 l/s

Variation of Air/water ratio with Droplength for Various Discharges on 1:10.9 Model

Fig. 5.5



Variation of Air/water ratio with Droplength for Various Discharges on 1:21.6 Model

Fig. 5.5 again exhibits a similar pattern but the limiting air/water ratio occurs at approximately 0.12. The change in flow regime occurs not only at a lesser ratio but also at a shorter droplength. This occurrence is again a result of the smaller model scale, and clearly displays the problems associated with previous methods of analysing air entraining model data.

In keeping with the results of previous investigators ⁽²⁾⁽¹⁰⁾, the experimental results showed the effects of the droplength approaching the total length of the shaft. The air demand rapidly increased as the shaft outlet began to affect the system by intercepting the lower end of the recirculation zone. However, the results are presented for only 7.0m. of the dropshaft as it was considered to be of little practical value to plot the upturn in demand due to 'end effects'.

In both models, the limiting air/water ratio occurs when the nominal water velocity in the shaft $\left(\frac{Q_w}{A}\right)$ is greater than 0.6m/s. The relation $\frac{Q_a}{Q_w}$, versus droplength is thus independent of discharge beyond this point and forms an envelope to all further curves.

It is difficult to interpret the results further to give a clearer understanding of the mechanisms involved from the dropshaft studies. This is because only the net air demand is measured, which is the difference between the air entrained at the ambient water surface, and the air released by recirculation. Hence it is difficult to draw firm conclusions about the way in which air entrained

and air released are affected by changes in discharge and droplength. Whillock and Thorn⁽³⁾ propose that when limiting shaft water velocities are reached, the net air demand, for a given droplength, is a constant proportion of discharge. Since the volume of air entrained is independent of droplength and discharge, the air demand increases due to more air being carried down by the shaft water velocities, conversely less air is released at the ambient surface.

For this reason, the rectangular column was developed to investigate the affects of varying the parameters controlling the rates of air entrainment.

5.3. Rectangular Column Dropshaft - Model Results

The rectangular column dropshaft was constructed with the particular aim of determining the affects of discharge velocities on air demand in air entraining models. The adjustable column wall thus provided a means of varying the cross-sectional area while maintaining all other parameters constant.

The results obtained from this section of the investigation cover a broad range. The control parameters used in these experiments are presented in Tables 5.1, 5.2 and 5.3, together with their respective experimental run numbers.

The general air demand results are shown in the form of air/water ratio against increasing droplength at each flow rate and for each column width in Figs. 5.6, 5.7. and 5.8. The characteristic air demand curves are

Table 5.1

Test No.	Q_w (1/s)	q (1/s/m)	$nwv = \frac{Q_w}{A}$ (m/s)	slot width (mm)	entry vel. v_i (m/s)	terminal Q_a/Q_w
A1	2.507	9.29	0.358	5.0	2.62	0.243
A2	3.35	12.41	0.479	7.5	2.62	0.235
A3	2.519	9.33	0.260	7.5	1.98	0.230
-	-	-	-	-	-	-
B1	2.484	9.20	0.233	5.0	2.62	0.195
B2	3.332	12.34	0.313	7.5	2.62	0.225
B3	2.472	9.16	0.232	7.5	1.98	0.165
B4	4.39	16.26	0.413	10.0	2.62	0.300
B5	3.341	12.37	0.314	10.0	1.98	0.190
B6	2.519	9.33	0.237	10.0	1.47	0.196
B7	5.715	21.17	0.537	12.5	2.62	0.327
B8	4.403	16.31	0.414	12.5	2.01	0.285
B9	3.376	12.50	0.317	12.5	1.53	0.264
B10	2.495	9.24	0.234	12.5	1.21	0.155
B11	6.962	25.79	0.654	15.0	2.62	0.330
B12	5.710	21.15	0.537	15.0	2.12	0.300
B13	4.416	16.36	0.415	15.0	1.66	0.292
B14	3.35	12.41	0.315	15.0	1.29	0.198
B15	2.519	9.33	0.237	15.0	0.94	0.180

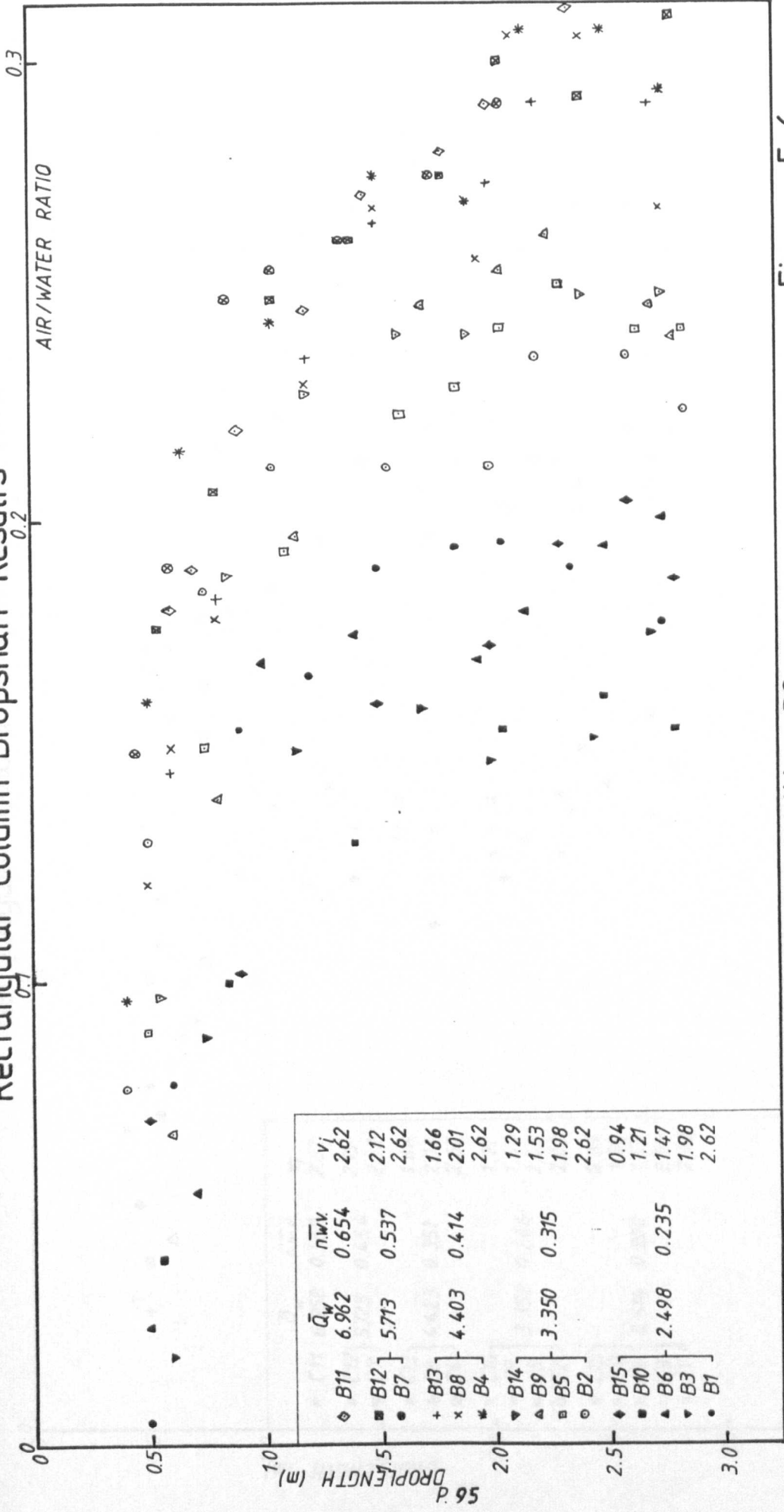
Table 5.2

Test No.	Q_w (1/s)	q (1/s/m)	$nwv = Q_w$ (m/s) \overline{A}	slot width (mm)	entry vel. v (m/s) i	terminal Q_a/Q_w
C1	2.519	9.33	0.200	5.0	2.62	0.135
C2	3.332	12.34	0.264	7.5	2.62	0.198
C3	2.519	9.33	0.200	7.5	2.01	0.135
C4	4.423	16.38	0.351	10.0	2.62	0.270
C5	3.358	12.44	0.267	10.0	2.03	0.205
C6	2.519	9.33	0.200	10.0	1.53	0.145
C7	5.72	21.19	0.454	12.5	2.62	0.302
C8	4.423	16.38	0.351	12.5	2.03	0.256
C9	3.358	12.44	0.267	12.5	1.53	0.220
C10	2.519	9.33	0.200	12.5	1.21	0.147
C11	6.958	25.77	0.552	15.0	2.62	0.310
C12	5.725	21.20	0.454	15.0	2.15	0.286
C13	4.423	16.38	0.351	15.0	1.66	0.280
C14	3.358	12.44	0.267	15.0	1.21	0.222
C15	2.495	9.24	0.198	15.0	0.89	0.133

Table 5.3

Test No.	Q_w (1/s)	q (1/s/m)	$nwv = Q_w$ (m/s) $\frac{1}{A}$	slot width (mm)	entry vel. v (m/s) i	terminal Q_a/Q_w
D1	2.519	9.33	0.180	5.0	2.62	0.100
D2	3.35	12.41	0.239	7.5	2.62	0.165
D3	2.53	9.37	0.181	7.5	2.006	0.107
D4	4.383	16.23	0.313	10.0	2.62	0.245
D5	3.35	12.41	0.239	10.0	2.03	0.177
D6	2.519	9.33	0.180	10.0	1.53	0.115
D7	5.715	21.17	0.408	12.5	2.62	0.285
D8	4.41	16.33	0.315	12.5	2.03	0.288
D9	3.385	12.54	0.242	12.5	1.53	0.185
D10	2.507	9.29	0.179	12.5	1.21	0.110
D11	6.953	25.75	0.497	15.0	2.62	0.300
D12	5.715	21.17	0.408	15.0	2.15	0.290
D13	4.423	16.38	0.316	15.0	1.66	0.248
D14	3.358	12.44	0.240	15.0	1.25	0.185
D.15	2.530	9.37	0.181	15.0	0.94	0.105
-	-	-	-	-	-	-
E7	5.700	21.11	0.270	12.5	2.62	0.271
E8	4.410	16.33	0.286	12.5	2.03	0.220
E11	6.962	25.79	0.452	15.0	2.62	0.295
E12	5.715	21.17	0.371	15.0	2.15	0.261
E13	4.410	16.33	0.286	15.0	1.66	0.234

Rectangular Column Dropshaft Results



Column width = 38 mm

Figure 5.6

Rectangular Column Dropshaft Results

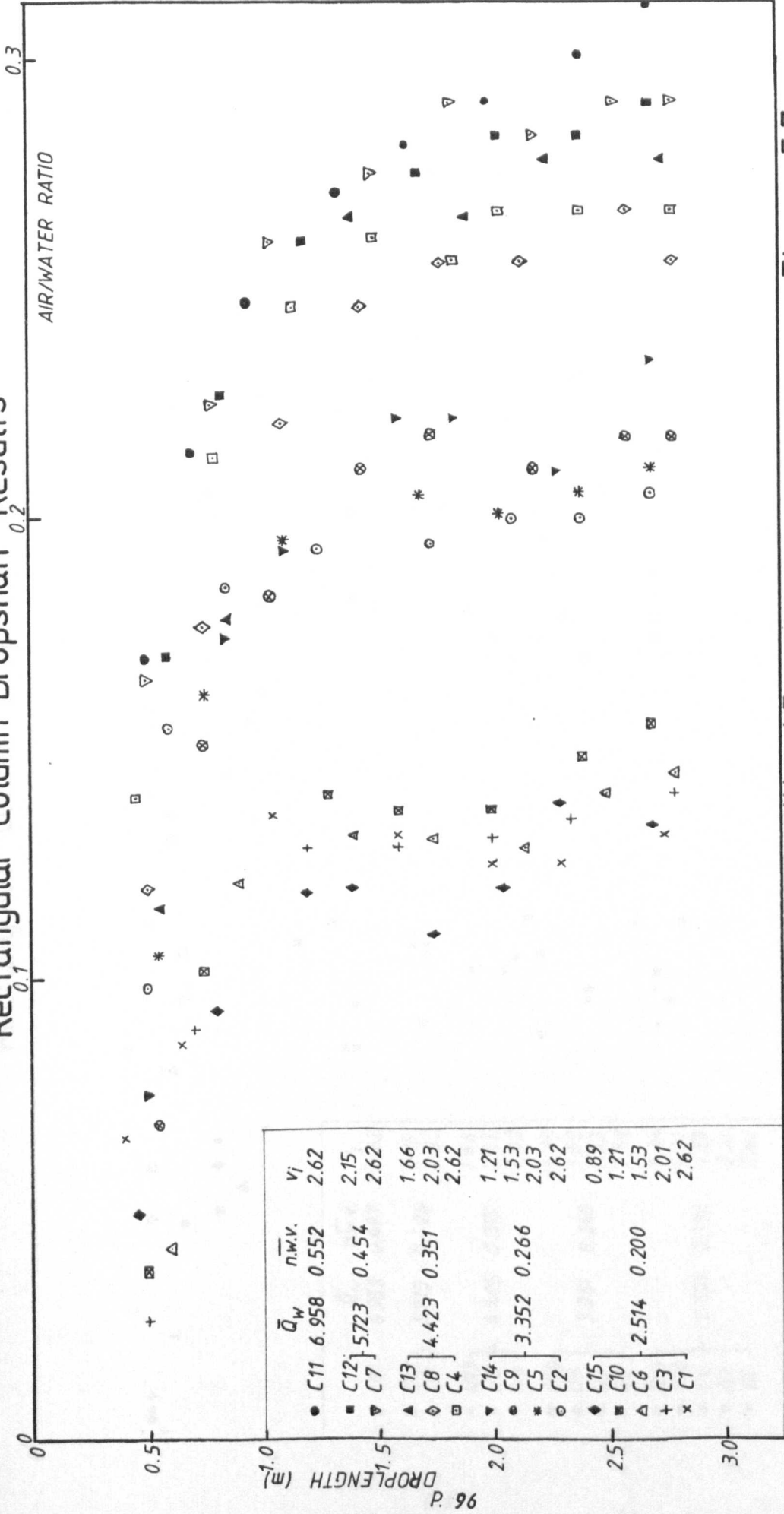
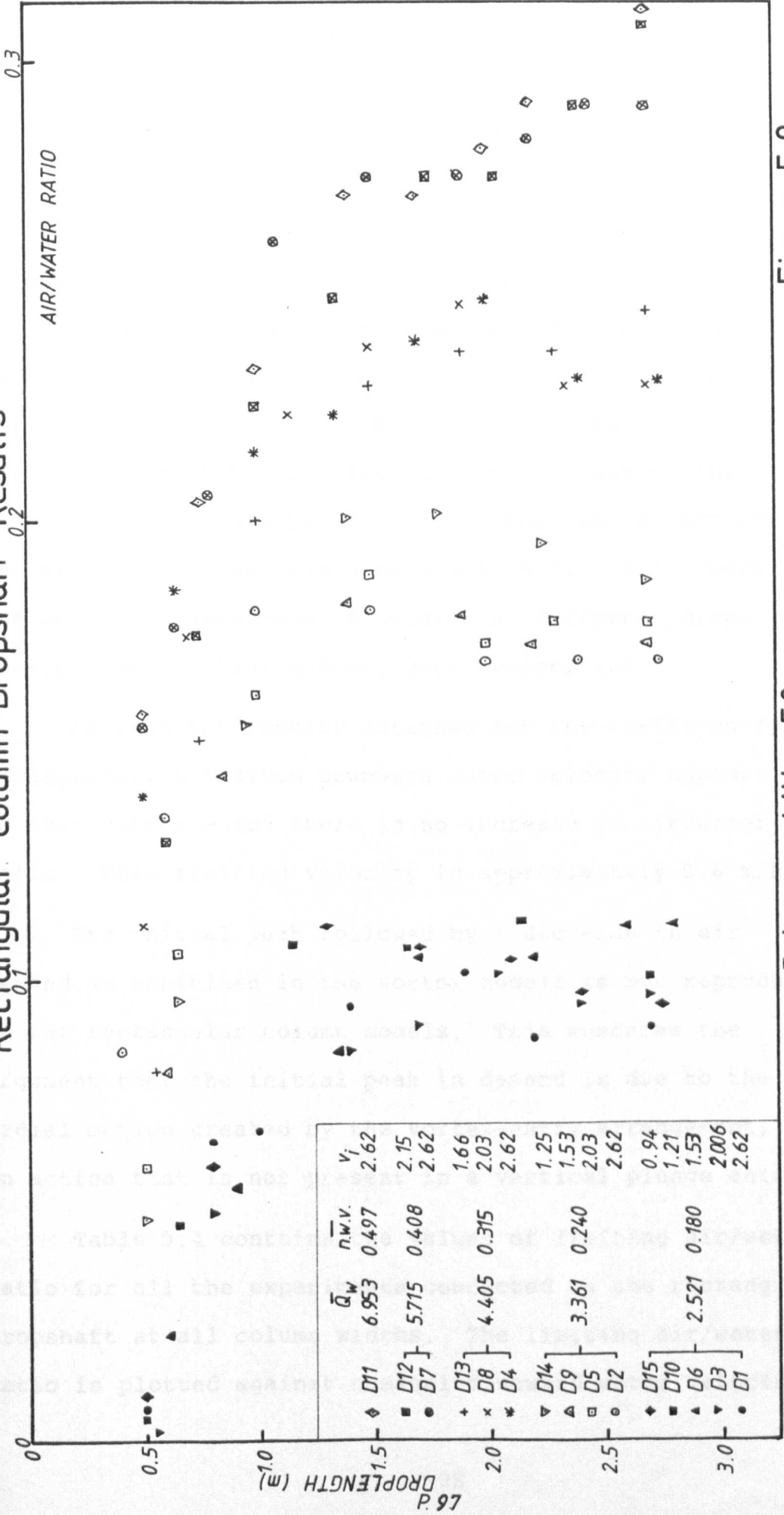


Figure 5.7

Column width = 45 mm.

Rectangular Column Dropshaft Results



Column width = 50 mm

Figure 5.8

again produced in these results i.e. increase in air/water ratio up to a terminal value as droplength increases for each flow rate. At constant droplength, the air demand increases for increasing discharge. It is apparent that variation of the inlet velocity does not significantly affect the terminal value of air/water ratio, hence the results are seen to exist in zones or bands of constant downward nominal water velocity (n.w.v.). The effect of varying the inlet velocity will be discussed later. The concentration of the results in bands is most obvious in Figs. 5.7 and 5.8 however, the trend also exists for the narrowest column width as shown in Fig. 5.6, where the spread of each band is greater at different droplengths for constant nominal water velocities.

As with the results obtained for the vortex-entry arrangement, a maximum downward water velocity appears to exist after which there is no increase in air/water ratio. This limiting velocity is approximately 0.6 m/s.

The initial peak followed by a decrease in air demand as exhibited in the vortex models is not reproduced in the rectangular column models. This enhances the argument that the initial peak in demand is due to the radial motion created by the vortex-entry arrangement, an action that is not present in a vertical plunge entry.

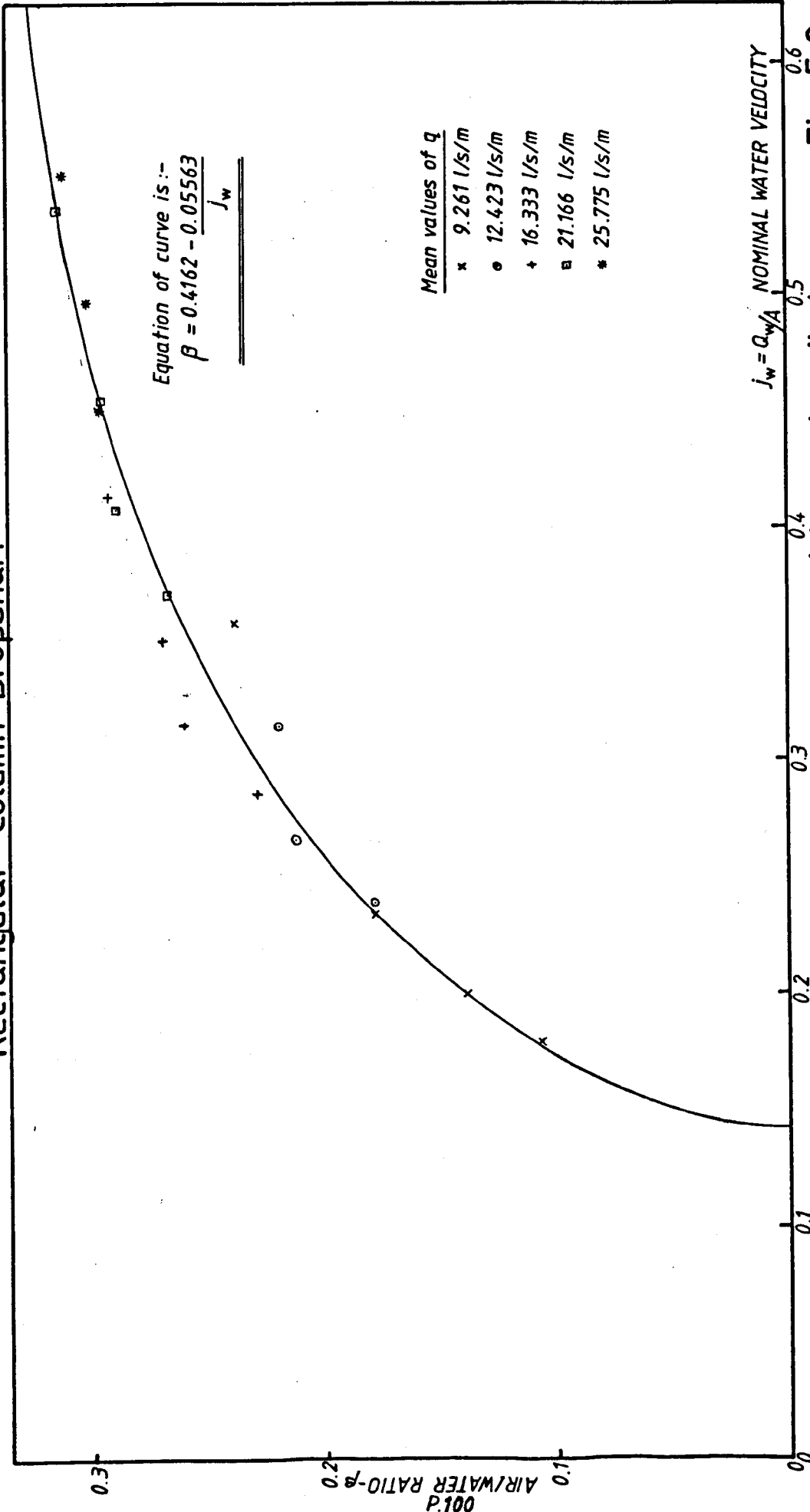
Table 5.4 contains the values of limiting air/water ratio for all the experiments conducted on the rectangular dropshaft at all column widths. The limiting air/water ratio is plotted against nominal downward water velocity

Mean values of limiting air/water ratios, nominal water velocities and flows per unit width, for each width of column dropshaft.

Table 5.4

Column Width	25mm	38mm	45mm	50mm	55mm
q_w	9.14	9.252	9.312	9.338	
n.w.v.	0.359	0.235	0.200	0.180	
Q_a/Q_w	0.237	0.178	0.139	0.107	
q_w		12.405	12.415	12.450	
n.w.v.		0.315	0.266	0.240	
Q_a/Q_w		0.219	0.211	0.178	
q_w		16.310	16.380	16.313	16.330
n.w.v.		0.414	0.351	0.315	0.286
Q_a/Q_w		0.292	0.269	0.260	0.227
q_w		21.160	21.195	21.170	21.140
n.w.v.		0.537	0.454	0.408	0.371
Q_a/Q_w		0.314	0.294	0.288	0.266
q_w		25.790	25.770	25.750	25.790
n.w.v.		0.654	0.552	0.497	0.452
Q_a/Q_w		0.330	0.310	0.300	0.295

Rectangular Column Dropshaft



Relationship between limiting air/water ratio & n.w.v. at increasing discharge. Fig. 5.9

($j_w = Q_{wA}$) at various discharges in Fig. 5.9. The relationship between these parameters was established by applying the statistical 'method of least squares' to various forms of the variables to obtain the best fit for the curve. An inverse logarithmic function was established as the relationship describing the curve attained from the experimental results. The equation of the curve is:-

$$\beta = 0.4162 - (0.05563/j_w)$$

where $\beta = Q_a/Q_w$ and $j_w = Q_w/A$

The curve intersects the horizontal axis at $j_w = 0.134$ m/s (i.e. $\beta = 0$), which corresponds to the values predicted by previous investigators for onset of downward air transport for air bubbles in the range under consideration.^(5,6) The curve also is asymptotic to a maximum air/water ratio; as j_w increases, the air/water ratio tends towards a value of 0.41. Higher values are considered attainable, but it is thought that on approaching this value, the bubbly regime becomes unstable and eventually becomes a bulking slug flow operation.

Figs. 5.10 to 5.12 are plotted to indicate that for constant nominal water velocity, the air/water ratio attains a maximum value at equal droplengths irrespective of discharge and inlet velocity. Fig. 5.10 is presented for a low nominal water velocity, the limiting air demand being approximately 0.18. As water velocity increases, see Fig. 5.12, the maximum air/water ratio increases to 0.30, and occurs at a longer droplength than at the lower velocity.

Rectangular Column Dropshaft

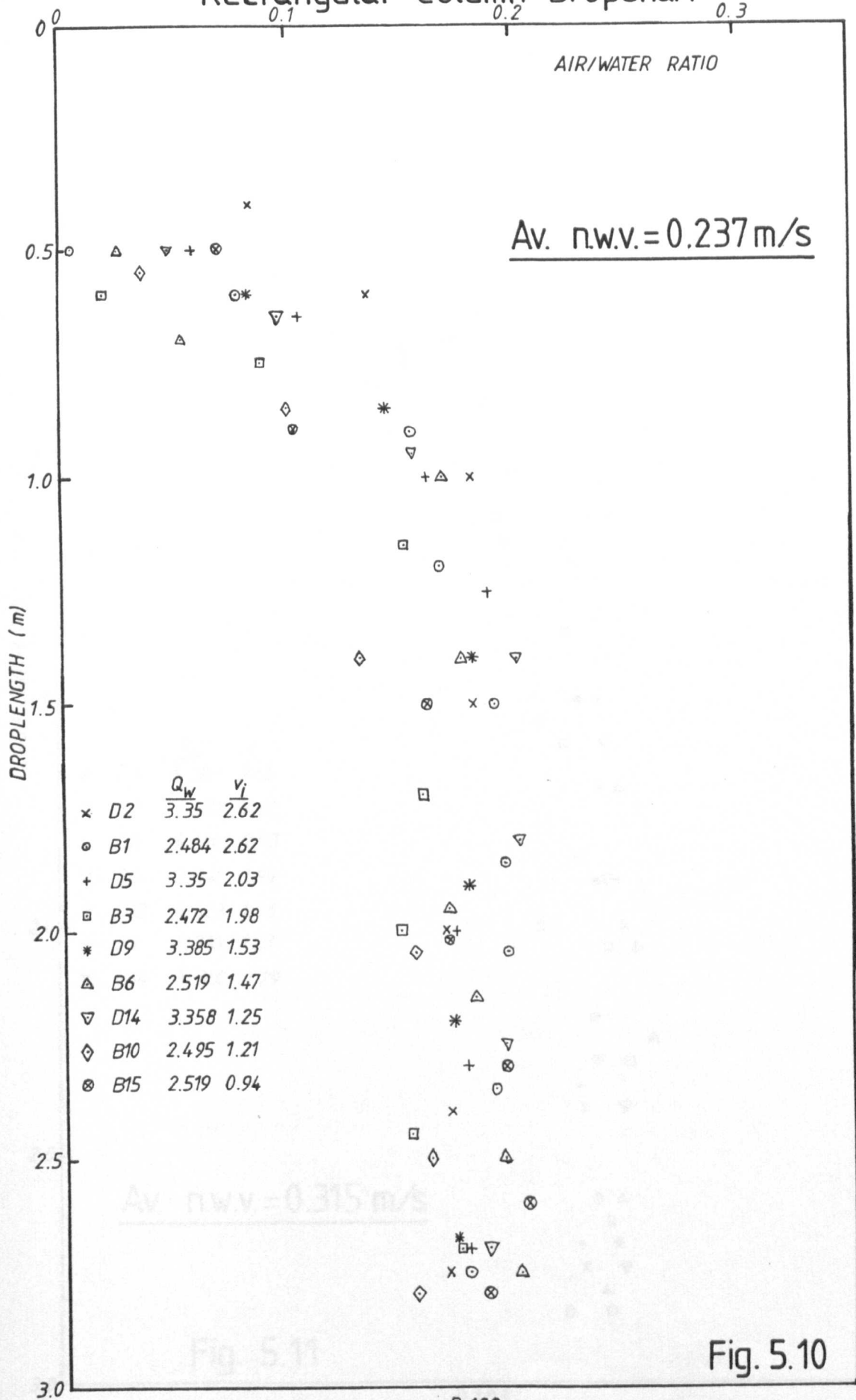


Fig. 5.11

Fig. 5.10

Rectangular Column Dropshaft

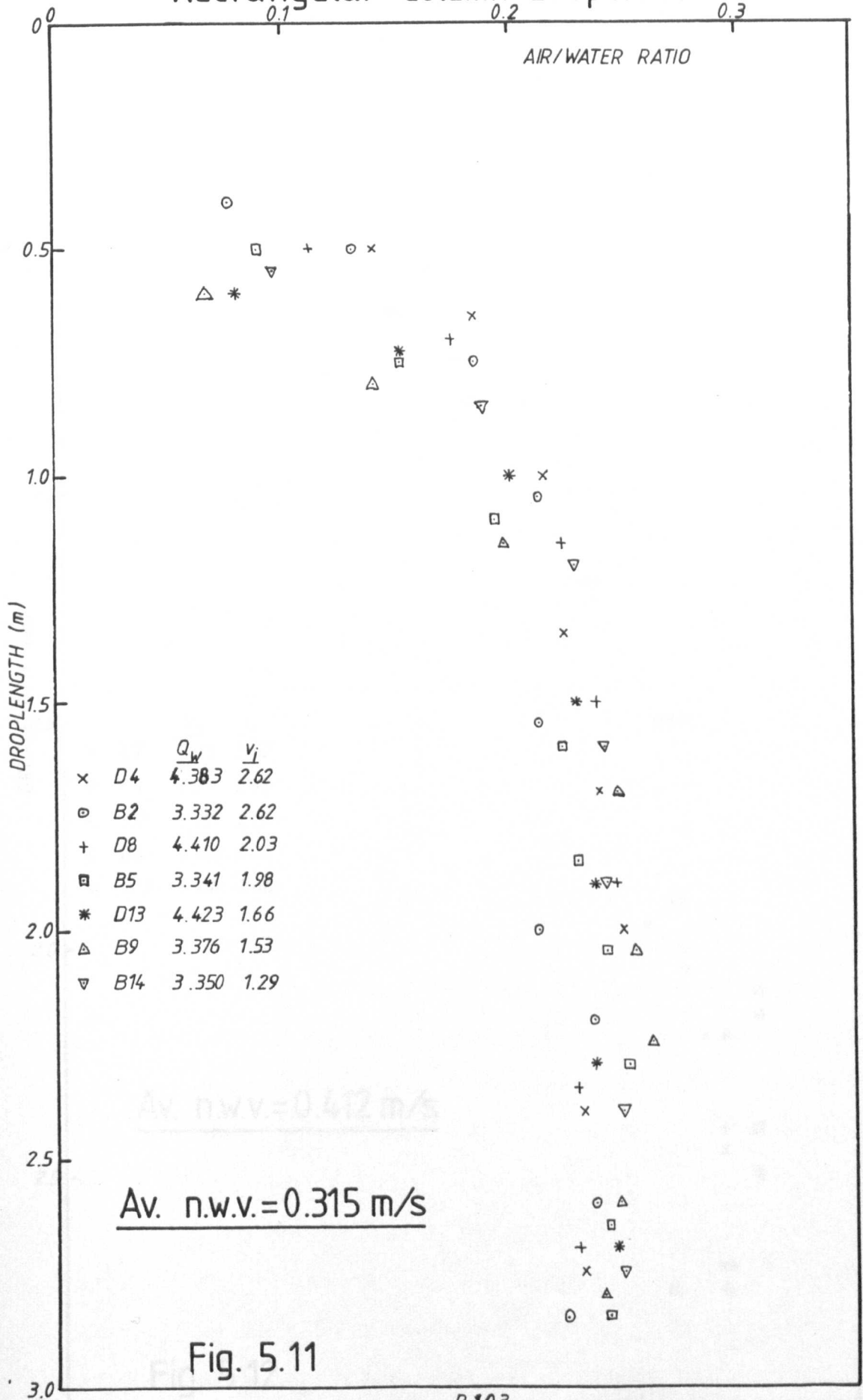


Fig. 5.11

Rectangular Column Dropshaft

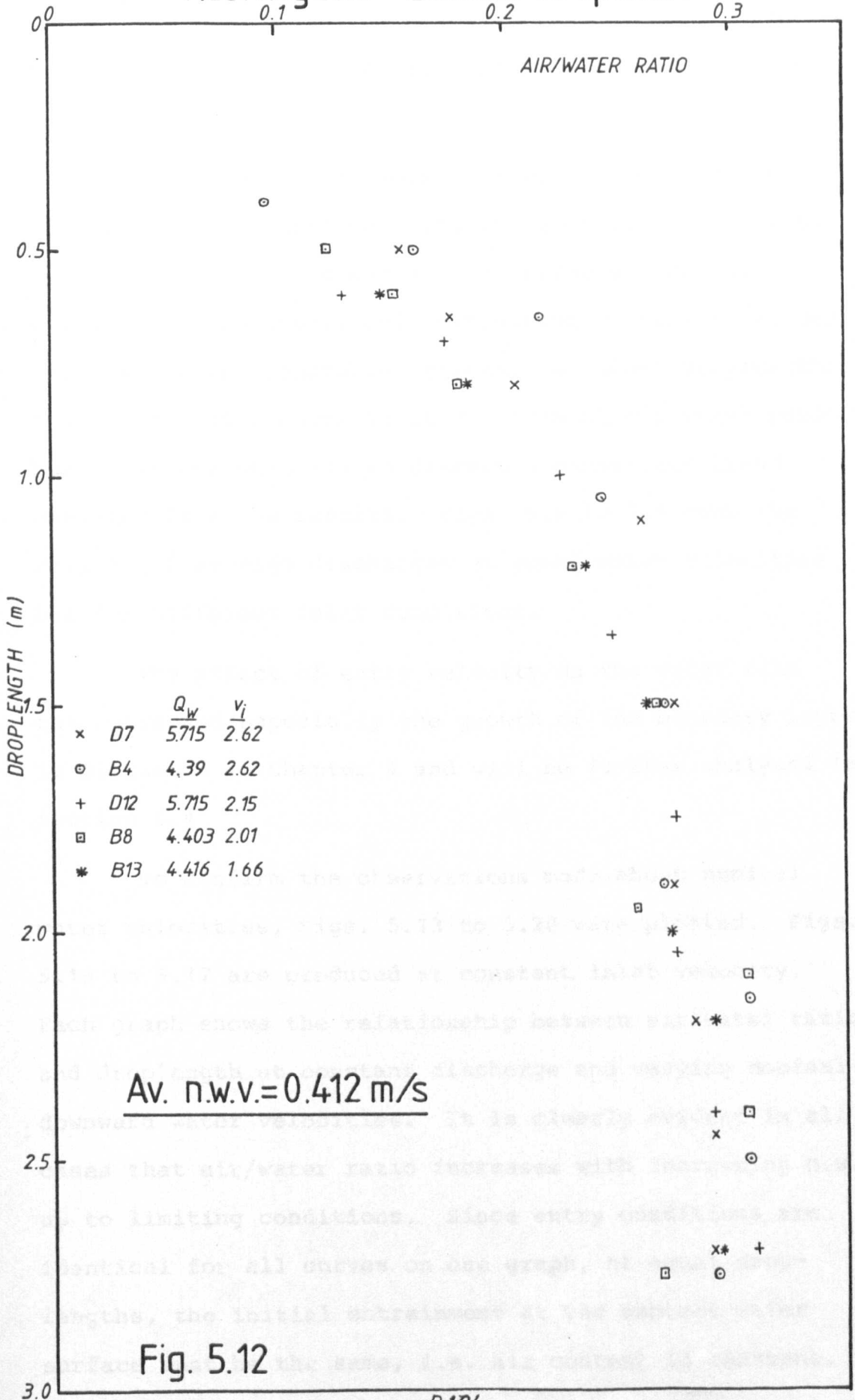


Fig. 5.12

This corresponds to the pattern observed in the vortex-entry dropshafts which displayed a limiting air demand at longer droplengths for increasing discharge and hence nominal water velocity.

The variation in inlet velocity appears to be effective to a degree only for the shorter droplengths. As the droplength increases, the spread of results becomes less apparent, and terminating or maximum values are reached in comparable regions. At short droplengths, the scatter of results is larger than at any other position, but it is not possible to discern a consistent trend emerging from the results. Figs. 5.6 to 5.8 show the results of average discharges at equal water velocities but for different inlet conditions.

The effect of entry velocity on the water film thickness and especially the growth of the boundary layer is discussed in Chapter 4 and will be further analysed in section 5.4

To confirm the observations made about nominal water velocities, Figs. 5.13 to 5.20 were plotted. Figs. 5.13 to 5.17 are produced at constant inlet velocity. Each graph shows the relationship between air/water ratio and droplength at constant discharge and varying nominal downward water velocities. It is clearly evident in all cases that air/water ratio increases with increasing n.w.v. up to limiting conditions. Since entry conditions are identical for all curves on one graph, at equal droplengths, the initial entrainment at the ambient water surface must be the same, i.e. air content is constant.

Rectangular Column Dropshaft

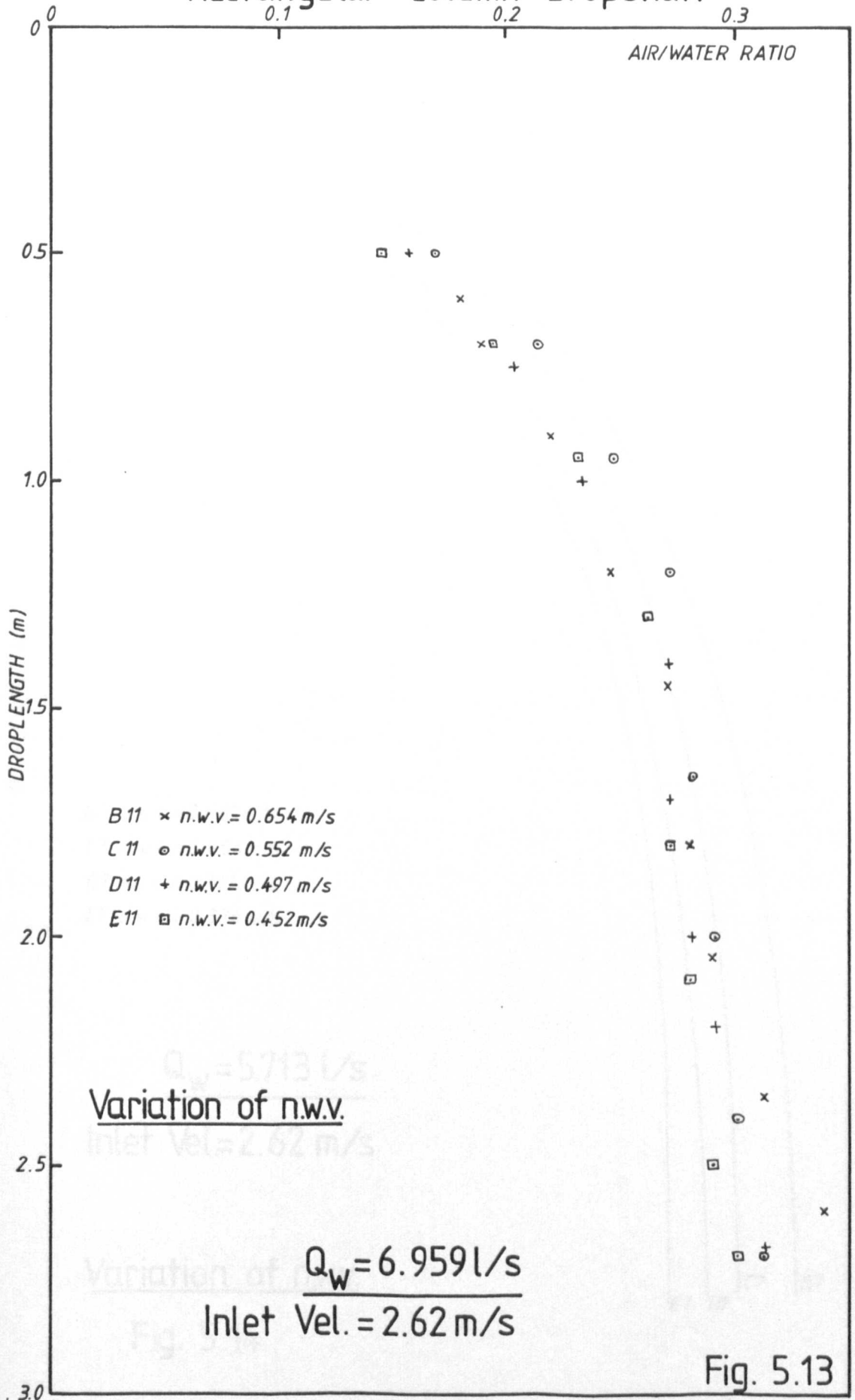
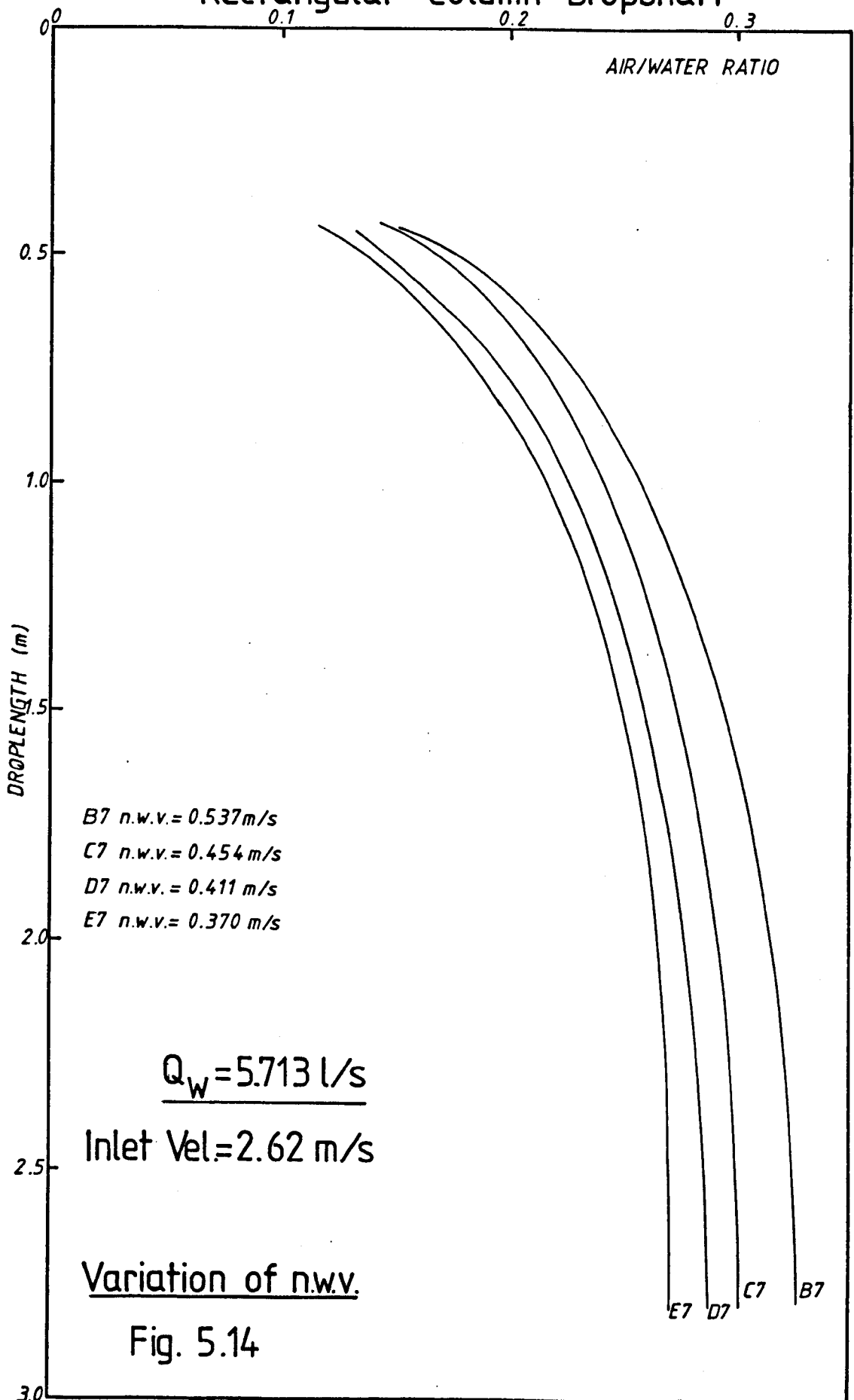


Fig. 5.13

Rectangular Column Dropshaft



B7 n.w.v. = 0.537 m/s
C7 n.w.v. = 0.454 m/s
D7 n.w.v. = 0.411 m/s
E7 n.w.v. = 0.370 m/s

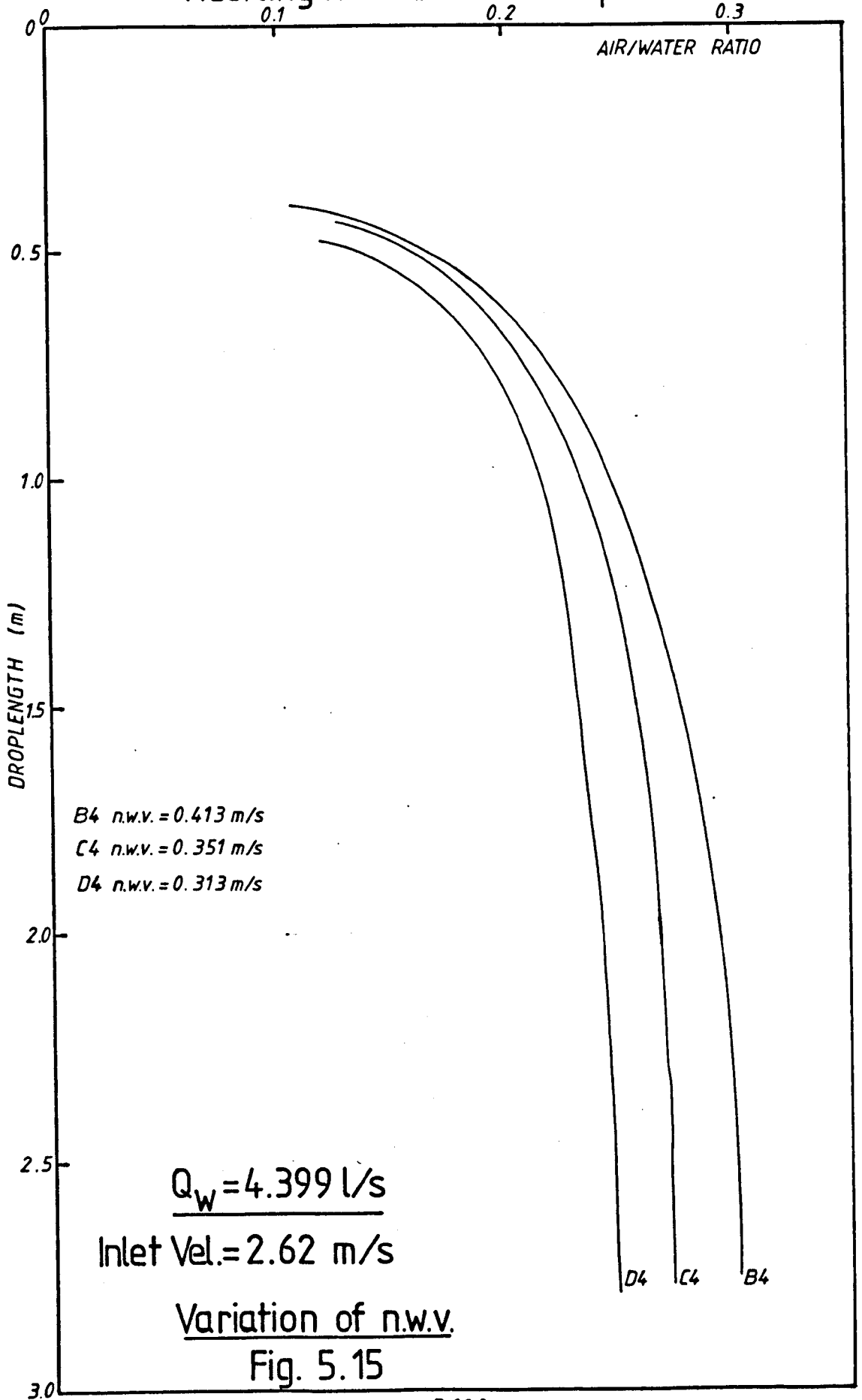
$Q_w = 5.713 \text{ l/s}$

Inlet Vel. = 2.62 m/s

Variation of n.w.v.

Fig. 5.14

Rectangular Column Dropshaft



Rectangular Column Dropshaft

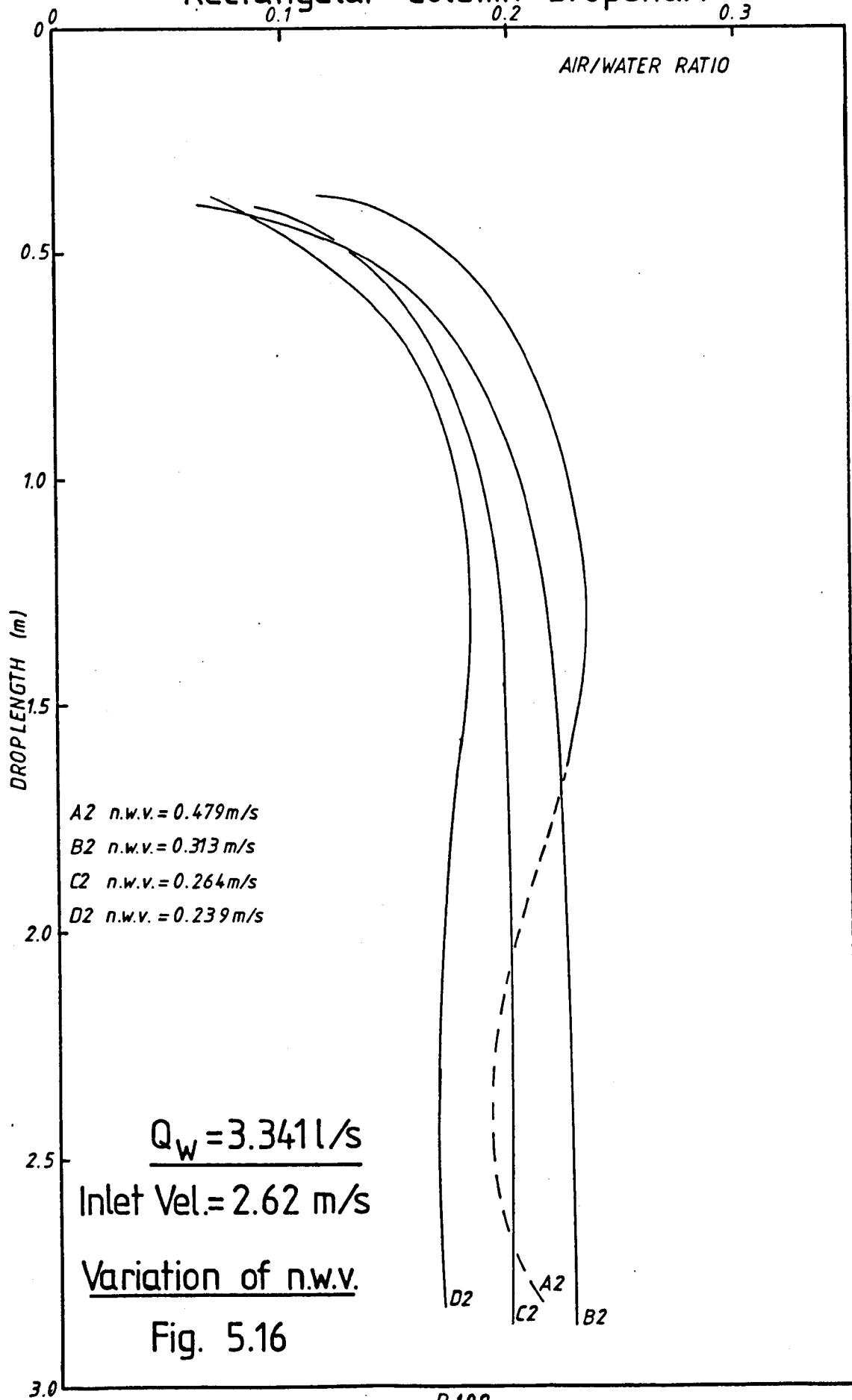
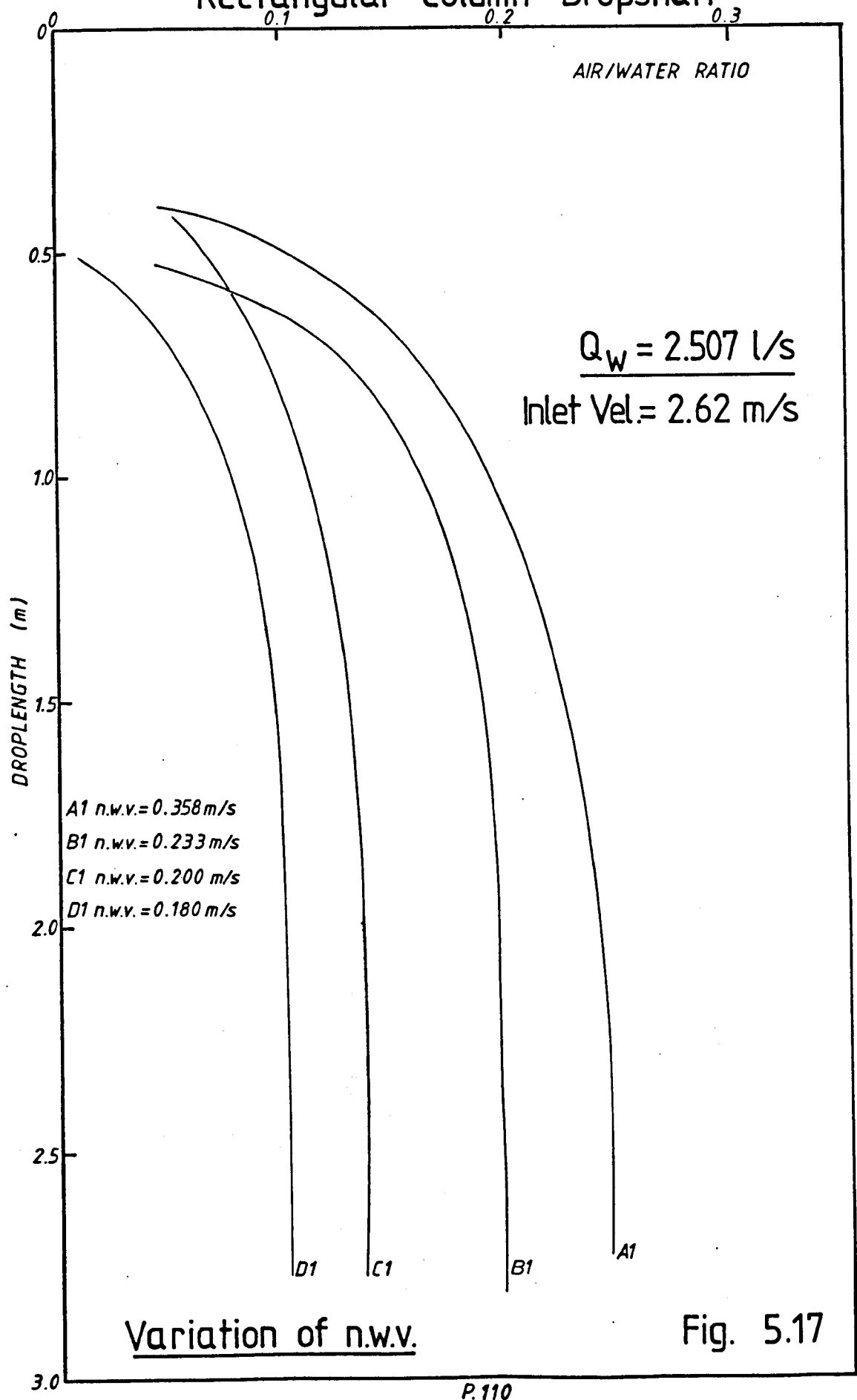


Fig. 5.16

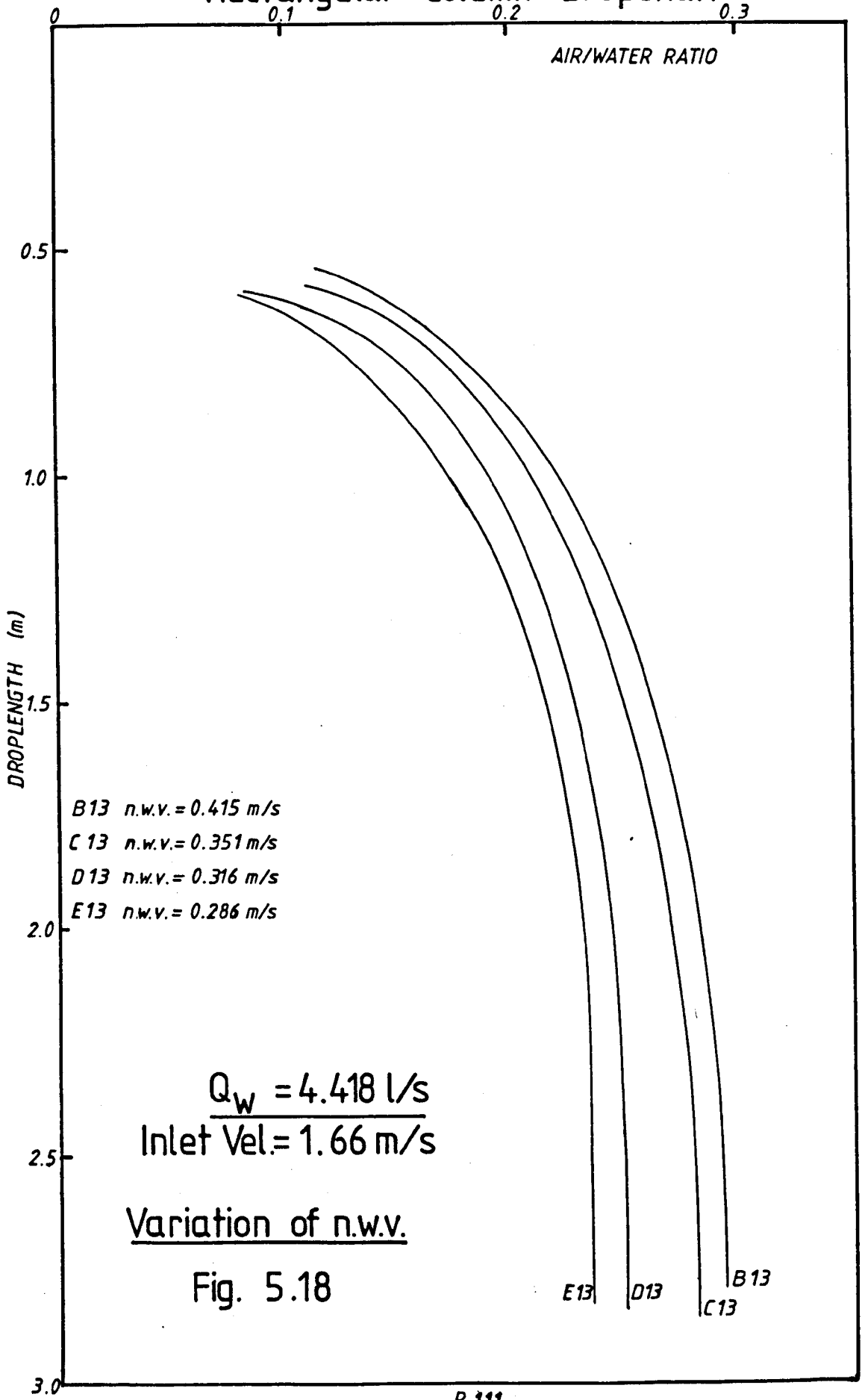
Rectangular Column Dropshaft



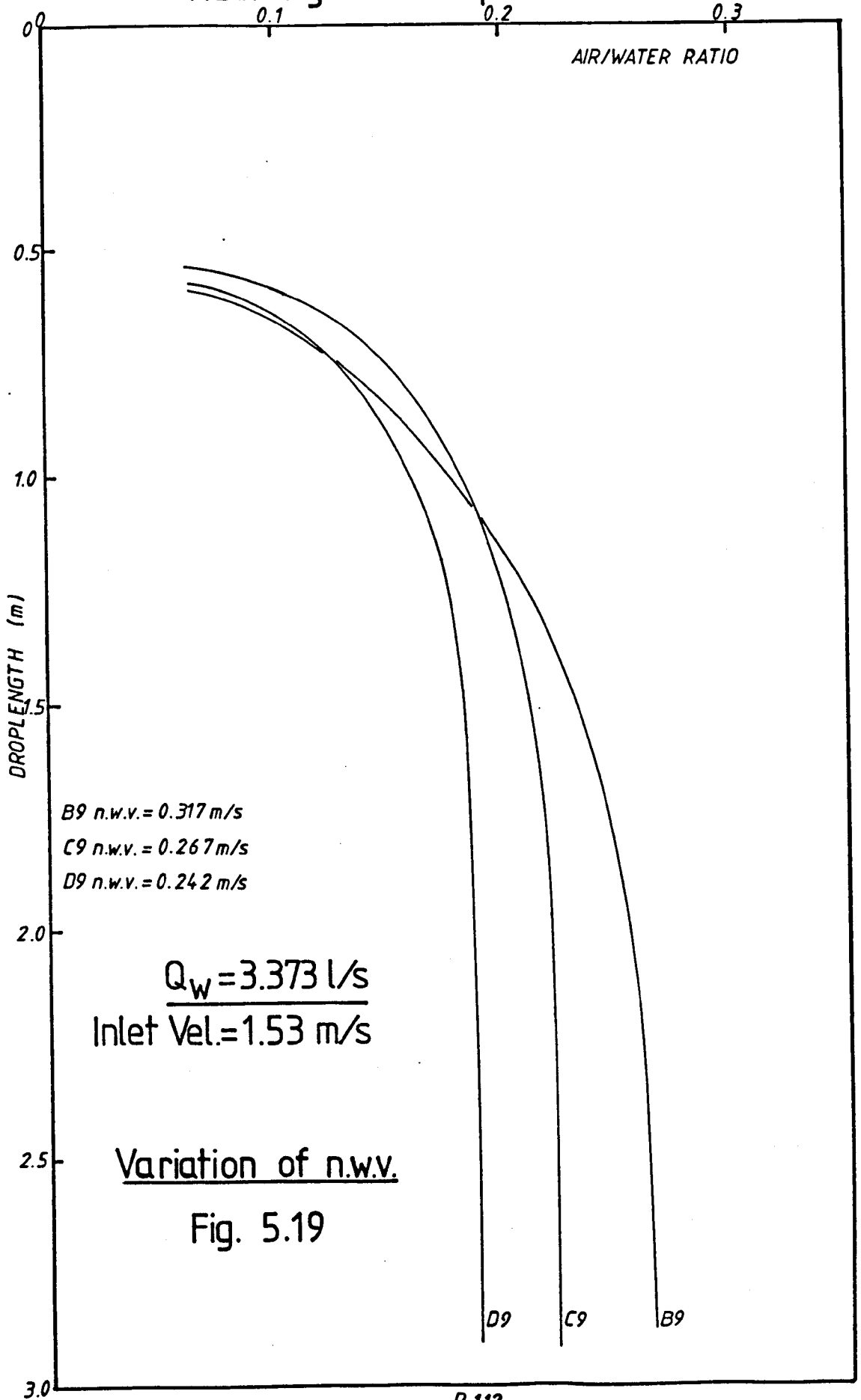
Variation of n.w.v.

Fig. 5.17

Rectangular Column Dropshaft



Rectangular Dropshaft

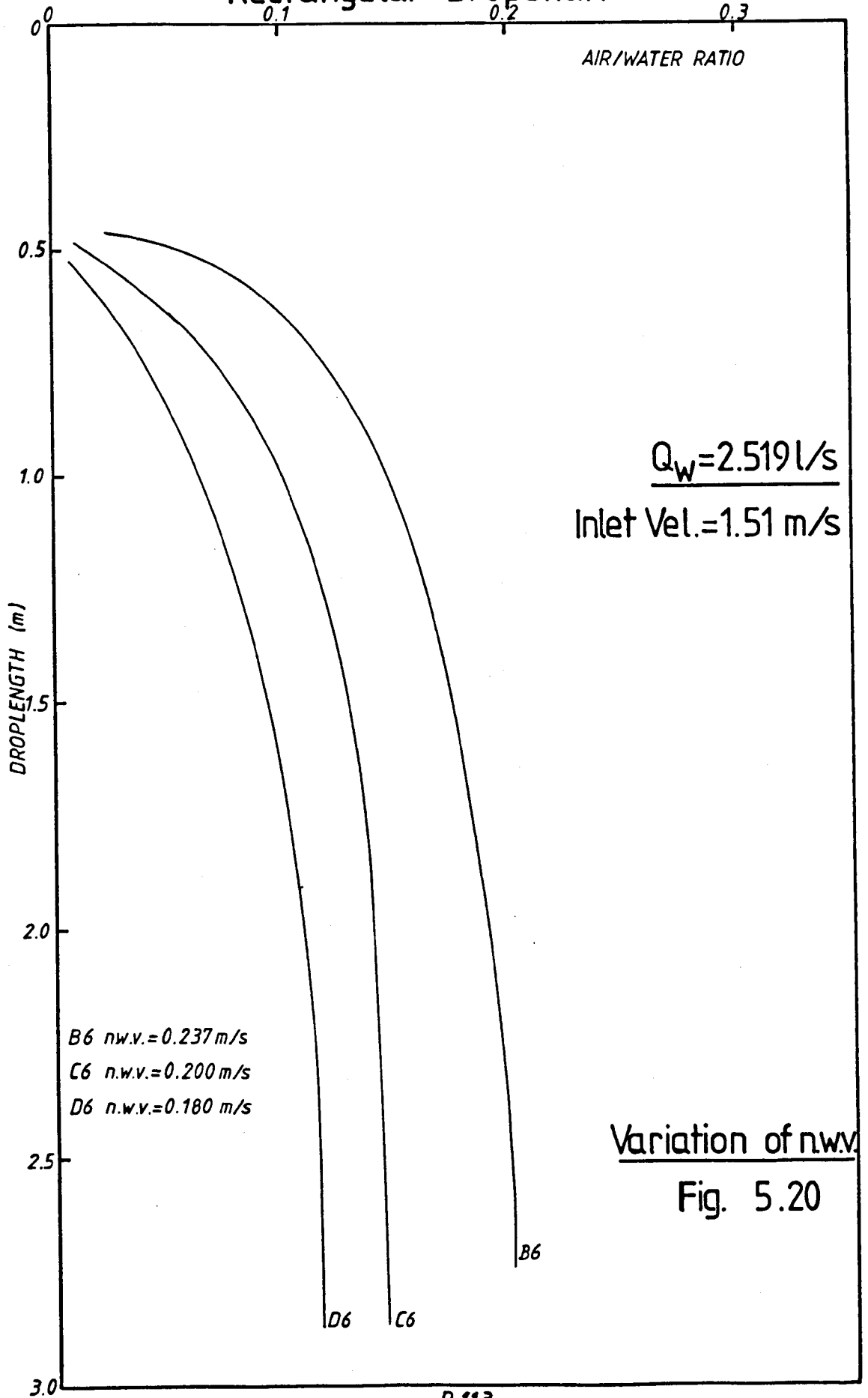


$Q_w = 3.373 \text{ l/s}$
Inlet Vel. = 1.53 m/s

Variation of n.w.v.

Fig. 5.19

Rectangular Dropshaft



Variation of n.w.v.

Fig. 5.20

The interstitial water velocity increases as the column width decreases, hence the relative velocity of water to bubble cloud increases and more air is carried down the shaft. Thus the air transport mechanism is a function of the water velocity (both nominal and interstitial).

The established trends of increasing air/water ratio with increasing discharge at constant droplength; and of maximum air/water ratio occurring at longer droplengths for increasing flow-rate are both clearly illustrated in this series of graphs.

In Fig. 5.13, the results plot in a narrow band and show very minor, though apparent, differences in air/water ratio at equal droplengths for increasing discharge, the water velocity increasing to about 0.6 m/s. This curve forms an envelope which is the limiting curve for air entrainment in this arrangement of dropshaft, for transport of bubble emulsions only. In Fig. 5.16 curve A2, the flow in the narrowest column width, shows a distinct anomaly. This is due to the development of slug flow by coalescence of the air bubbles instigated in this case by the very narrow column width (25mm).

The series of Figs. 5.18 to 5.20 are produced on the same basis but for a lower inlet velocity.

5.4. Dimensional analysis of vortex-entry dropshaft results.

5.4.1 Determination of relevant parameters.

The determination of the parameters is presented in section 4.1.2. The flow rate per unit width is determined from the measured discharge using the calibration for the orifice plate and the particular drop-pipe under consideration. Air flow is measured using the air meter described. The air bubbles are assumed to be of mean diameter 4mm after the work of Rosenberg et al⁽²¹⁾. The terminal film thickness, (δ) is calculated from equation 4.1.7.

The inlet velocities are obtained using the method devised by Ackers and Crump⁽¹⁹⁾ and presented in the appendices. Assuming these calculated values to be the radial entry velocity only, i.e. neglecting the swirl component of velocity, the length at which the boundary layer projects beyond the surface of the falling water film can be evaluated thus;

$$\delta^{12} = k \cdot q^7 \quad 4.1.7a$$

$$0 = W^{1.75} - (W_c^{5.857} - W^{-4.107}) - \left[\frac{(\delta^{1.25} \gamma_c^{1.25}) g}{0.0016727} \right] \quad 4.1.20a$$

Hence

$$z_t = \frac{W^2 - W_0^2}{2g}$$

Equation 4.1.20a can be solved using Newton-Raphson's method. This has been achieved by computer program and the results are presented in Table 5.5a for the circular shafts and Table 5.5b for the rectangular shafts.

Table 5.5a

Pipe dia.	Q_w	q_w	W_o	W	δ	z_t
	(l/s)	(l/s/m)	(m/s)	(m/s)	(mm)	(m)
51mm	0.62	3.87	0.608	2.515	1.81	0.304
L'pool	0.75	4.68	0.688	2.567	2.02	0.312
Poly.	0.91	5.68	0.777	2.629	2.26	0.322
	0.98	6.12	0.820	2.658	2.36	0.326
	1.06	6.62	0.859	2.688	2.47	0.331
	1.19	7.43	0.925	2.738	2.64	0.339
	1.33	8.30	0.992	2.793	2.82	0.348
	1.51	9.42	1.095	2.866	3.03	0.358
	1.69	10.55	1.185	2.939	3.24	0.369
	1.84	11.48	1.260	3.000	3.41	0.378
101mm	2.03	6.39	0.633	2.636	2.42	0.334
L'pool	2.63	8.30	0.739	2.741	2.82	0.355
Poly	3.26	10.28	0.841	2.849	3.19	0.378
	3.51	11.07	0.890	2.893	3.33	0.386
	3.92	12.34	0.945	2.962	3.55	0.402
	4.16	13.10	0.987	3.005	3.68	0.411
	4.48	14.11	1.028	3.057	3.84	0.423
	4.84	15.24	1.070	3.117	4.02	0.437
	5.19	16.37	1.120	3.176	4.19	0.450
	5.63	17.75	1.180	3.248	4.39	0.467
	6.01	18.93	1.230	3.310	4.56	0.481
	6.40	20.18	1.282	3.373	4.73	0.496
	7.18	22.62	1.380	3.497	5.06	0.526
	7.76	24.46	1.465	3.588	5.29	0.547
4in.	2.87	8.99	0.863	2.795	2.95	0.360
H.R.S.	4.02	12.59	1.040	2.992	3.59	0.401
	5.17	16.19	1.210	3.187	4.16	0.443
	6.32	19.79	1.367	3.376	4.68	0.485
	7.47	23.39	1.506	3.556	5.16	0.529
	8.61	26.98	1.660	3.734	5.61	0.570
6in.	6.33	13.22	1.352	3.098	3.70	0.396
H.R.S.	7.91	16.52	1.572	2.396	4.21	0.428
	9.49	19.83	1.770	3.487	4.68	0.460
	11.08	23.13	1.970	3.687	5.16	0.495
	12.66	26.44	2.165	3.861	5.54	0.521
	14.24	29.74	2.360	4.043	5.93	0.549
12in.	17.89	18.67	0.948	3.248	4.52	0.492
H.R.S.	26.86	28.03	1.142	3.684	5.73	0.625
	35.81	37.37	1.320	4.084	6.78	0.761
	44.75	46.70	1.485	4.446	7.72	0.895
	53.69	56.04	1.650	4.776	8.58	1.025
	60.12	62.74	1.754	4.999	9.17	1.117
	71.61	74.74	1.938	5.367	10.15	1.277
	80.56	84.07	2.168	5.643	10.88	1.383

Table 5.5b

Test No.	q_w (1/s/m)	W_o (m/s)	W (m/s)	δ (mm)	z_t (m)
B1	9.20	2.62	3.539	2.992	0.289
B2	12.34	2.62	3.633	3.551	0.323
B3	9.16	1.98	3.182	2.985	0.316
B4	16.26	2.62	3.749	4.171	0.366
B5	12.37	1.98	3.295	3.556	0.354
B6	9.33	1.47	2.976	3.017	0.341
B7	21.17	2.62	3.895	4.865	0.423
B8	16.31	2.01	3.448	4.179	0.400
B9	12.50	1.53	3.123	3.578	0.378
B10	9.24	1.21	2.890	3.000	0.351
B11	25.79	2.62	4.032	5.459	0.479
B12	21.15	2.12	3.662	4.863	0.454
B13	16.36	1.66	3.318	4.186	0.421
B14	12.41	1.29	3.046	3.563	0.388
B15	9.33	0.94	2.826	3.017	0.362
C1	9.33	2.62	3.543	3.017	0.290
C2	12.34	2.62	3.633	3.551	0.323
C3	9.33	2.02	3.202	3.017	0.317
C4	16.38	2.62	3.753	4.189	0.368
C5	12.44	2.02	3.321	3.568	0.352
C6	9.33	1.53	2.997	3.017	0.339
C7	21.19	2.62	3.895	4.868	0.423
C8	16.38	2.03	3.459	4.189	0.400
C9	12.44	1.53	3.121	3.568	0.377
C10	9.33	1.21	2.894	3.017	0.352
C11	25.77	2.62	4.032	5.457	0.479
C12	21.20	2.15	3.676	4.869	0.453
C13	16.38	1.66	3.319	4.189	0.421
C14	12.44	1.21	3.026	3.568	0.392
C15	9.24	0.89	2.812	3.000	0.363
D1	9.33	2.62	3.543	3.017	0.290
D2	12.41	2.62	3.635	3.563	0.324
D3	9.37	2.01	3.204	3.024	0.317
D4	16.23	2.62	3.749	4.167	0.366
D5	12.41	2.03	3.320	3.563	0.352
D6	9.33	1.53	2.997	3.017	0.339
D7	21.17	2.62	3.895	4.865	0.423
D8	16.33	2.03	3.457	4.182	0.399
D9	12.54	1.53	3.125	3.585	0.378
D10	9.29	1.21	2.892	3.009	0.352
D11	25.75	2.62	4.031	5.454	0.478
D12	21.17	2.15	3.675	4.865	0.453
D13	16.38	1.66	3.319	4.189	0.421
D14	12.44	1.25	3.036	3.568	0.390
D15	9.37	0.94	2.828	3.024	0.363
E7	21.11	2.62	3.893	4.857	0.422
E8	16.33	2.03	3.457	4.182	0.399
E11	25.79	2.62	4.032	5.459	0.479
E12	21.17	2.15	3.675	4.865	0.453
E13	16.33	1.66	3.317	4.182	0.420

A modification to the program produces a complete analysis for the growth of a boundary layer on a flat vertical plate. If the results of this analysis are studied, it can be seen that the initial growth of the boundary layer is suppressed as the discharge, hence initial velocity, increases. This is an interesting phenomenon and it was thought that this occurrence could possibly be used to explain the initial air entrainment characteristics displayed in the dropshaft model results.

However, the suppression is limited to very short vertical distances, and the difference in laminar boundary layer thickness at equal distances down the plate are only of the order of hundredths of a millimetre. Thus it is unlikely to have a measurable effect and since it proved difficult to establish a consistent pattern developing for air demand at short droplengths, the argument cannot be extended.

5.4.2. Dimensional Analysis

In Section 4.1.1, it was proposed that the variables considered to be relevant to the rate of air entrainment could be combined to form the following non-dimensional groups;

$$\frac{Q_a}{Q_w} , \frac{Q_w^2}{D^5 g} , \frac{L}{D} , \frac{b}{D} , \frac{\delta}{D} , \frac{\mu D}{\rho Q_w} , \frac{\sigma D^3}{\rho Q_w^2}$$

for circular dropshafts of diameter, D.

Standardisation of these groups for both the circular and rectangular shafts can be achieved by expressing the water flow rate, Q_w , as flow intensity, q_w . This further removes the necessity to include the geometrical shape factor

$\frac{B}{d}$, for the cross-section of the rectangular column. It is also considered that the geometrical ratio, $\frac{L}{D}$, relating droplength, L , should be modified to $\frac{L - z_t}{D}$. The distance, z_t , is the distance down the shaft at which the thickness of the turbulent boundary layer becomes equal to the film thickness. The modified droplength, $(L - z_t)$, recognizes that entrainment commences only when the ambient water surface is some distance below the inlet to the shaft.

The film thickness, δ , is uniquely related to the intensity of the rate of water flow, so $\frac{\delta}{D}$ can be omitted from the analysis. It has previously been postulated that the Reynolds and Weber non-dimensional groups are unlikely to significantly influence the air entrainment process as compared with the effects associated with the Froude non-dimensional group. Hence, it would appear that four groups only need to be considered; for the rectangular column, D being replaced by column width, d .

The data for the dropshafts plotted in Fig. 5.4 to 5.5 for the circular shafts, and Fig. 5.6 to 5.8 for the rectangular dropshafts, show that the air/water ratio increases with droplength, and in certain tests, attains a peak value at a specific droplength, the ratio being maintained notwithstanding further increase in droplength. The values of the relevant dimensionless groups applicable at these terminal conditions of constant air/water ratio are contained in the tables given in Appendix D.

Fig. 5.21 shows that the maximum air/water ratio

Variation of β with Non-Dimensional Group $\frac{q_w}{(g \cdot D^3)^{0.5}}$ - Circular shafts

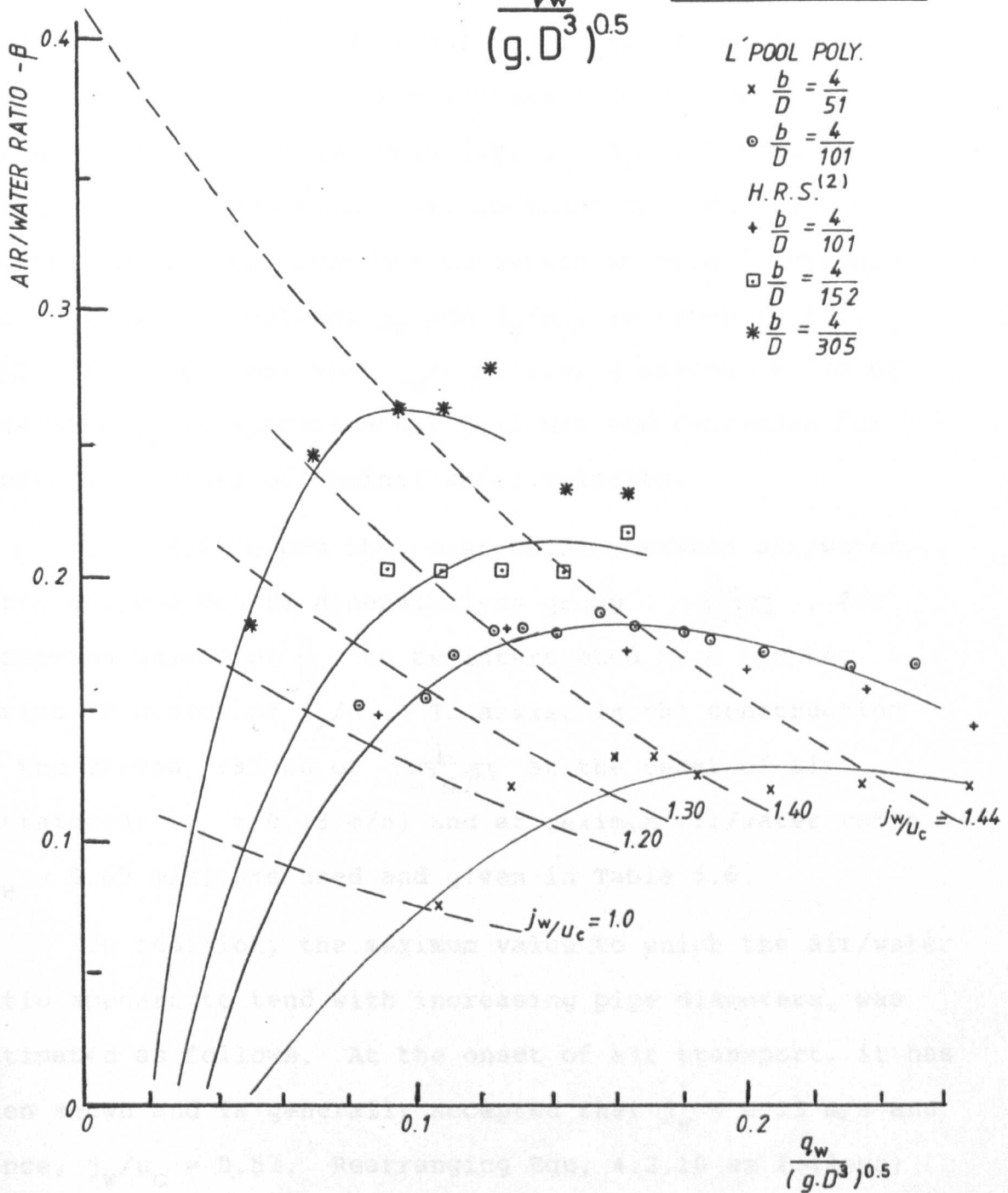


Figure 5.21

for each water flow in the circular pipes to plot as a series of curves, each curve being peculiar to the geometrical ratio of bubble diameter/pipe diameter. Each data point also refers to a specific nominal downward water velocity, j_w and it is apparent that this value increases along each curve. This velocity was made dimensionless by dividing by the relative velocity, u_c , derived from the relationship in equation 5.9a, obtained from the radio-isotope absorption technique to determine void fraction. The relationship between j_w and j_w/u_c , is shown in Fig. 5.22; it is apparent that j_w/u_c attains a maximum value of 1.44 when j_w is approximately 0.65 m/s and decreases for increasing values of nominal water velocity.

Fig. 5.21 shows the relationship between air/water ratio and the Froude dimensionless group $\frac{q_w}{(D^3g)^{0.5}}$, for differing values of $\frac{b}{D}$, to be intersected by a further series of curves of j_w/u_c . To assist in the construction of the curves, values of $\frac{q_w}{(D^3g)^{0.5}}$ at the onset of air entrainment ($j_w = 0.13$ m/s) and at maximum air/water ratio ($j_w = 0.65$ m/s) are used and given in Table 5.6.

In addition, the maximum value to which the air/water ratio appears to tend with increasing pipe diameters, was estimated as follows. At the onset of air transport, it has been shown and is generally accepted that $j_w = 0.13$ m/s and hence, $j_w/u_c = 0.57$. Rearranging Equ. 4.2.10 as follows;

$$\beta \frac{(1-\alpha)}{\alpha} = 1 - \frac{u_c}{j_w} (1-\alpha) \quad 4.2.10a$$

Relationship between j_w and j_w/u_c

(derived from Equation 5.9a)

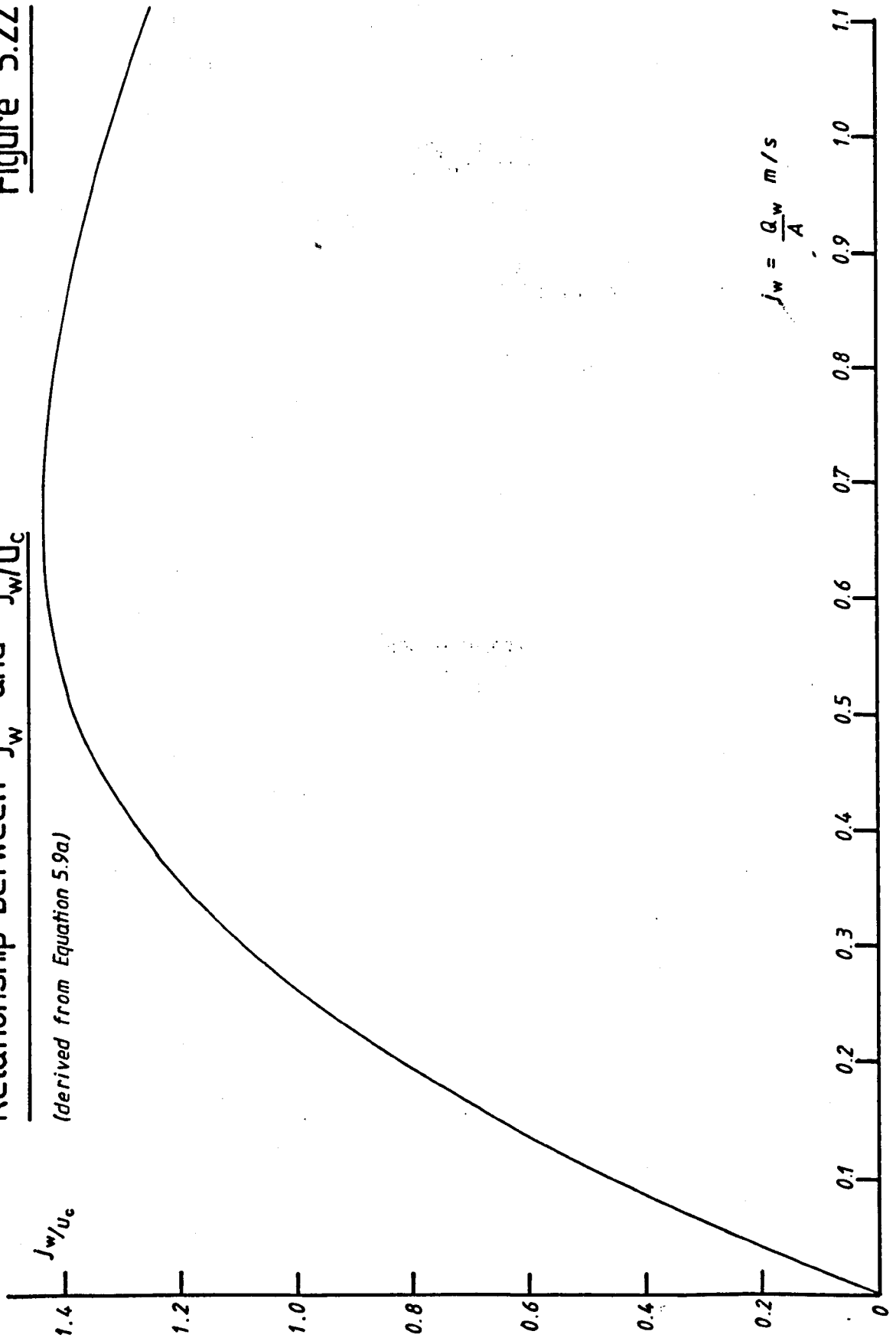


Table 5.6

Values of modified Froude non-dimensional group for circular shafts and rectangular columns for onset and maximum air/water ratios.

Circular shaft (D mm)		$\frac{q_w}{(D^3 \cdot g)^{0.5}}$			
D	=	51	101	152	305
n.w.v.	= 0.13 m/s	0.046	0.033	0.027	0.019
n.w.v.	= 0.65 m/s	0.233	0.166	0.135	0.096
Rectangular column (d mm)		$\frac{q_w}{(d^3 \cdot g)^{0.5}}$			
d	=	25	38	45	50
n.w.v.	= 0.13 m/s	0.263	0.213	0.196	0.186
n.w.v.	= 0.65 m/s	1.33	1.08	1.00	0.94

then as air/water ratio $\beta = 0$, $\alpha = 0.42$ and the absolute interstitial water velocity is 0.23 m/s. A small increase in the water flow rate and hence in j_w/u_c , would then be sufficient to cause air bubbles to be transported. Fig. 5.35 showing the plot of the experimental data illustrates this point. For a fixed flow rate, the relationship between α and β plotting along lines of constant j_w/u_c values, with α varying from 0.2 to 0.38 for a j_w/u_c value of 1.09. All values recorded were less than the voids ratio at which air transport is possible, hence it is postulated that a voids ratio of 0.42 is the maximum that is possible for bubbly flow regimes.

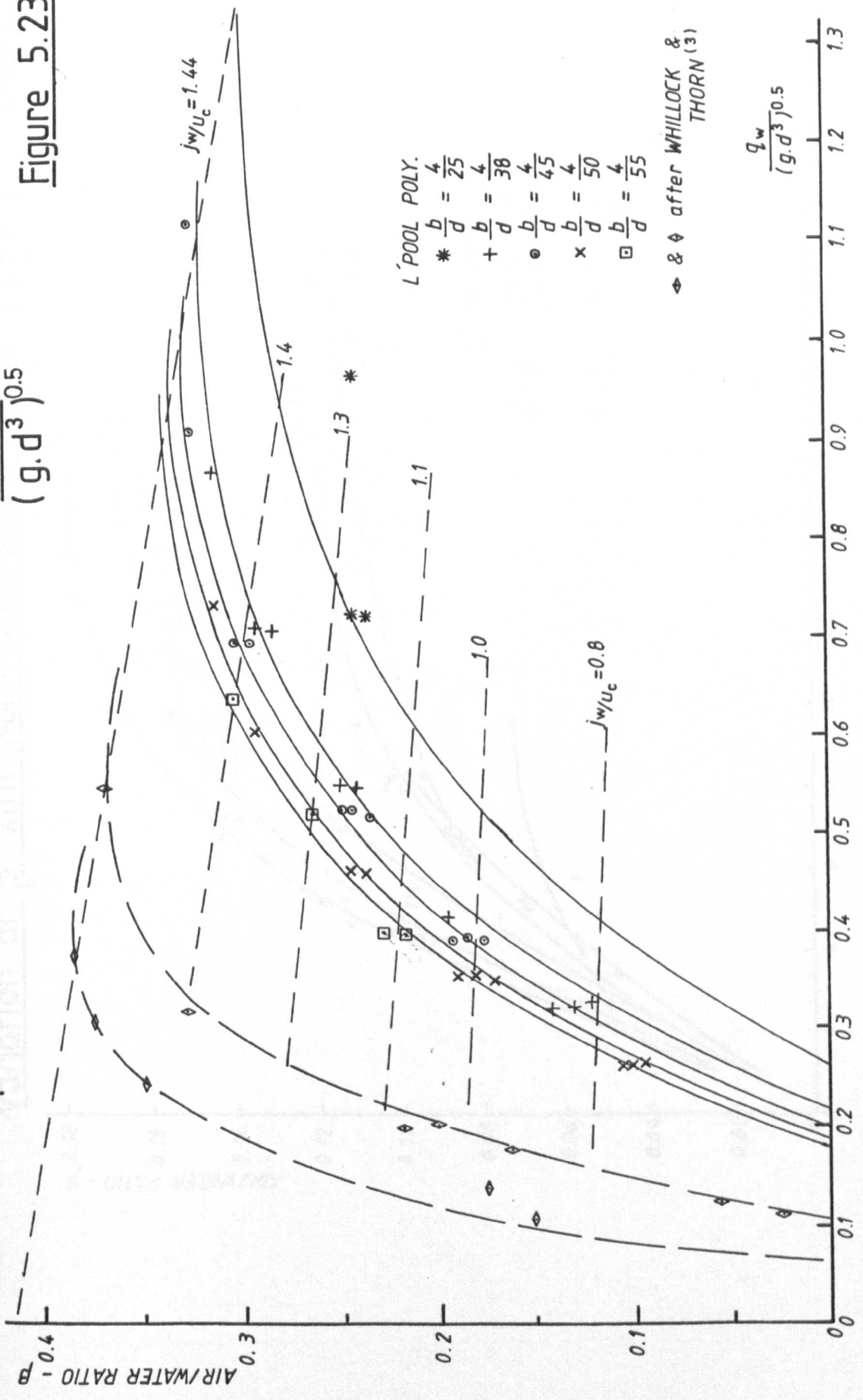
Using 4.1.10a with $\alpha = 0.42$ and the condition for maximum flow ratio as $j_w/u_c = 1.44$, it is apparent that β cannot exceed 0.43, which is in reasonable agreement with the value of 0.42 derived from statistical analysis of the raw data as plotted in Fig. 5.9.

Fig. 5.23 is plotted for the rectangular column dropshaft data on a similar basis to Fig. 5.21 for the circular shaft. It can be seen that the family of curves for air/water ratio plotted against the Froude dimensionless group at different values of $\frac{b}{d}$, is contained within an envelope formed by the curve $j_w/u_c = 1.44$. This curve intersects the air/water ratio axis to give a peak value of approximately 0.41.

The variation of air/water ratio with the effective droplength non-dimensional group $\frac{L - zt}{D}$, for each pipe diameter, and hence constant values of $\frac{b}{D}$, is plotted as a series of curves in Fig. 5.24. Each curve represents a

Variation of β with Non-Dimensional Group $\frac{q_w}{(g.d^3)^{0.5}}$ - Rectangular shafts

Figure 5.23



L'POOL POLY.

- * $\frac{b}{d} = \frac{4}{25}$
- + $\frac{b}{d} = \frac{4}{38}$
- o $\frac{b}{d} = \frac{4}{45}$
- x $\frac{b}{d} = \frac{4}{50}$
- $\frac{b}{d} = \frac{4}{55}$

\diamond & \square after WHILLOCK & THORN (3)

Variation of β with Non-Dimensional Group $\left(\frac{L-z_t}{D}\right)$

Figure 5.24

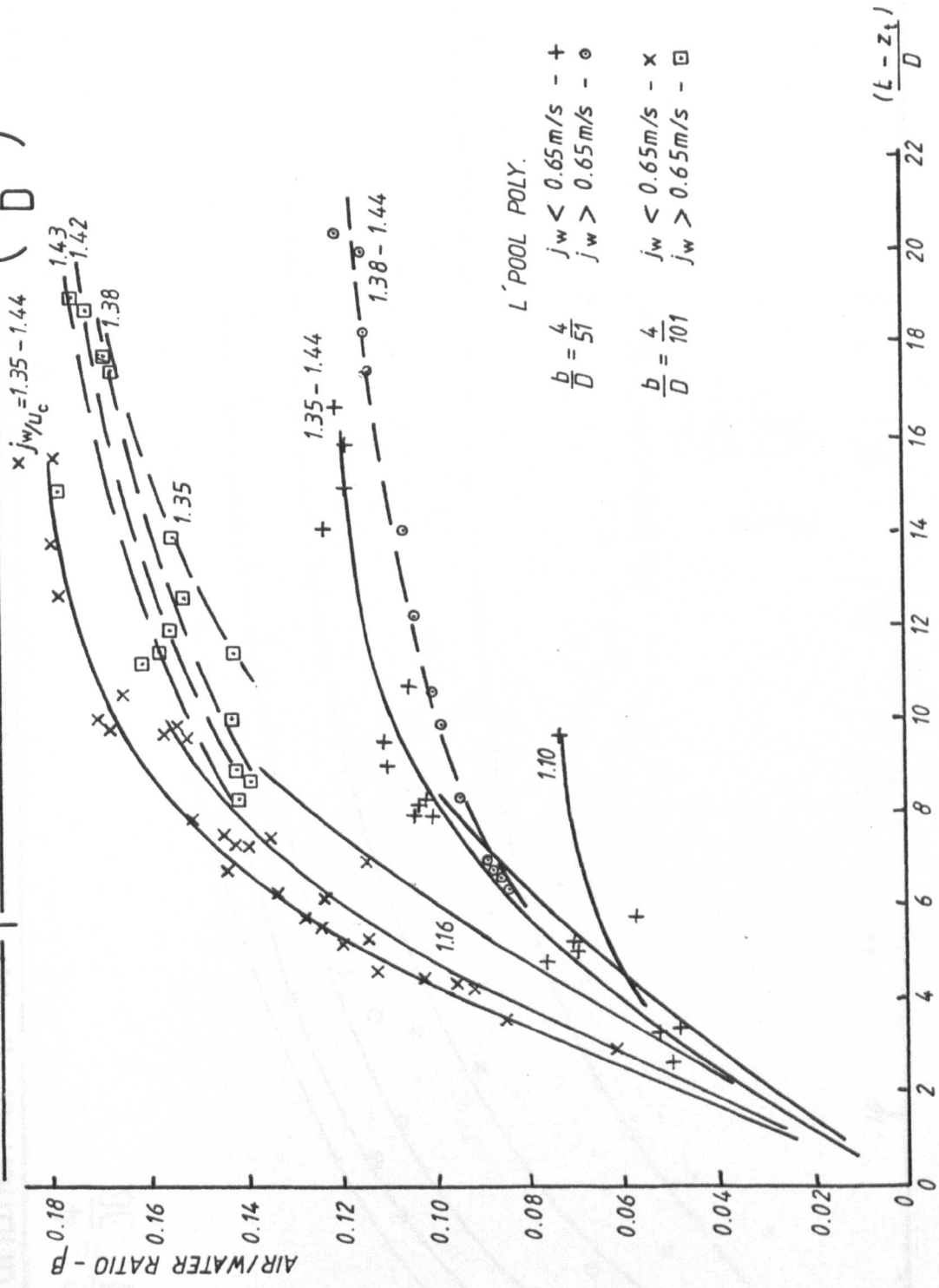
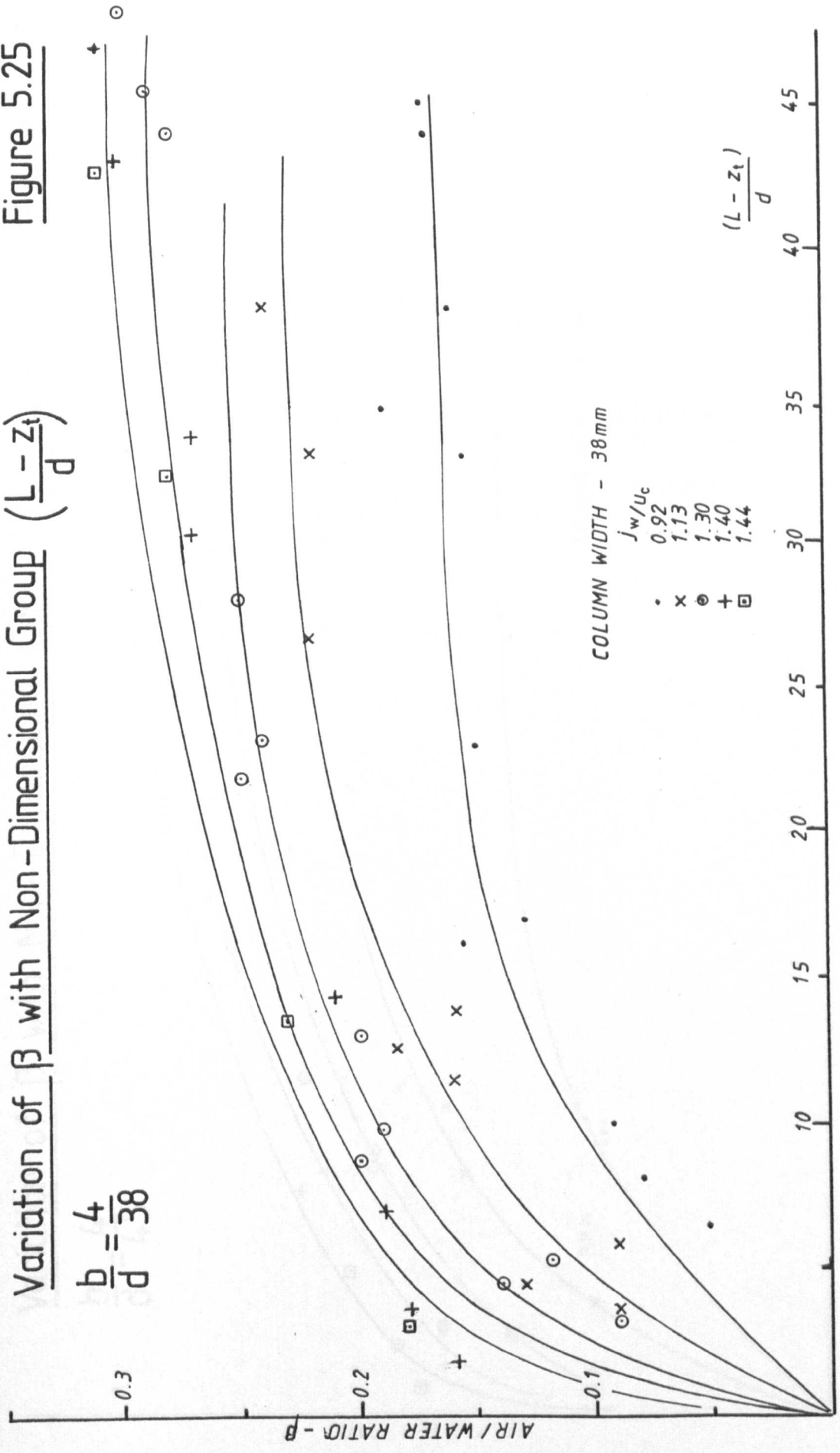


Figure 5.25

Variation of β with Non-Dimensional Group $(\frac{L-z_t}{d})$

$$\frac{b}{d} = \frac{4}{38}$$



Variation of β with Non-Dimensional Group $\left(\frac{L-z_t}{d}\right)$

Figure 5.26

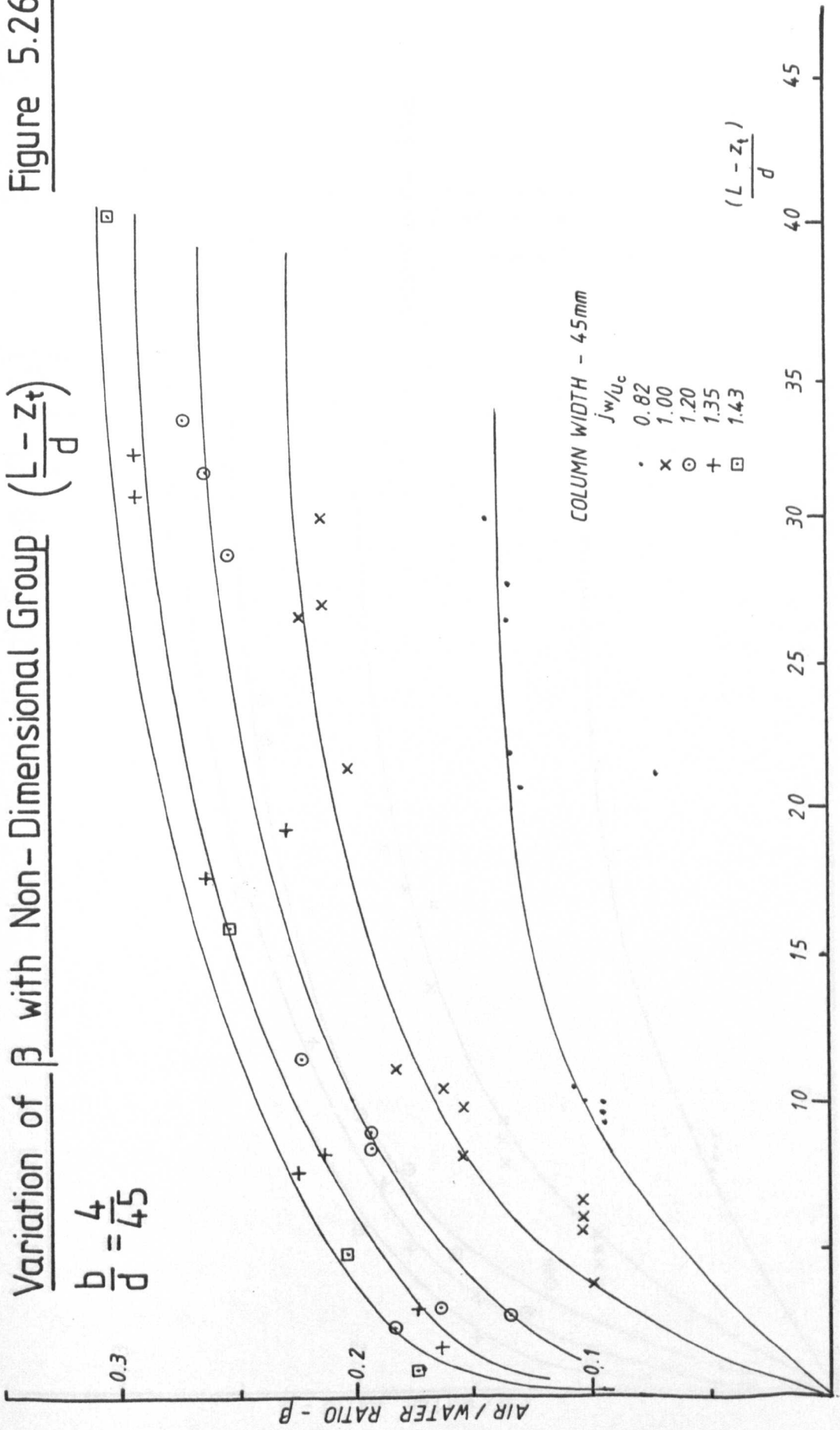
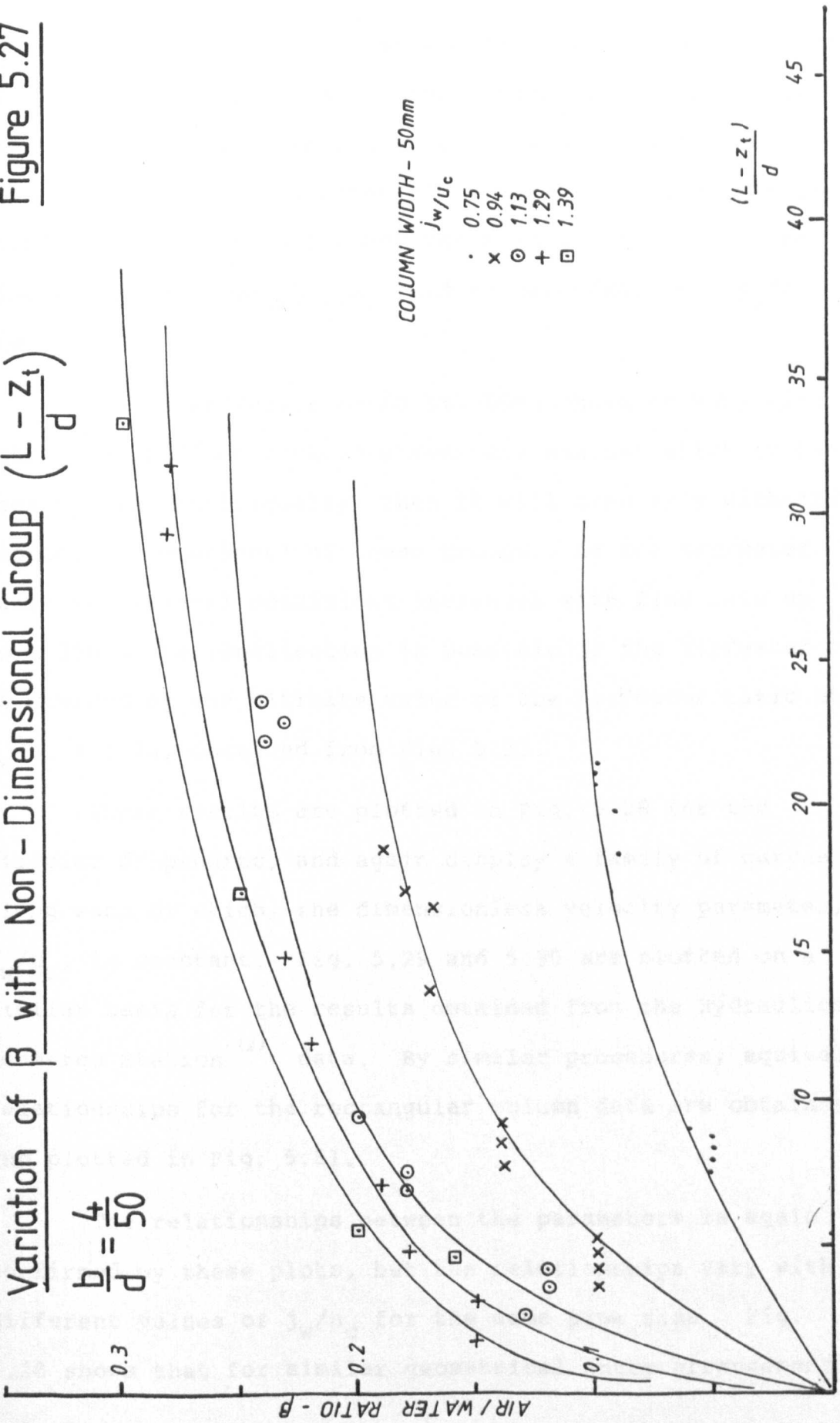


Figure 5.27

Variation of β with Non-Dimensional Group $(\frac{L-z_t}{d})$

$$\frac{b}{d} = \frac{4}{50}$$



different flow rate, and hence, along each curve the value of j_w/u_c is constant, indicating unique relationships as expected. Similar relationships are indicated by the data from the rectangular columns plotted in Fig. 5.25 to 5.27. These show that the air/water ratio is a function of the dimensionless group $\frac{L - z_t}{D}$ and is dependant upon j_w/u_c and $\frac{b}{d}$.

As the air/water ratio has been shown to vary with both sets of dimensionless parameters against which it has been plotted individually, then it will also vary with the product (or quotient) of these groups. As the air/water ratio at terminal conditions increases with flow rate up to a limit, rationalisation is possible if the air/water ratio is divided by the ultimate value of the air/water ratio at $j_w/u_c = 1.44$, obtained from Fig. 5.21.

These results are plotted in Fig. 5.28 for the circular dropshafts, and again display a family of curves along each of which, the dimensionless velocity parameter, j_w/u_c , is constant. Fig. 5.29 and 5.30 are plotted on a similar basis for the results obtained from the Hydraulics Research Station ⁽²⁾ data. By similar procedures, equivalent relationships for the rectangular column data are obtained and plotted in Fig. 5.31.

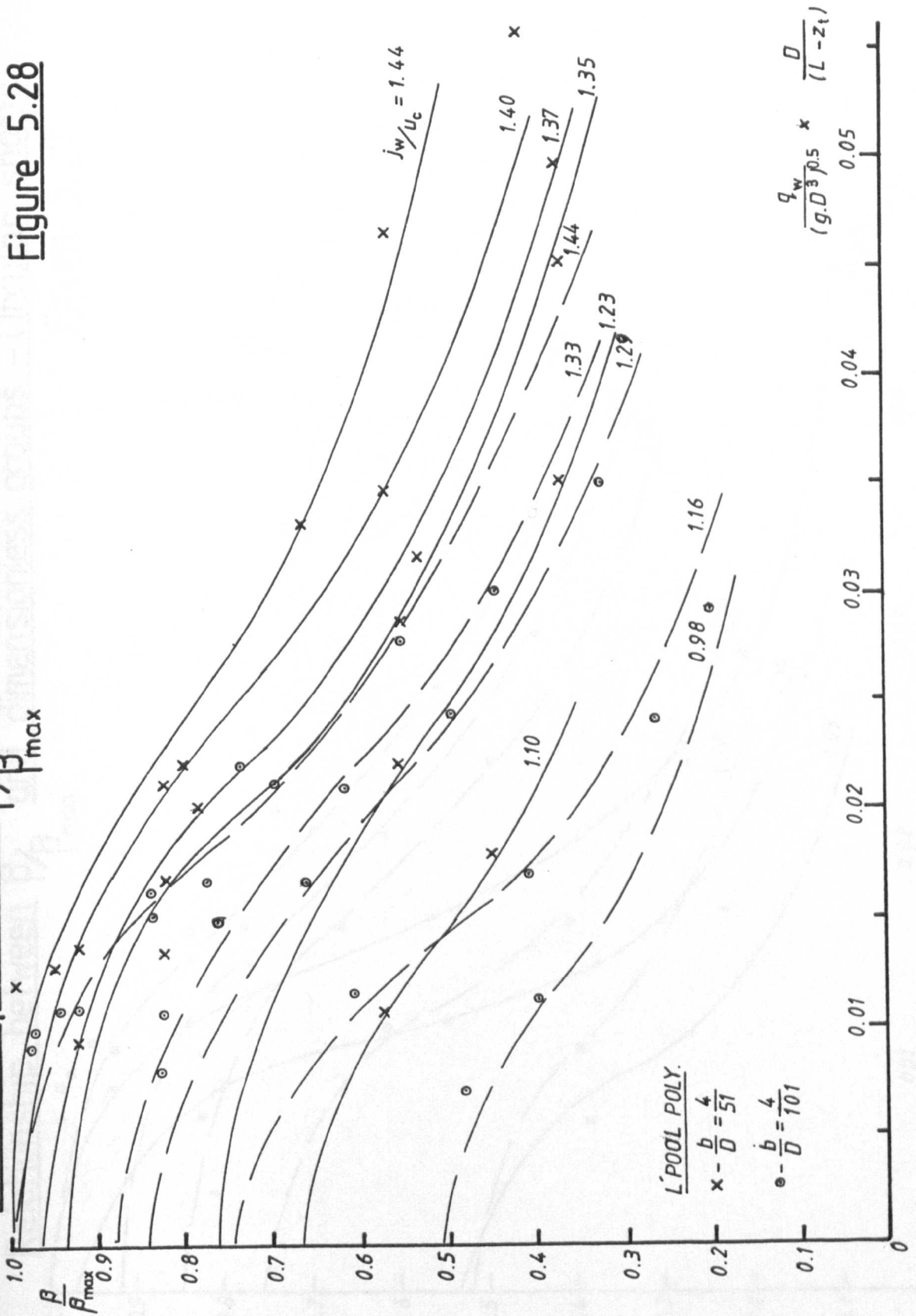
The relationships between the parameters is again confirmed by these plots, but the relationships vary with different values of j_w/u_c for the same pipe size. Fig. 5.28 shows that for similar geometrical entry arrangements

to the dropshaft, the relationship varies with pipe diameter; the curves of equal dimensionless velocity do not coincide. If the results for equal pipe diameters, but different geometrical inlet conditions, are compared, as in Fig. 5.29, it is apparent that no direct comparisons can be made. Data plotted in Fig. 5.30 for pipes of 152mm and 305mm diameter, confirm the deductions derived from Fig. 5.28, that direct relationships do not exist between geometrically similar arrangements of differing scale.

It is evident that although the parameters Q, D, d and L have been varied, and the effects on the air entrainment ratio recorded, the bubble diameter has not been changed to any appreciable extent. Some variation may have occurred due to variation in water temperature, which, whilst recorded, was not controlled, and is not considered significant.

The experimental investigation of the voids ratio in the two-phase downward flow condition, indicated that the relative velocity between the phases depended on the velocity of the predominant phase. This indicates that the drag force exerted on the individual bubbles would vary with this velocity. It is possible for each bubble to become relatively distorted in shape, and hence the individual bubbles can move at different relative velocities at the same void ratio in the two-phase condition. This shows that the inability to model the bubble sizes has an effect in the complete dimensional analysis of the air entraining parameters.

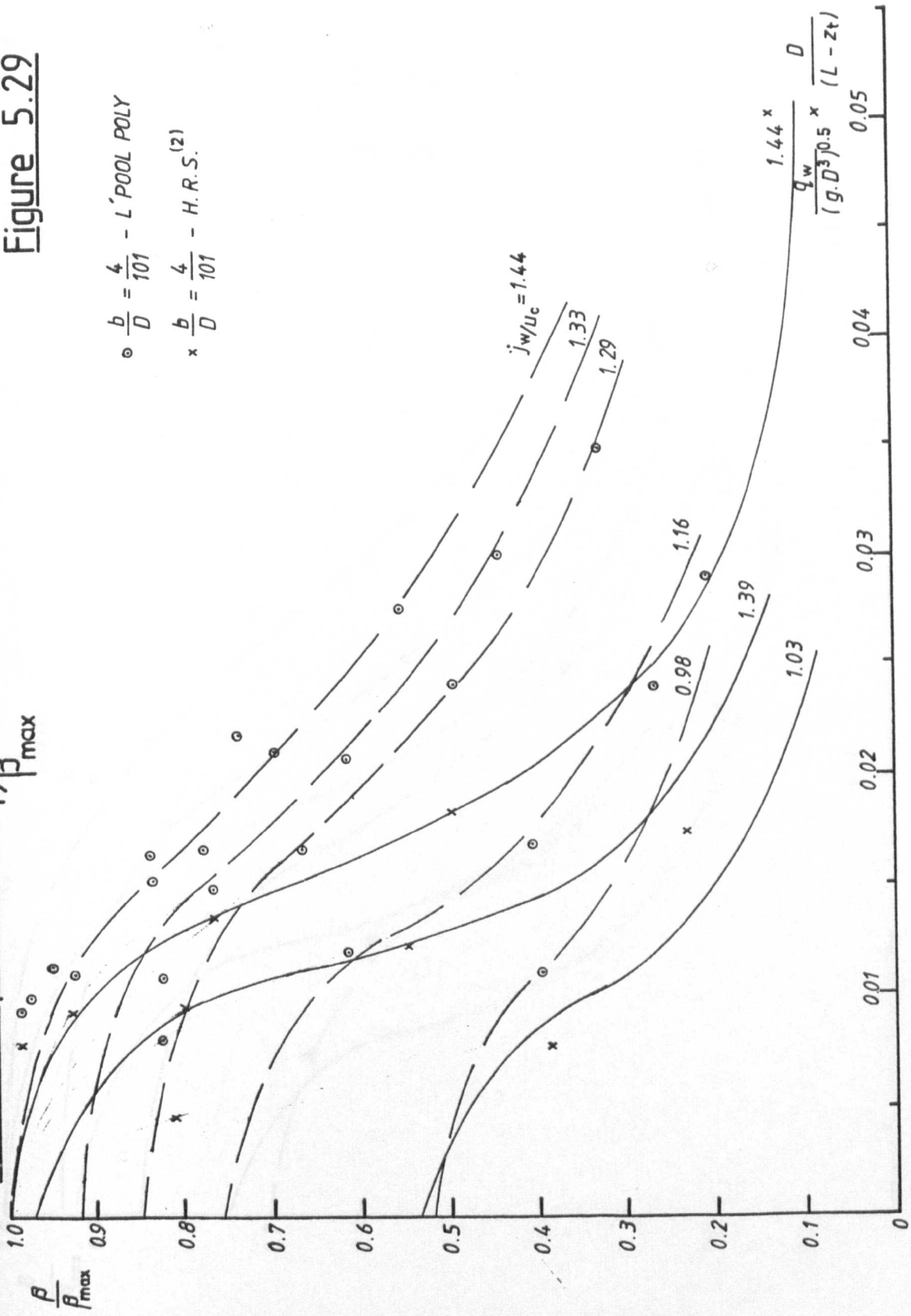
Relationship between β/β_{\max} and dimensionless groups - Circular shafts
 Figure 5.28



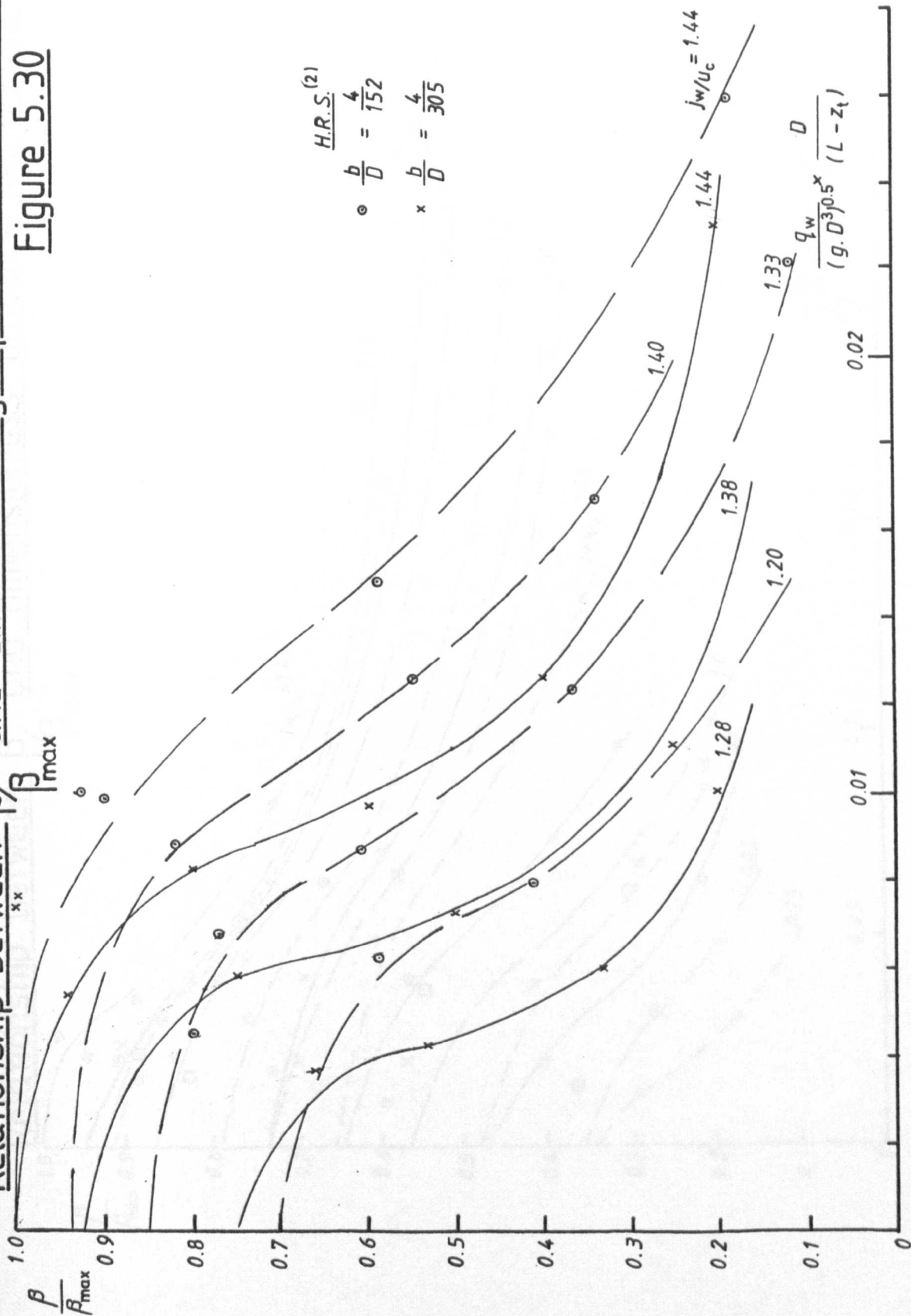
Relationship between β/β_{max} and dimensionless groups - Circular shafts

Figure 5.29

$\circ \frac{b}{D} = \frac{4}{101} - L'POOL \text{ POLY}$
 $\times \frac{b}{D} = \frac{4}{101} - H.R.S. (2)$

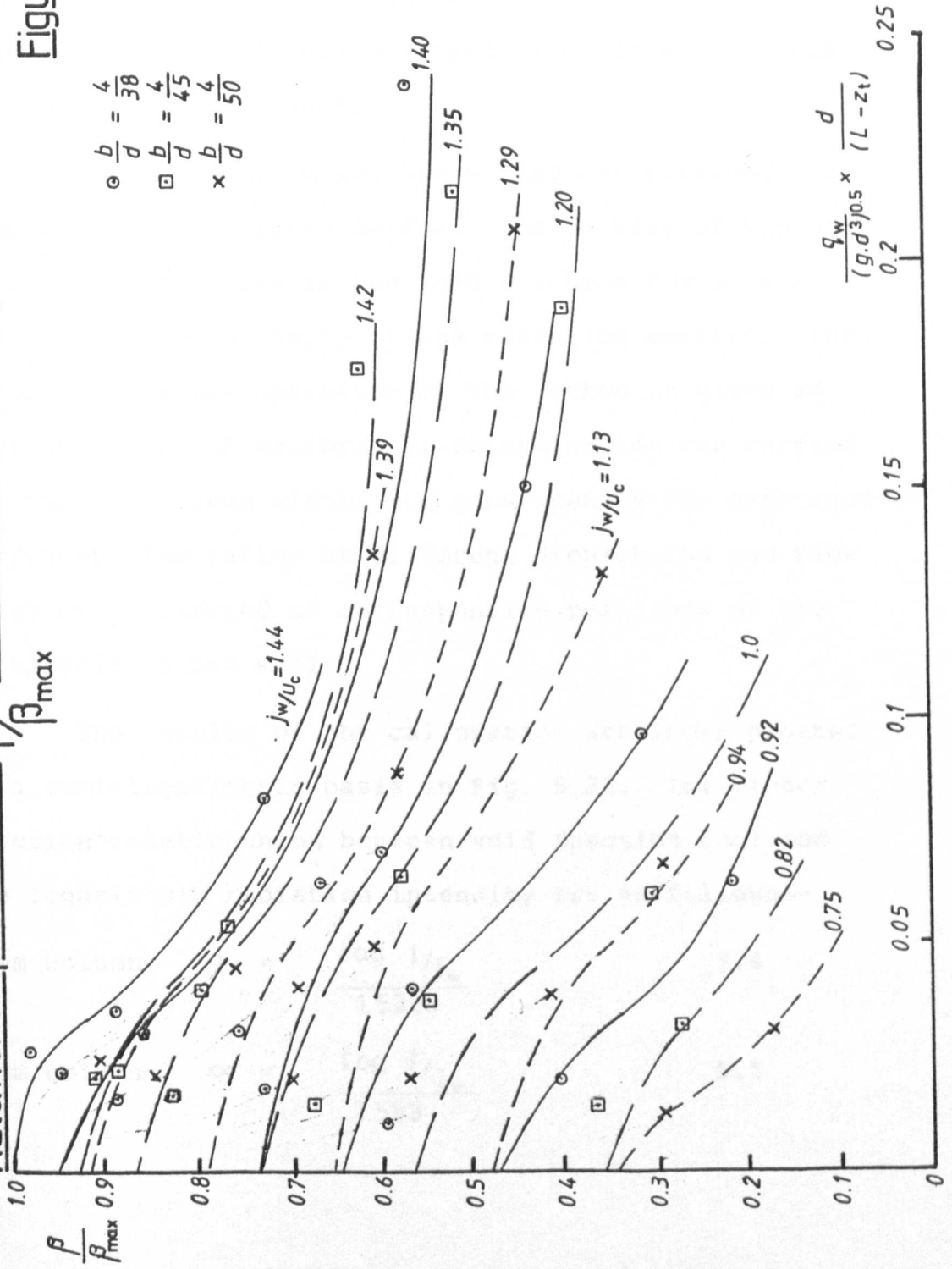


Relationship between β_x and dimensionless groups - Circular shafts
 Figure 5.30



Relationship between β/β_{\max} and dimensionless groups - Rectangular shafts

Figure 5.31



5.5. Void Fraction Determination

Since the bubble emulsions in the shafts showed no visual variation in appearance, yet the measured flow ratios (Q_a/Q_w) differed, the void fraction or air content of the shaft was measured directly using a gamma-ray absorption technique.

The calibration for the method was obtained using a specifically designed device. The density of the air/water mixture, which is the void fraction (α), was related to the intensity of the radiation emitted. The theory behind the operation of the method is given in section 4.2.2. A calibration determination was carried out for two column widths and consequently the experimental air/water flow ratios at different droplengths and flow rates were measured at corresponding positions of the adjustable column wall.

The results of the calibration are shown plotted on a semi-logarithmic basis in Fig. 5.32. The linear function relationships between void fraction (α) and the logarithmic radiation intensity are as follows:-

38mm column	$\alpha = \frac{\log I/I_w}{1.5325}$	5.4
45mm column	$\alpha = \frac{\log I/I_w}{1.553}$	5.5

where I = intensity of radiation at counter
 I_w = intensity of radiation when shaft
contains 100% water

The tests carried out as described previously on the rectangular column dropshaft were repeated for the 38mm and 45mm column widths. The gamma-ray absorption technique was used to determine the void fraction for each measurement of air/water flow ratio. The recirculation zone was not permitted to impinge upon the gamma-ray beam during the tests since this region contains a higher air content which would be misleading. The results obtained are tabulated in Tables 5.7 and 5.8, together with the experimentally determined void fraction obtained from the calibration for the respective column. The absolute air and water velocities and relative velocity are also calculated from the equations given in section 4.2

$$\text{Absolute air velocity} \quad v_a = \frac{Q_a}{A\alpha} \quad 5.6$$

$$\text{Absolute water velocity} \quad v_w = \frac{Q_w}{A(1-\alpha)} \quad 5.7$$

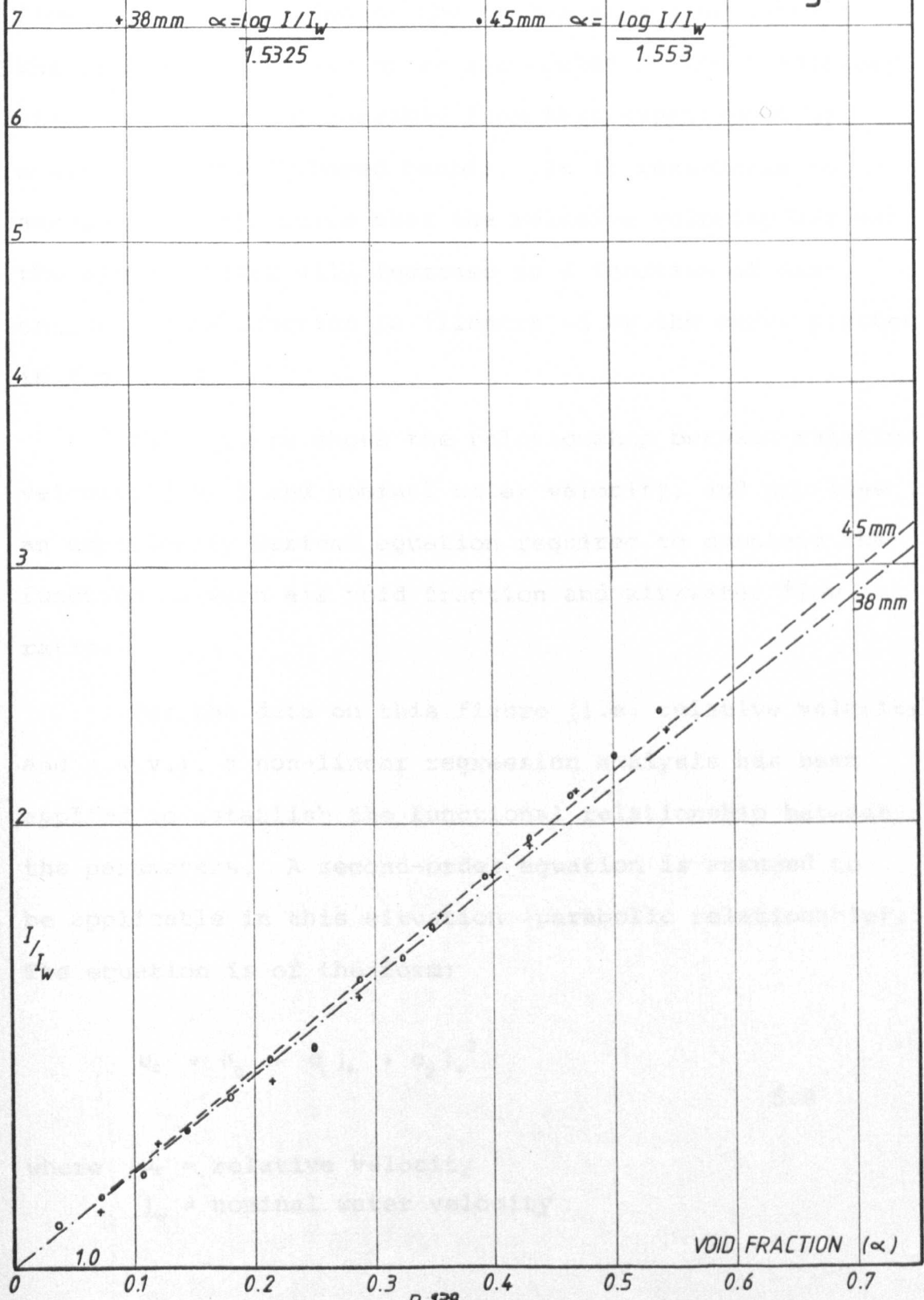
$$\text{Relative velocity} \quad u_c = v_w - v_a \quad 5.8$$

The absolute air and water velocities are plotted in Fig.5.33. The apparent result from this plot is that the absolute water velocity required to transport air is 0.24 m/s. This value is in agreement with that obtained by previous investigators.

Fig. 5.33 indicates that a non-linear relationship exists between the absolute air and water velocities as

Calibration curves for determination of Void Fraction Gamma-ray absorption technique

Fig. 5.32



determined by the void fraction measurements. It would appear that the curve attains a limiting air velocity for increase in water velocity. It is thought that this occurs when the stable bubble swarm changes to a different flow regime consisting of the random slug flow pattern. The drag force exerted on an air pocket in the transitory state will vary considerably from that experienced by a single spheroid shaped bubble. It is reasonable to assume from this curve that the relative velocity between the air and water will increase as a function of discharge. This function is illustrated by the curve plotted in Fig. 5.34.

This figure shows the relationship between relative velocity (u_c) and nominal water velocity, and provides an empirically derived equation required to complete the function between air void fraction and air/water flow ratio.

For the data on this figure (i.e. relative velocity and n.w.v.), a non-linear regression analysis has been applied to establish the functional relationship between the parameters. A second-order equation is assumed to be applicable in this situation (parabolic relationship). The equation is of the form;

$$u_c = a_0 + a_1 j_w + a_2 j_w^2$$

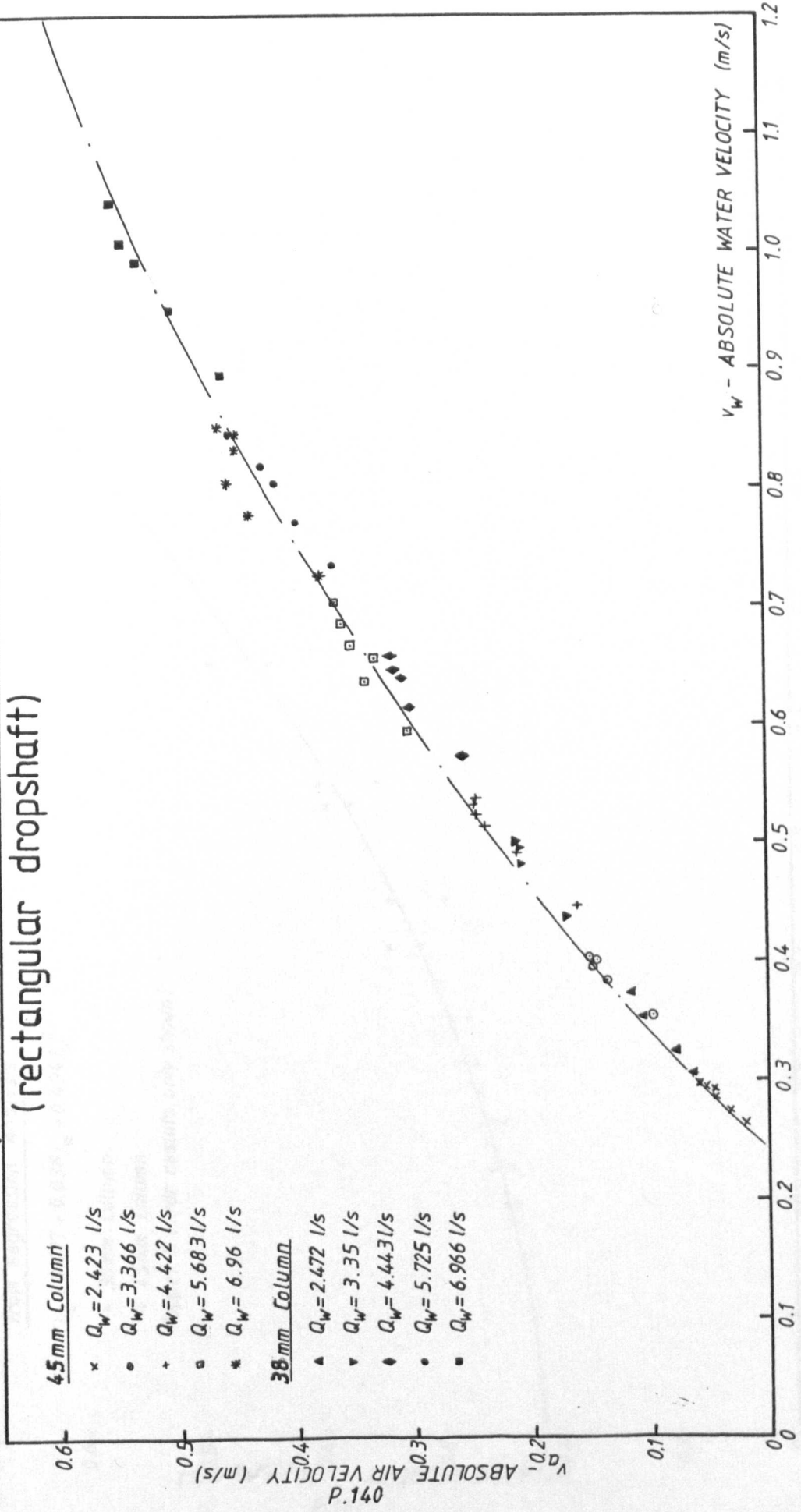
5.9

where u_c = relative velocity
 j_w = nominal water velocity

Relationship between Absolute air & water velocities
 (rectangular dropshaft)

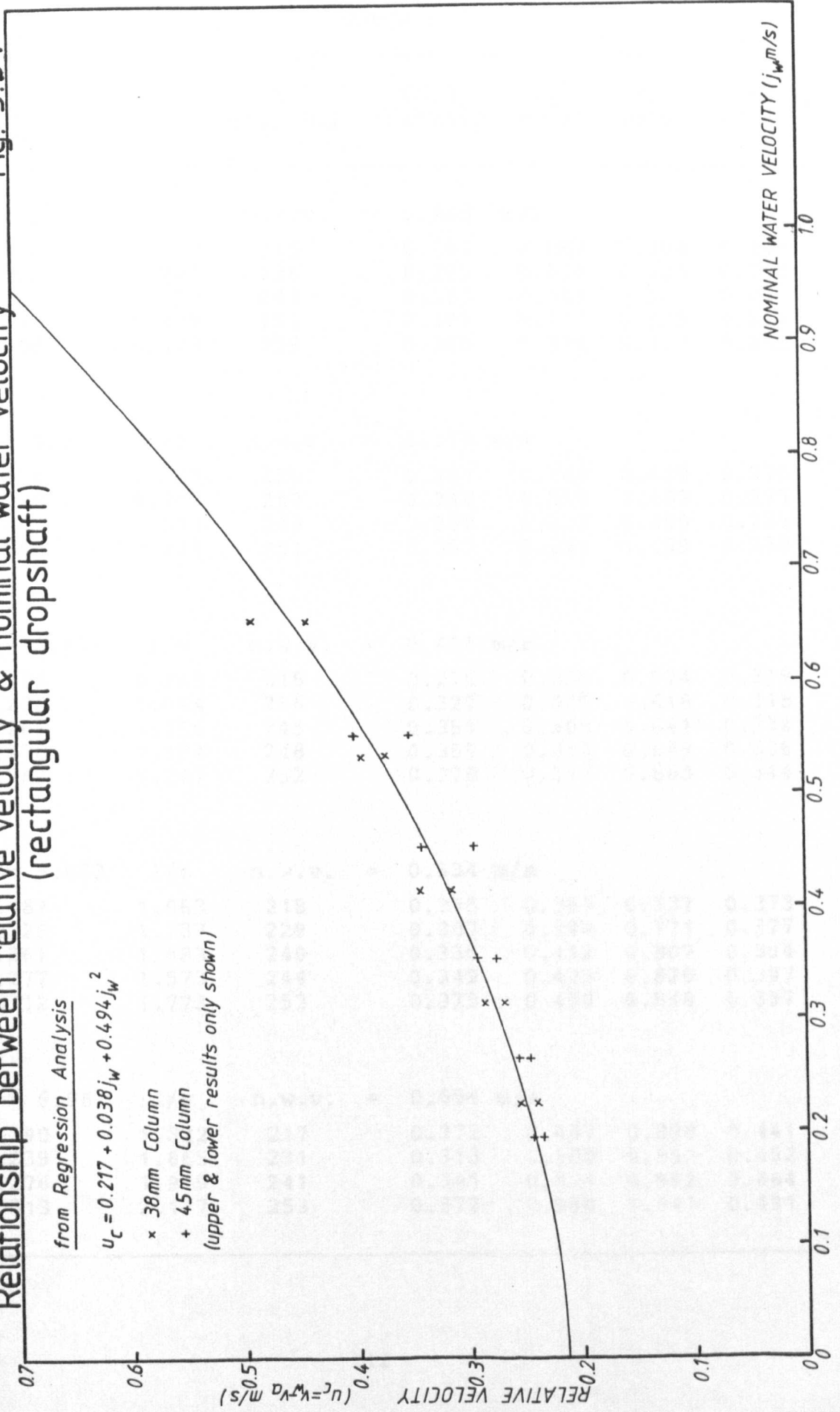
Figure 5.33

- | | |
|--------------------|-------------------|
| 45mm Column | |
| x | $Q_w = 2.423$ l/s |
| o | $Q_w = 3.366$ l/s |
| + | $Q_w = 4.422$ l/s |
| ◊ | $Q_w = 5.683$ l/s |
| * | $Q_w = 6.96$ l/s |
| 38mm Column | |
| ▲ | $Q_w = 2.472$ l/s |
| ▼ | $Q_w = 3.35$ l/s |
| ◆ | $Q_w = 4.443$ l/s |
| • | $Q_w = 5.725$ l/s |
| ◼ | $Q_w = 6.966$ l/s |



Relationship between relative velocity & nominal water velocity
 (rectangular dropshaft)

Fig. 5.34



Results of Void Fraction Determination by Radio-isotope
Measurements: 38mm Column Width

Table 5.7

$\frac{Q_a}{Q_w}$	Q_a (l/s)	I (c.p.s.)	Void Fraction	v_a (m/s)	v_w (m/s)	$u_c = v_w - v_a$ (m/s)
$Q_w = 2.423$	1/s	n.w.v.	= 0.228	m/s		
0.070	0.170	210	0.251	0.064	0.304	0.241
0.102	0.247	226	0.299	0.078	0.325	0.248
0.161	0.390	245	0.351	0.104	0.351	0.247
0.173	0.419	251	0.367	0.107	0.355	0.248
0.195	0.473	259	0.388	0.114	0.373	0.258
$Q_w = 3.366$	1/s	n.w.v.	= 0.316	m/s		
0.150	0.505	220	0.281	0.169	0.439	0.270
0.228	0.767	243	0.346	0.208	0.483	0.275
0.241	0.811	249	0.362	0.211	0.495	0.285
0.245	0.825	251	0.367	0.211	0.499	0.288
$Q_w = 4.422$	1/s	n.w.v.	= 0.416	m/s		
0.168	0.745	218	0.275	0.255	0.574	0.319
0.236	1.044	236	0.327	0.300	0.618	0.318
0.261	1.155	245	0.351	0.309	0.641	0.332
0.270	1.194	248	0.359	0.313	0.649	0.336
0.282	1.247	252	0.370	0.317	0.660	0.344
$Q_w = 5.683$	1/s	n.w.v.	= 0.534	m/s		
0.187	1.063	218	0.275	0.363	0.737	0.373
0.226	1.287	229	0.307	0.394	0.771	0.377
0.261	1.483	240	0.338	0.412	0.807	0.394
0.277	1.573	244	0.349	0.423	0.820	0.397
0.312	1.773	252	0.370	0.450	0.848	0.397
$Q_w = 6.96$	1/s	n.w.v.	= 0.654	m/s		
0.190	1.322	217	0.272	0.457	0.898	0.441
0.239	1.665	231	0.313	0.500	0.952	0.452
0.276	1.919	241	0.341	0.529	0.992	0.464
0.313	2.177	253	0.372	0.550	1.041	0.491

Results of Void Fraction Determination by Radio-isotope Measurement: 45mm Column Width

Table 5.8

$\frac{Q_a}{Q_w}$	Q_a (1/s)	I (c.p.s.)	Void Fraction	v_a (m/s)	v_w (m/s)	$u_c = v_w - v_a$ (m/s)
$Q_w = 2.472$ 1/s n.w.v. = 0.196 m/s						
0.070	0.062	405	0.259	0.019	0.265	0.246
0.049	0.121	425	0.290	0.033	0.276	0.243
0.070	0.173	444	0.318	0.043	0.287	0.244
0.088	0.218	456	0.335	0.052	0.295	0.243
0.102	0.252	459	0.339	0.059	0.297	0.238
0.077	0.190	451	0.328	0.046	0.292	0.246
$Q_w = 3.35$ 1/s n.w.v. = 0.266 m/s						
0.094	0.315	402	0.254	0.098	0.357	0.258
0.156	0.523	436	0.307	0.135	0.384	0.249
0.184	0.616	452	0.330	0.148	0.397	0.249
0.192	0.643	460	0.341	0.150	0.404	0.254
0.188	0.630	459	0.339	0.147	0.402	0.255
$Q_w = 4.443$ 1/s n.w.v. = 0.353 m/s						
0.097	0.431	378	0.214	0.160	0.449	0.289
0.168	0.746	420	0.282	0.210	0.492	0.282
0.212	0.942	442	0.315	0.237	0.515	0.278
0.228	1.013	451	0.328	0.245	0.525	0.280
0.236	1.049	459	0.339	0.246	0.534	0.288
0.240	1.066	463	0.345	0.245	0.539	0.294
$Q_w = 5.725$ 1/s n.w.v. = 0.454 m/s						
0.159	0.910	393	0.240	0.301	0.597	0.296
0.215	1.231	424	0.288	0.339	0.638	0.298
0.225	1.288	439	0.310	0.330	0.658	0.328
0.247	1.414	446	0.321	0.350	0.669	0.319
0.267	1.529	459	0.339	0.358	0.687	0.329
0.283	1.620	470	0.355	0.362	0.704	0.342
$Q_w = 6.966$ 1/s n.w.v. = 0.553 m/s						
0.163	1.140	393	0.240	0.377	0.728	0.351
0.226	1.581	425	0.290	0.433	0.779	0.346
0.254	1.777	440	0.312	0.452	0.804	0.352
0.271	1.896	457	0.337	0.447	0.834	0.388
0.280	1.959	465	0.348	0.447	0.848	0.401
0.290	2.029	467	0.350	0.460	0.851	0.391

The method of least squares is applied to estimate the regression parameters a_0 , a_1 and a_2 . The resultant equation is as follows:-

$$u_c = 0.217 + 0.038j_w + 0.494j_w^2$$

5.9a

This equation is used to calculate corresponding values of relative velocity which are then utilised in equation 4.2.9 to give computed values for the air void fraction. These results are tabulated in Table 5.9 for both 38mm and 45mm column widths.

$$\alpha^2 \frac{u_c \cdot A}{Q_w} + \alpha \left(1 + \beta - \frac{u_c \cdot A}{Q_w}\right) - \beta = 0 \quad 4.2.9$$

$$\alpha = \frac{-(1 + \beta - \frac{u_c}{j_w}) \pm \left[(1 + \beta - \frac{u_c}{j_w})^2 + 4 \cdot \beta \cdot \frac{u_c}{j_w} \right]^{0.5}}{2 \frac{u_c}{j_w}} \quad 4.2.9a$$

where α = void fraction
 u_c = relative velocity
 β = air/water flow ratio
 Q_w = discharge
 A = cross-sectional area of flow
 j_w = nominal water velocity

Equation 4.2.10 derived in Chapter 4 and plotted in Fig. 4.2.9 to illustrate the significance of variations in the relative velocity, is reproduced in Fig. 5.35. The experimental values of void fraction and air/water ratio are plotted on the graph and show good correlation

Experimental values of Q_{a0}/Q_w against Void Fraction
 (rectangular dropshaft)

Figure 5.35

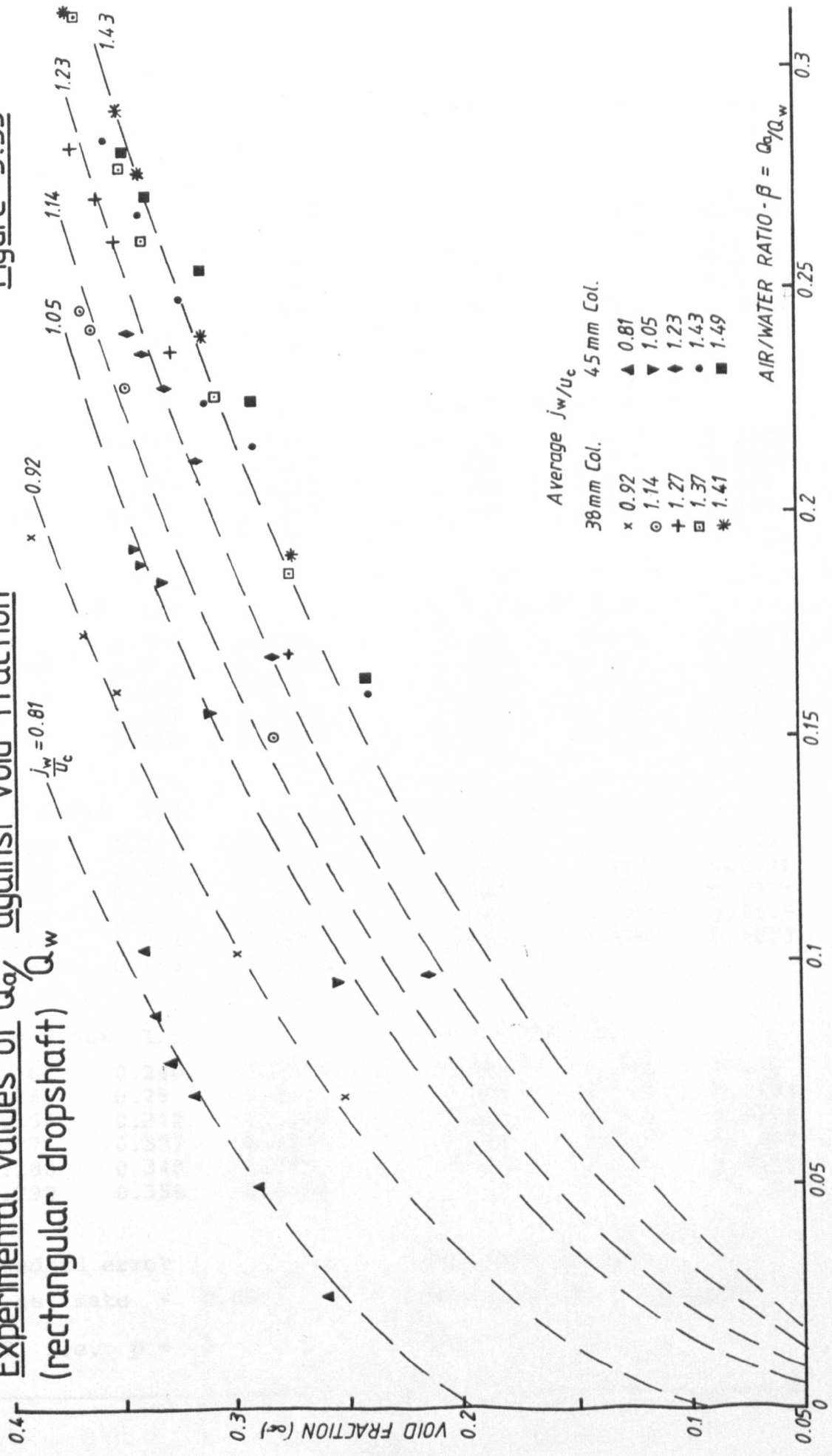


Table 5. 9

45mm	expt. α	calc. α	38mm	expt. α	calc. α
$Q_w = 2.472$ 1/s			$Q_w = 2.423$ 1/s		
0.025	0.259	0.2537	0.070	0.251	0.2675
0.049	0.290	0.2905	0.102	0.299	0.3047
0.070	0.318	0.3162	0.161	0.351	0.3568
0.088	0.335	0.3352	0.173	0.367	0.3657
0.102	0.339	0.3481	0.195	0.388	0.3809
0.077	0.328	0.3236			
$Q_w = 3.35$ 1/s			$Q_w = 3.366$ 1/s		
0.094	0.254	0.2587	0.150	0.281	0.2872
0.156	0.307	0.3208	0.228	0.346	0.3484
0.184	0.330	0.3249	0.241	0.362	0.357
0.192	0.341	0.3488	0.245	0.367	0.3596
0.188	0.339	0.346			
$Q_w = 4.443$ 1/s			$Q_w = 4.422$ 1/s		
0.097	0.214	0.2163	0.168	0.275	0.2474
0.168	0.282	0.3246	0.236	0.327	0.3273
0.228	0.328	0.336	0.261	0.351	0.3441
0.236	0.339	0.3416	0.270	0.359	0.3496
0.240	0.345	0.3442	0.282	0.370	0.357
$Q_w = 5.725$ 1/s			$Q_w = 5.683$ 1/s		
0.159	0.240	0.26	0.187	0.275	0.277
0.215	0.288	0.3064	0.226	0.307	0.3076
0.225	0.310	0.3137	0.261	0.338	0.3314
0.247	0.321	0.3291	0.277	0.349	0.3415
0.267	0.339	0.3423	0.312	0.370	0.3625
0.283	0.355	0.3522			
$Q_w = 6.966$ 1/s			$Q_w = 6.96$ 1/s		
0.163	0.240	0.2557	0.190	0.272	0.276
0.266	0.29	0.307	0.239	0.313	0.3133
0.254	0.312	0.3265	0.276	0.341	0.3376
0.271	0.337	0.3376	0.290	0.351	0.3467
0.280	0.348	0.3433	0.313	0.372	0.3599
0.290	0.350	0.3494			
Standard error of estimate = 0.0076			Standard error of estimate = 0.0072		
n-3 i.e. p = 3			n-3 i.e. p = 3		

with the theoretically predicted curves. It is considered that this validates the absorption technique used in the determination of air content.

5.6 Review of previous investigations

The characteristic air demand curves obtained for the vortex-entry dropshaft arrangement display a similarity to those presented by H.R.S.⁽²⁾ The initial peak is attributed to the presence of the swirl component of velocity in the annular flow in the shaft. The upturn in air demand recorded at droplengths approaching the end of the shaft can be explained by "end effects", i.e. the recirculation zone of very high air content extending beyond the outlet to the shaft.

These curves are dissimilar to the results presented by Laushey and Mavis⁽⁹⁾ and Viparelli⁽¹⁰⁾. In the former case, the relationship is formulated to be a linear function between air/water ratio and droplength. This is an oversimplification of the case. For spiral entry arrangements, the air demand is shown to commence immediately from the point of entry and do not exhibit any early peak in air demand. The upturn in air/water ratio at longer droplengths is attributed to the "end effect" condition.

Viparelli⁽¹⁰⁾ presents a relationship predicting air entrainment as a function of free fall height/pipe diameter. He argues that air entrainment depends on the flow both upstream and downstream of the hydraulic jump in the shaft. The analysis is based on the assumption that the air core

attains the same velocity as the water film on striking the standing water in the shaft. Thus, the volume of air entrained is the product of the air core area and the water velocity. This proposition, however, does not take into account the re-circulation of air above the ambient water surface due to air rejection in this zone.

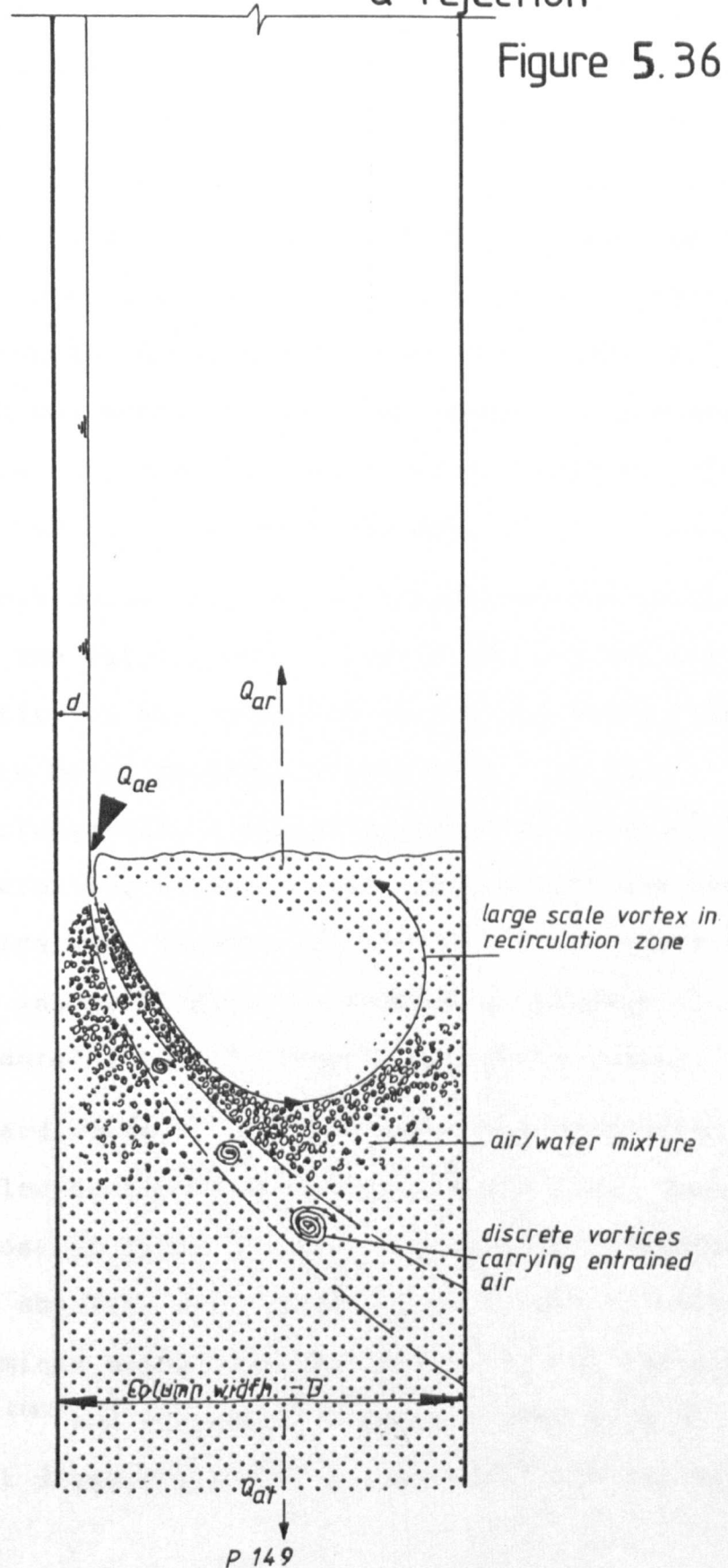
This investigation identifies the differences between the initial air entrained and the net air transported by the downward flow of water. It is only in recent years that investigators have begun to appreciate that air rejection occurs at the ambient water surface from the volume of air initially entrapped. Whillock and Thorn⁽³⁾ develop Nuttall's⁽²⁷⁾ work in estimating the effect of air rejection in spiralling water. No attempts were made in this study to analyse this effect but from observations, it was evident that rejection does occur in vertical dropshafts.

Ervine and Kolkman⁽¹¹⁾ describe a mechanism for initial entrainment and rejection at the ambient water surface (see Fig. 5.36). The water film impinges into the standing water creating a roller action; discrete vortices may be established and a large scale vortex created in the re-circulation zone. This action would enable air to escape back into the air core through the ambient surface.

It is reasonable to assume that this mechanism is present in the circular shafts as well as the rectangular column. It is considered that the air rejection process is greater in a circular shaft, or net air transported is less, due to the additional swirl component of velocity

Proposed mechanism for air entrainment & rejection

Figure 5.36



present in the flow imparted by the entrance conditions.

Hack ⁽³⁹⁾ defined different stages of air entrainment in a circular dropshaft and developed a relationship for predicting entrainment rates for the annular flow regime. Analysis of the entrainment patterns in the bubbly regime and with two-phase flow in the shaft was not undertaken by Hack. Study of the annular flow regime did not form part of the current investigation, but the condition was permitted in several instances during the experimental stages, e.g., when droplength was equal to the total length of the shaft. The resulting net air demand was considerably higher than those recorded for the other flow regimes.

It is considered that the air demand is due to the drag effect of the falling water film on the central air core; the quantity of air entrained within the water film is considered to be of negligible magnitude. In the vortex-entry arrangement, a swirl component of velocity is present, thus creating a centripetal force within the water film. This force will inhibit the ability of the water film to entrain air into its mass, there being a tendency to displace air radially inwards towards the shaft centre.

Curtet and Djonin ⁽⁵⁾ investigated the transition from zero airflow to a positive airflow condition. Their results and those of Thorn ⁽⁶⁾ show the airflow threshold to occur at an absolute water velocity of 0.24 m/s, corresponding to a nominal water velocity of 0.13 m/s in the lower shaft. Wisner ⁽¹⁴⁾ and Marquetet ⁽⁴⁰⁾ experimented with a number of shaft diameters and also identified the air flow

threshold at nominal water velocities of about 0.13 m/s. In the current investigation, a nominal velocity of 0.14 m/s was determined as the onset of positive air flow. The true water velocity, or interstitial water velocity, at this threshold was computed as 0.222 m/s which compares favourably with Curtet and Djonin. It is evident that the zero airflow/positive airflow threshold is independent of scale and thus constitutes a fundamental dissimilarity in dropshaft models.

A limiting air demand constraint also exists in an air entraining system in dropshafts. The nominal water velocity at which this limit is attained was determined to be approximately 0.65 m/s. If the nominal velocity exceeds this value, there is no significant increase in air/water ratio for increase in discharge. This value of water velocity is approximately twice that of the bubble rise velocity. These results are in close agreement with the conclusions of Whillock and Thorn and Curtet and Djonin.

Whillock and Thorn suggest that the trend of the limiting air/water flow ratio against droplength curve indicates that the air/water ratio is a maximum when the droplength is greater than 3.7m. Dawson and Kalinske⁽⁸⁾ predicted that this maximum is attained when the droplength is between 4.0m and 5.0m. From the current investigation, the limiting value of air/water ratio is attained at droplengths of approximately 3.0m in the rectangular column. In the vortex-entry dropshafts, a limiting droplength is not clearly defined. It is considered that the variance in the droplength for limiting air/water ratio is due to the

configuration of the dropshaft model, e.g., the shaft geometry and entry arrangement. This influences the shape of the jet and consequently the degree and nature of the water film impinging on the standing water surface creating the initial entrainment process.

In recent years, it has become apparent that in vertical dropshafts the rate of air transported by the flowing water is less than the initial air entrained. Ervine and Kolkman present a relationship describing aeration in hydraulic structure which is of the form of a modified Froude relationship. However, several assumptions made to derive this relationship are considered to be inaccurate. In order to obtain a relationship between void ratio and volumetric ratio, the relative velocity between air and water was assumed constant; this is not evident in the voids ratio investigation undertaken in this study. The void ratio was also assumed to be proportional to the upstream air entrainment, however, it was found to be a function of the air transport capabilities of the downward flowing water.

Several investigators have reported the phenomenon of surface entrainment on inclined surfaces and have attempted to establish relationships predicting the factors influencing the mechanisms involved. Hickox⁽³⁶⁾ proposed that the length of film to onset of surface aeration is a function of the flow rate. Applying this relationship to the current investigation, yields a substantially longer distance from inlet before the film becomes wholly turbulent. It is considered there are several other

fundamental parameters involved in the determination of this critical length, e.g. slope, entry velocity and conditions, and bed roughness.

Novak and Cabelka ⁽³⁷⁾ , in analysing the measurements recorded by Hickox, propose that the ratio of critical length (l) to turbulent film thickness (h_{cr}) approximates to 100. In the present investigation, if the calculated length of film to become wholly turbulent (z_t) and the depth of the terminal film thickness (δ) are similarly expressed, the mean value of the ratio in the rectangular column shaft is approximately 100. However, in the vortex-entry circular shafts, the ratio decreases towards 100 as the flow rate increases. It is considered that the omission of any swirl component of velocity from the evaluation of the above parameters produces this trend in the circular shafts.

CHAPTER SIX

CONCLUSIONS

The present state of knowledge for understanding the air entrainment phenomena is insufficient to predict with certainty the performance of any particular arrangement of dropshaft. The scope of this current research investigation covers the theoretical and experimental analyses of air entraining dropshaft models.

6.1 General

The flow regimes observed throughout the operation of the experiments in both forms of the dropshafts (rectangular and circular), were reported in Chapter 5. Summarised they are as follows:

- a) Zero airflow - no net air demand, i.e. all the air entrained is subsequently rejected or retained in an emulsion within the shaft
- b) Positive airflow - bubbles are carried down in an emulsion by the flow of liquid towards the shaft outlet
- c) Slug flow - the bubbles coalesce to form large air pockets which are ejected spasmodically either upwards or downwards through the shaft outlet

In the case of a bubble emulsion being formed, the observed bubble sizes were of the order 3-5mm as reported by previous investigators. The slug regime was noticeably exhibited as the discharge increased in the smaller diameter circular shaft and in the narrowest rectangular

column width. This effect led to some of the anomalies reported in the results.

A phenomenon observed when testing the extended 1:10.9 scale model vortex-entry dropshaft was the appearance, at high flows, of wavefronts advancing down the wall of the shaft. The wavefronts were characterized as oblique rings at intervals moving down the shaft above the ambient water surface. The frequency of the waves was monitored and appeared steady; but at random intervals, a wave would accelerate through the preceding wave, this phenomenon remains unexplained. The ability to discern these waves was dependent on the lighting conditions and the angle of observation. It is considered that the effect was due to what is sometimes referred to as "roll waves". This manifestation has been investigated previously^(28,29,30) by experimenting with thin films flowing down inclined channels. The formation of the roll waves is thought to be due to some local instability generated in the flow by channel defects which is then propagated in the thin film. However, no quantitative assessment was made of this phenomenon and further research is required on the nature of roll waves and their effects on air entrainment.

The results obtained from this investigation can be broadly classified into two categories, viz direct comparisons with the reported findings of previous researchers and new hypotheses to substantiate the observed phenomena.

6.2 Conditions for Air Entrainment

For air entrainment to take place, it is necessary that the water film be wholly turbulent, which in this investigation occurred at distances below the throat depending on the intensity of the water flow related to the periphery of the water film. This is in accord with the findings of Whillock and Thorn⁽³⁾ on rectangular columns, and investigations into air entrainment on steep chutes and spillways. Entrainment of air at the surface of water flowing with high velocity at inclinations other than near vertical is recognised as being caused by water particles, having previously been ejected by the extreme turbulence of the flow, entraining air as they drop back into the main body of water. This mechanism cannot apply in vertical flows; it being observed that on the few occasions on which small droplets of water were ejected from the water film, they fell down the shaft and did not re-enter the vertically flowing water. Hence, the high speed jet on entry into the standing water contained no entrained air, the complex rotations at entry being solely responsible for the bubble formation.

The air initially entrained at the ambient water surface by the high speed jet, and the net air transported within the shaft have been clearly identified in this investigation. It has been established that the superficial or nominal water velocity necessary for transport of air must exceed 0.13 m/s, this corresponds to an absolute water velocity of 0.23 m/s. These values are in agreement with Curtet and Djonin⁽⁵⁾ and Whillock and Thorn.⁽³⁾

The air/water ratio has been shown to increase with the length of turbulent film, and to attain some constant value at a length dependent upon the water flow rate. As air bubbles are not formed within the vertically flowing turbulent film, but develop only on impingement, then the momentum input into the standing water is independent of the vertical distance over which the film is turbulent. Since the air entrained increases with this length, this increase must be due to an increase in the air flow rate into the standing water. This increase in the flow of air made available at the point of impingement must be related to the increasing length of the turbulent film. Energy transfer from the water to the air must take place in this region, dependent on the roughness of the water surface, and resulting in the enforced downward flow of a film of air adjacent to the air/water interface. Whillock and Thorn⁽³⁾ showed that when the water surface was artificially roughened an increased volume of air was entrained. A similar conclusion was reached by Ervine⁽¹¹⁾ for plunging circular jets. The importance of the turbulent length of film led to the development of the modified droplength parameter defined in Section 5.4.2.

The rectangular column of variable cross-section was developed to enable tests to be carried out for which the conditions of the impinging water jet were maintained constant, but the bubble transport potential in the lower shaft was variable. It has been established that under these circumstances, the air actually transported varied

with the cross-sectional area of the column, indicating that a proportion of the air initially entrained is transported downwards, the remainder being ejected back to the ambient surface. The air released by the flow from the recirculation zone complicates the understanding of the mechanisms involved in the entrainment process. The rejected air is recirculated within the air core in the shaft above the ambient water surface. This air may be then re-entrained as it is dragged down by the water film. An attempt was made to measure the velocity distributions of the air flows in the core but definitive patterns were not determined.

From observations of the performances of the models, it was apparent that the motion of bubbles near the walls of the pipes and column was not steady, and in certain instances, reverse motion of the bubbles occurred. It is possible that the velocity of the bubbles varies with distance from the wall but the variation was not quantified.

The gamma ray absorption technique was used to determine the void fraction in the rectangular column, the method measured the mean void ratio at a section in the shaft and hence cannot be compared with air concentration profiles determined by Curtet and Djonin ⁽⁵⁾ and Zuber and Findlay ⁽¹⁵⁾. It is considered that the air content is a function of the geometrical arrangement of the system and correlation between different systems is not possible. A theoretical analysis of the bubble motion

in a confined liquid medium yielded a series of relationships describing the relative motion of the two phases independent of the geometrical arrangement of the system.

Wallis⁽¹⁶⁾ describes the bubbly flow pattern as being characterised by a suspension of discrete bubbles in a continuous liquid medium. He also defines the change in regime to slug flow when the bubbles are large and assume a cylindrical shape almost filling the duct. The bubbly flow regime is rarely a stable flow situation and the formation of bubbles is commonly only a transitory state. The maximum possible rate of air entrainment, or more correctly, air transport, was found to occur at a nominal water velocity of about 0.65 m/s. For velocities in excess of this value, there are indications that the air transport rate is initially maintained prior to development of a slug flow regime.

The results of the void ratio measurements showed that the absolute velocity of the individual phases do not exhibit a linear relationship. Wallis and Zuber and Findlay infer that the slip velocity between the phases under all conditions is constant and equal in magnitude to that required to commence the downward motion of the air bubbles. Fig. 5.34 clearly shows the slip velocity to vary with the nominal water velocity and consequently with the voids ratio.

By plotting voids ratio against air/water flow ratio in Fig. 5.35, the results are seen to lie along

lines of equal $\frac{j_w}{u_c}$ values. The form of the relationship was developed from Nicklin's⁽¹⁷⁾ work with modifications proposed by Thorn⁽⁶⁾. Statistical analysis of the results yielded an empirical relationship described in Equation 5.9a. Hence, the nominal water velocity must exceed 0.13 m/s for air to be transported. It has also been established that $\frac{j_w}{u_c}$ attains a maximum value when the nominal water velocity is approximately 0.65 m/s. Utilising the above relationships, it follows that air transport commences when $\frac{j_w}{u_c} = 0.56$, from which the void ratio can be determined as 0.43. At maximum values of $\frac{j_w}{u_c} = 0.56$, from which the void ratio can be determined as 0.43. At maximum values of $\frac{j_w}{u_c} = 1.44$, and for the same voids ratio, air/water flow ratio was calculated as 0.41. Consequently, in the bubbly flow regime, the maximum air/water ratio tends towards 0.41 for voids ratio less than 0.43.

6.3 Dimensional Relationships

The dimensionless plots of the maximum performance of both the circular shafts and rectangular columns show that the air/water flow ratio increases with physical size from 0.12 for the 51mm diameter pipe to 0.25 for the 305mm pipe. The bubble diameter/pipe diameter ratio correspondingly changes by a factor of 6. The variation in air/water ratio in the rectangular columns is significantly lower, however, the bubble diameter/pipe diameter ratio only changes by a factor of 2.2

The plots of the product of the non-dimensional groups with air/water flow ratio show that the circular shafts with different vortex-entry arrangements, hence differing relative swirl velocities, exhibit differing performance curves. Results from pipes of different diameters, but the same design of inlet also do not coalesce for equal values of $\frac{j_w}{u_c}$. Even using a droplength modified to take into account of the length over which boundary layer growth occurs, the usual geometrical scaling rules do not apply for comparison of air/water flow ratios.

The plots of air/water ratio against the modified Froude dimensionless group clearly show that the usual scaling relationships do not apply, the bubble diameter being assumed constant by virtue of the surface tension effects of the water. Hence, geometrical similarity cannot be maintained at all diameters. Inclusion of the non-dimensional velocity parameter ($\frac{j_w}{u_c}$), which is shown to vary uniquely because the slip velocity is not constant, as has been presumed by all previous investigators, enables the air/water flow rate to be determined for any water flow rate in any size of pipe or column, providing the droplength is sufficiently long for the flow rate to reach its peak.

REFERENCES

1. HALL L.S.
Conformity between model and prototype
Trans. A.S.C.E. Paper 2207, Vol.109, 1944.
2. HYDRAULICS RESEARCH STATION
Plover Cover Water Supply Scheme, Hong Kong
Report on hydraulic model investigation of a
typical dropshaft and de-aeration chamber.
Report No. Ex.264 August 1965.
3. WHILLOCK A.F. & THORN M.F.C.
Air entrainment in dropshafts
CIRIA Technical Note 48, April 1973.
4. COTILLON J.
Pressure tunnel supply shafts and the problem
of air entrainment
I.A.H.R. 8th Congress, Montreal 1959, Paper 17D.
5. CURTET R. & DJONIN K.
Study of a vertical downward mixed air and
water flow: Flor and concentration conditions
La Houille Blanche, October 1967, Vol.22, (No.5).
6. THORN M.F.C.
Modelling the air demand of vertical dropshafts
I.A.H.R. 17th Congress, Baden-Baden 1977.
7. PETERKA A.J.
Morning-Glory shaft spillways: performance
tests on prototype and model
Trans. A.S.C.E. Paper 2802, Vol.121, 1956.
8. DAWSON F.M. & KALINSKE A.A.
Report on hydraulics and pneumatics of plumbing
drainage systems
University of Iowa Studies in Engineering,
Bulletin 10, 1937.
9. LAUSHEY L.M. & MAVIS F.T.
Air entrained by water flowing down vertical
shafts
I.A.H.R. 5th Congress, Minneapolis 1953.
10. VIPARELLI M.
Air and water currents in vertical shafts
La Houille Blanche, 1961, Vol.16, (No.6).
11. ERVINE D.A. & KOLKMAN P.A.
Air entrainment and transport in closed conduit
hydraulic structures
Delft Hydraulics Laboratory, Report S330, August 1980.

12. KENN M.J.
Dynamical similarity for flow systems in
which inertia effects are small
J. Instn. Water Engineers, June 1969, Vol.23, (No.4).
13. KENN M.J. & ZANKER K.J.
Aspects of similarity for air-entraining water
flows
Nature, 7.Jan 1967, Vol.213, (No.5071).
14. WISNER P.
On the role of Froude criterion in the study
of air entrainment by high velocity flows
I.A.H.R. 11th Congress, Leningrad 1965, Paper 1.15.
15. ZUBER N. & FINDLAY J.A.
Average volumetric concentration in two-phase
flow systems
Trans. A.S.M.E. J. Heat Transfer, Vol.87, Nov.1965.
16. WALLIS G.B.
One-dimensional two-phase flow
McGraw-Hill, Published 1969.
17. NICKLIN D.J.
Two-phase bubble flow
Chem. Eng. Sci., Vol.17, 1962.
18. BLAND J.A.
A vertical laminar boundary layer
Int. J. Math. Educ. Sci. Technol., 1981, 12 No.4.
19. ACKERS P. & CRUMP E.S.
The vortex drop
Proc. I.C.E., Vol.16, Paper 6430, August 1960.
20. HABERMAN W.L. & MORTON R.K.
An experimental study of bubbles moving in
liquids
Proc. A.S.C.E., Vol.80, Separate No. 387, 1954.
21. ROSENBERG B.
The drag and shape of air bubbles moving in
liquids
David Taylor Model Basin (Washington) Report 272
September 1950.
22. CHANISHVILI A.G.
Air entrainment and vertical downward motion of
aerated flows
I.A.H.R. 8th Congress, Montreal 1959, Paper 8D.
23. GARNER F.H. & HAMMERTON D.
Circulation inside gas bubbles
Chem. Eng. Sci., Vol.3, (No.1), February 1954.

24. HOLROYD A. & PARKER H.B.
Investigations on the dynamics of
aeration
J. Instn. Sew. Purif. , 1949 (Part 3).
25. BAKER J.L.L. & CHAO B.T.
An experimental investigation of air bubble
motion in a turbulent water stream
J. Am. Instn. Chem. Engrs., Vol.11, (Part 2)
March 1965.
26. FRANCIS J.R.D.
Fluid Mechanics for Engineering Students
Edward Arnold, 4th Edition 1975.
27. NUTTAL J.B.
Axial flow in a vortex
Nature, 26 September 1953, Vol.172.
28. RENNER J.
Air Entrainment in Surface Rollers
Symp. on Design & Operation of Siphons
& Siphon Spillways
Paper A4, May 1975.
29. MAYER P.G.
Roll waves and slug flows in inclined open
channels
Proc. A.S.C.E. Paper 2085, Vol.85, No. HY7
July 1959.
30. DRESSLER R.F.
Mathematical solution of the problem of roll
waves in inclined open channels
Communication on Pure & Applied Maths, 2, 1949.
31. FRANCIS J.R.D.
The aerodynamic drag of a free water surface
Royal Society, Series A, 1951.
32. PETRICK M.
Two-phase air/water flow phenomena
A.N.L. Report No.5787 March 1958.
33. SMISSAERT G.E.
Two-component two-phase flow parameters for
low circulation rates
A.N.L. Report No.6755 July 1963.
34. HALL L.S.
Open channel flow at high velocities
Trans. A.S.C.E., Vol. 108, 1943.

35. STRAUB L.G. & ANDERSON A.G.
Self-aerated flow in open channels
Trans. A.S.C.E., Paper No. 3029, 1958.
36. HICKOX G.H.
Aeration of spillways
Trans. A.S.C.E., Paper No. 2215, Vol 109, 1942.
37. NOVAK P. & CABELKA J.
Models in Hydraulic Engineering
Pitman, 1st Edition, 1981.
38. ELSAWY E.M. & MCKEOGH E.J.
Study of self-aerated flow with regard to
modelling criteria
I.A.H.R. 17th Congress, Baden-Baden, 1977.
39. HACK H.P.
Air entrainment in dropshafts with annular
flow by turbulent diffusion
I.A.H.R. 17th Congress, Baden-Baden, 1977.
40. MARQUENET G.
Air entrainment by flow in a vertical pipe
and application to secondary supply shafts
I.A.H.R. 5th Congress, Minneapolis, 1953.

FURTHER READING

1. ABRAMOVICH G.N.
The Theory of Turbulent Jets
Massachusetts Inst. of Tech. 1973
2. ERVINE D.A.
The entrainment of air in water
Water Power & Dam Construction, December 1976.
3. JEVDEVICH V. & LEVIN L.
Entrainment of air in flowing water and
technical problems connected with it
I.A.H.R. 5th Congress, Minneapolis 1953.
4. KALINSKE A.A. & ROBERTSON J.M.
Closed conduit flow
Trans. A.S.C.E. Vol. 108, 1943.
5. KINORI B.Z. & NIR Z.
Scaling problems for hydraulic models
Water Power & Dam Construction, December, 1976.
6. LAUSHEY L.M.
Studies show Pittsburgh how to drop sewage
90ft. vertically to tunnel interceptors
Engineering News Record, 5 March 1953.
7. LIPSON C. & SHETH N.J.
Statistical Design and Analysis of Engineering
Experiments
McGraw-Hill 1973.
8. MIRONER A.
Engineering Fluid Mechanics
McGraw-Hill 1979.
9. SCHLICHTING H.
Boundary Layer Theory
McGraw-Hill 7th Edition, 1979.
10. SHARP J.J.
Hydraulic Modelling
Butterworths, 1st Edition 1981.
11. SHERIDAN A.T.
Surface entrainment of air by a water jet
Nature Vol.209, 19 February 1966.
12. HALL L.S. & KALINSKE A.A.
Entrainment of air in flowing water-A Symposium
Trans. A.S.C.E. Paper No. 2205, September 1942.

13. SHARMA H.R.
Air entrainment in high head gated conduits
Proc. A.S.C.E. HY9, Vol.102, November 1976.
14. JAIN A.K., RAJU K.G.R. & GARDE R.J.G.
Air entrainment in radial flow towards intakes
Proc. A.S.C.E. HY11, Vol.104 September 1978.
15. STRAUB L.G., KILLEN J.M. & LAMB O.P.
Velocity measurements of air/water mixtures
St. Anthony Falls Hyd. Lab. Univ. of Minnesota
Tech. Paper No.10, Series B, March 1952.

A P P E N D I C E S

APPENDIX A

Calibration of Orifice Meter

The orifice plate was calibrated by measuring the volume of water retained in a collection tank over a timed period at different head readings on the differential pressure manometer. The results are plotted in Fig. A, and the following relationship is established;

$$Q_w = C_d \frac{a_0 a_1}{\sqrt{a_1^2 - a_0^2}} \cdot (2gH)^{0.5}$$

where C_d = coefficient of discharge
 a_0 = pipe diameter
 a_1 = orifice diameter
 Q_w = discharge
 H = differential head reading

$$\text{If } k = \frac{0.051^2 \times 0.031^2 \cdot \pi}{\sqrt{0.051^4 - 0.031^4}} \cdot \frac{1}{4} = 8.1224 \times 10^{-4}$$

$$\therefore C_d = \frac{1}{k} \cdot \frac{1}{\sqrt{2g}} \cdot \frac{Q}{H^{0.5}} \cdot \frac{1}{10^3} \quad \text{where } Q \text{ is in l/s}$$

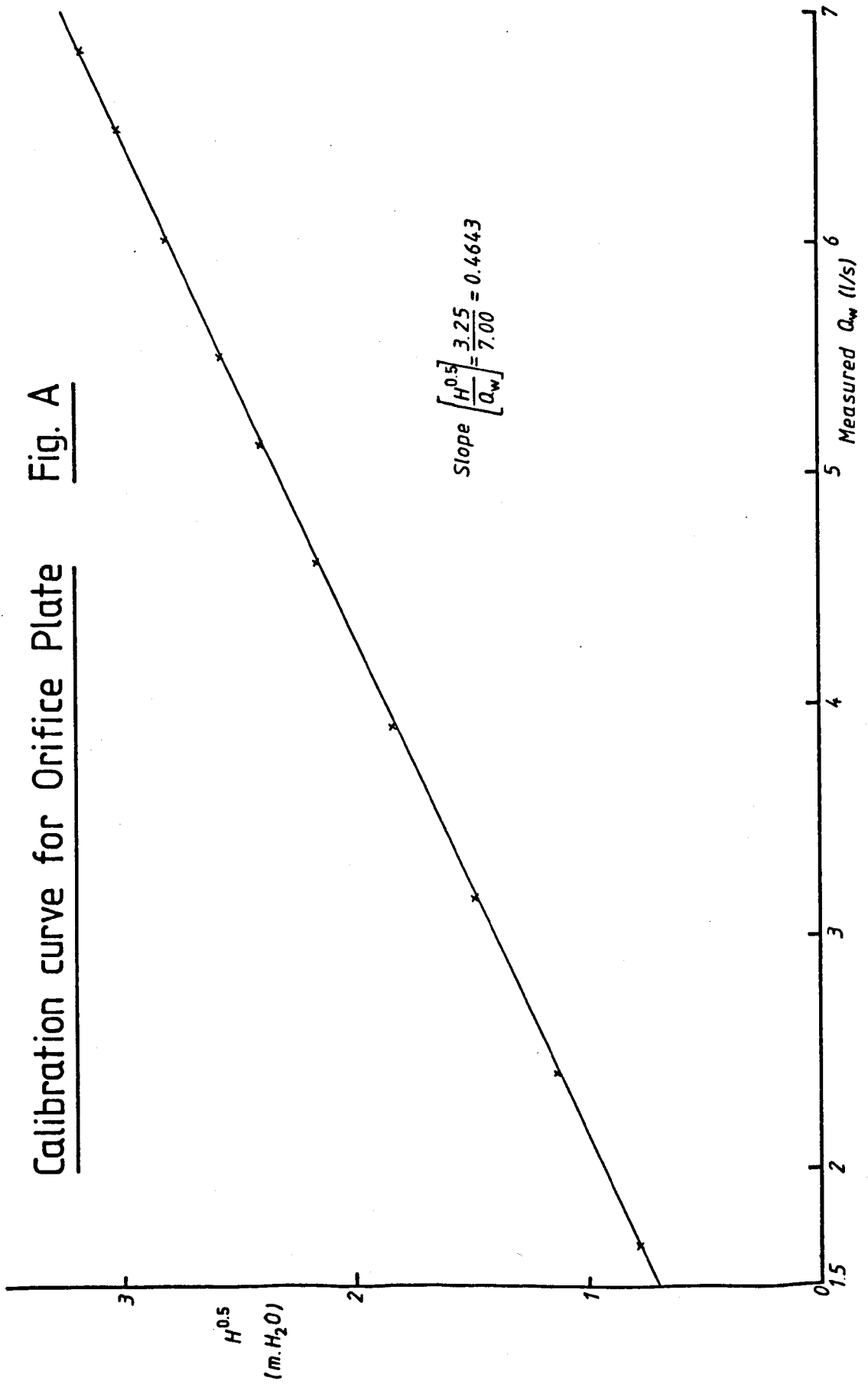
$$= \frac{1}{8.1224 \times 10^{-4}} \cdot \frac{1}{\sqrt{2g}} \cdot \frac{1}{0.4643} \cdot \frac{1}{10^3}$$

$$= 0.599$$

$$Q_w = 0.599 \times 8.1224 \times 10^{-4} \cdot \sqrt{2g} \cdot H^{0.5} \cdot 10^3 \quad (H \text{ in } \text{mH}_2\text{O})$$

$$Q_w = 2.1551 \times H^{0.5} \text{ l/s} \quad (Q_w \text{ in l/s})$$

Calibration curve for Orifice Plate Fig. A



Calibration of Wet-Drum Gas Meter

The air flow meter was calibrated by a positive displacement method. The rectangular column was filled completely with standing water; the water level was lowered a measured distance and hence a volume of air was drawn through the gas meter to replace the water. Thus a direct comparison was established for the accuracy of the drum's measuring gauges. An allowance was made for the volume occupied by the perspex dividing wall, supports and control mechanism.

Volume of Water Displaced	Metered volume through drum	
(l/s)	(ft/s)	(l/s)
152.5	5.57	157.66
114.3	4.135	117.04
172.7	6.37	180.30
166.1	5.96	168.70

APPENDIX B

Determination of Inlet Velocity at throat for Vortex Dropshaft

Utilising the method proposed by Ackers and Crump ⁽¹⁹⁾, the Figures C,D,E,F,G were produced to give the inlet velocity at the throat for a known discharge in each model considered. Figure B defines the parameters used in the system of analysis.

G_1 and G_2 are geometric properties depending solely on the relative radii of the structural elements.

F_1 and F_2 are parameters depending solely on the fractional area of the air core.

f is the air core ratio = $\frac{a^2}{d^2}$

$$G_1 = \log_e \left(\frac{r_2}{r_1} \right)$$

$$G_2 = \frac{d^2}{r_2^2} \left(\frac{r_2^2}{r_1^2} - 1 \right)$$

For a series of f values

$$F_1 = f^2 / 4 (1 + f)$$

$$F_2 = \frac{\pi}{4} (1 / (f - 1) \sqrt{2(1 - f)})$$

Hence

$$\frac{E}{d} = \frac{F_2 + \frac{t}{d} \cdot F_1 \cdot G_2}{G_1 - F_1 \cdot G_2}$$

evaluate Q from

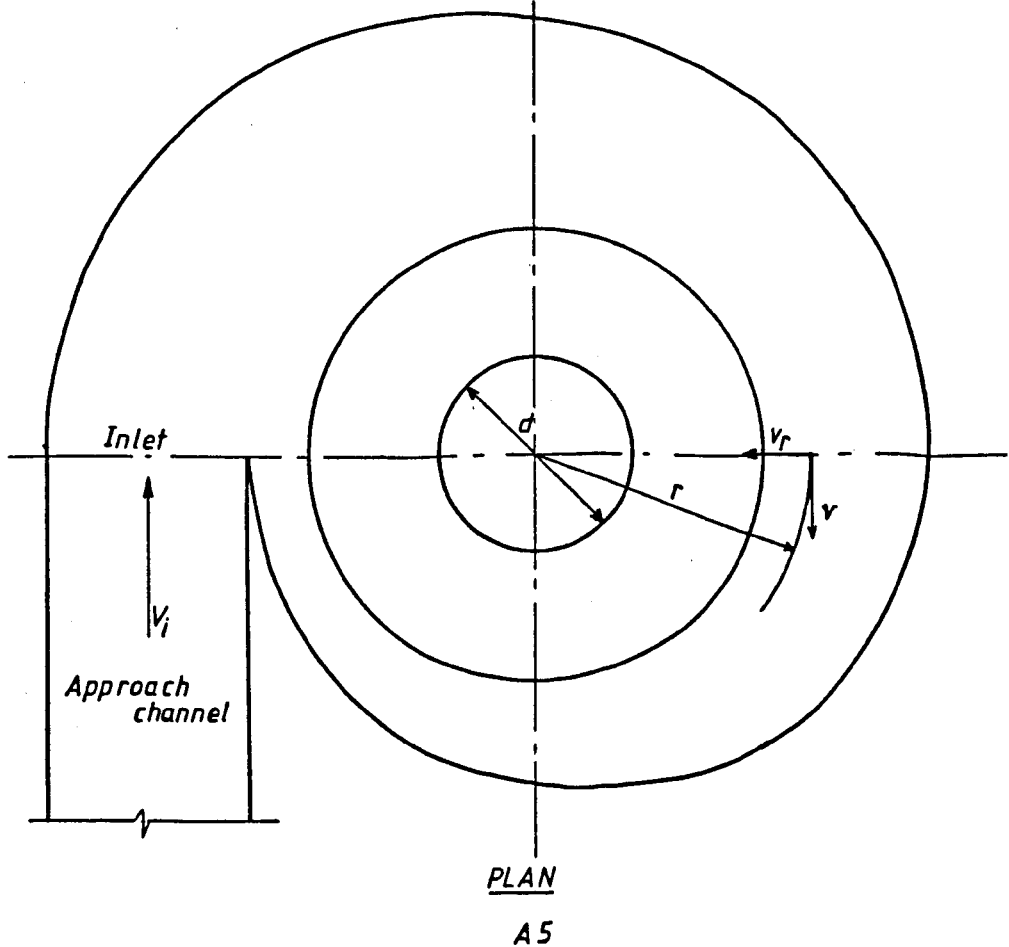
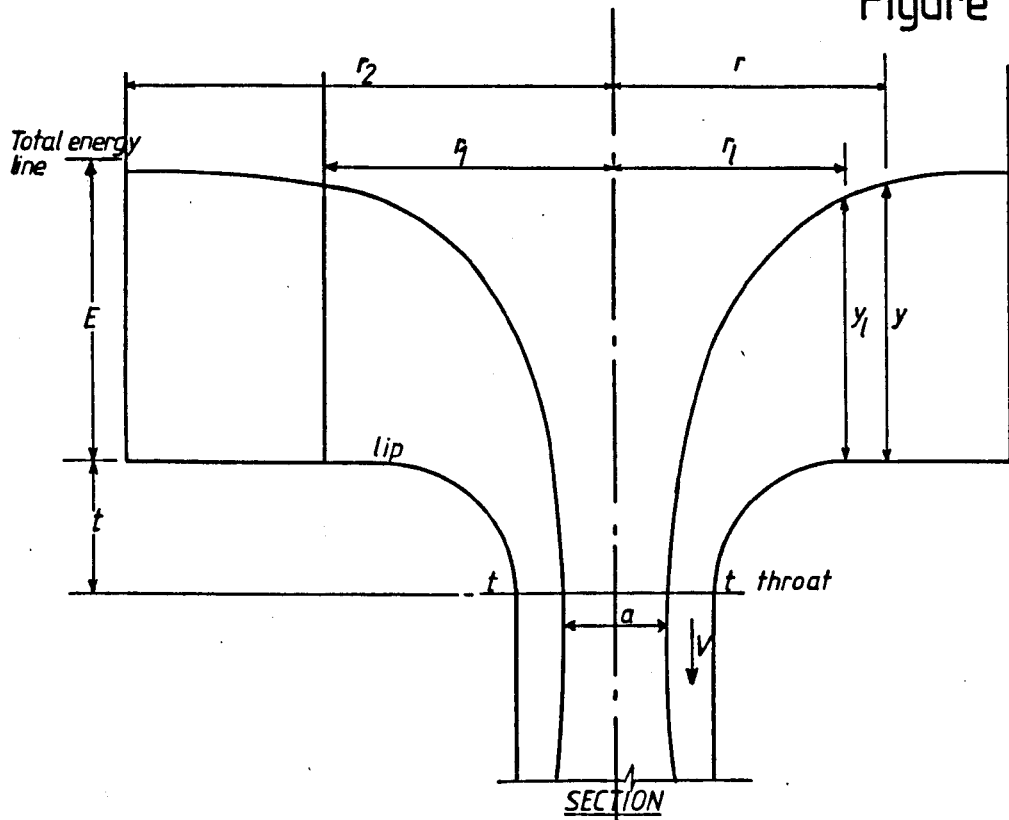
$$\frac{Q}{\sqrt{gd^5}} = F_2 \sqrt{(4F_1 \cdot (E + t) / d)}$$

& velocity at throat

$$v_1 = \frac{4 \cdot Q}{\pi d^2 (1 - f)}$$

The Vortex Drop after Ackers & Crump

Figure B



Relationship between Discharge and Velocity

51 mm ϕ Dropshaft (L'pool)

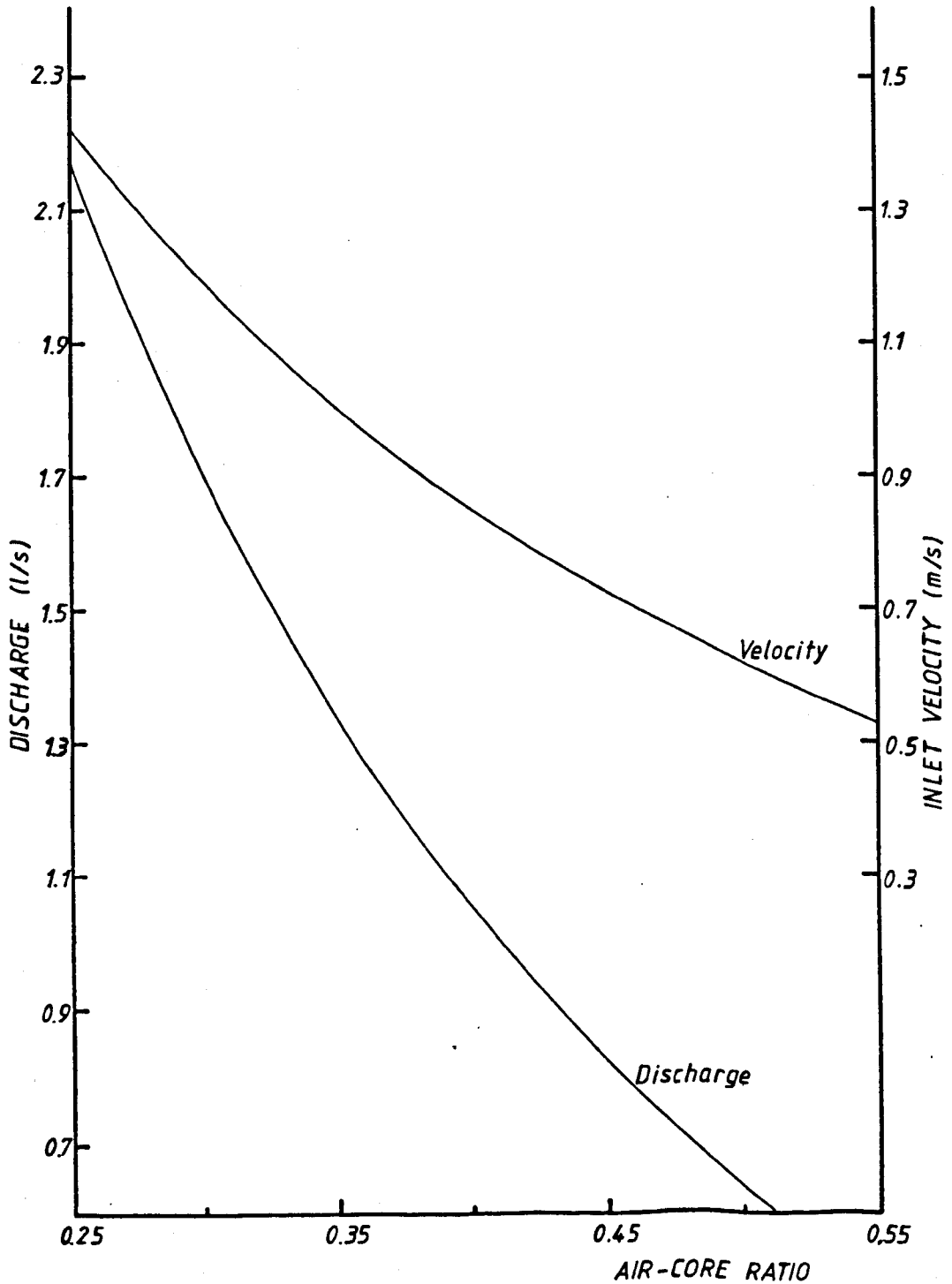


Figure C

Relationship between Discharge and Inlet Velocity

101mm ϕ Dropshaft (L'pool)

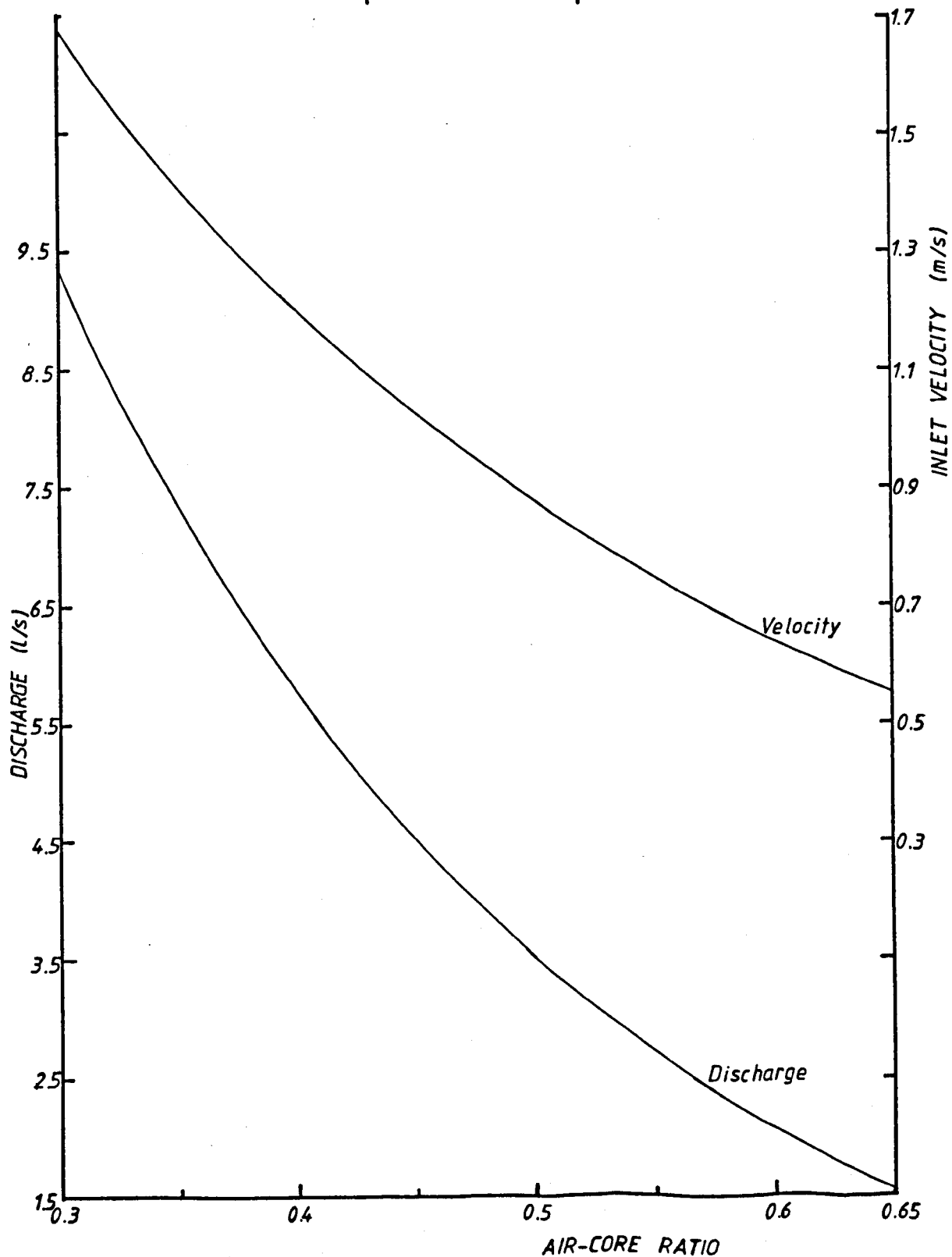


Figure D

Relationship between Discharge and Velocity

1:10 Scale model (H.R.S.)

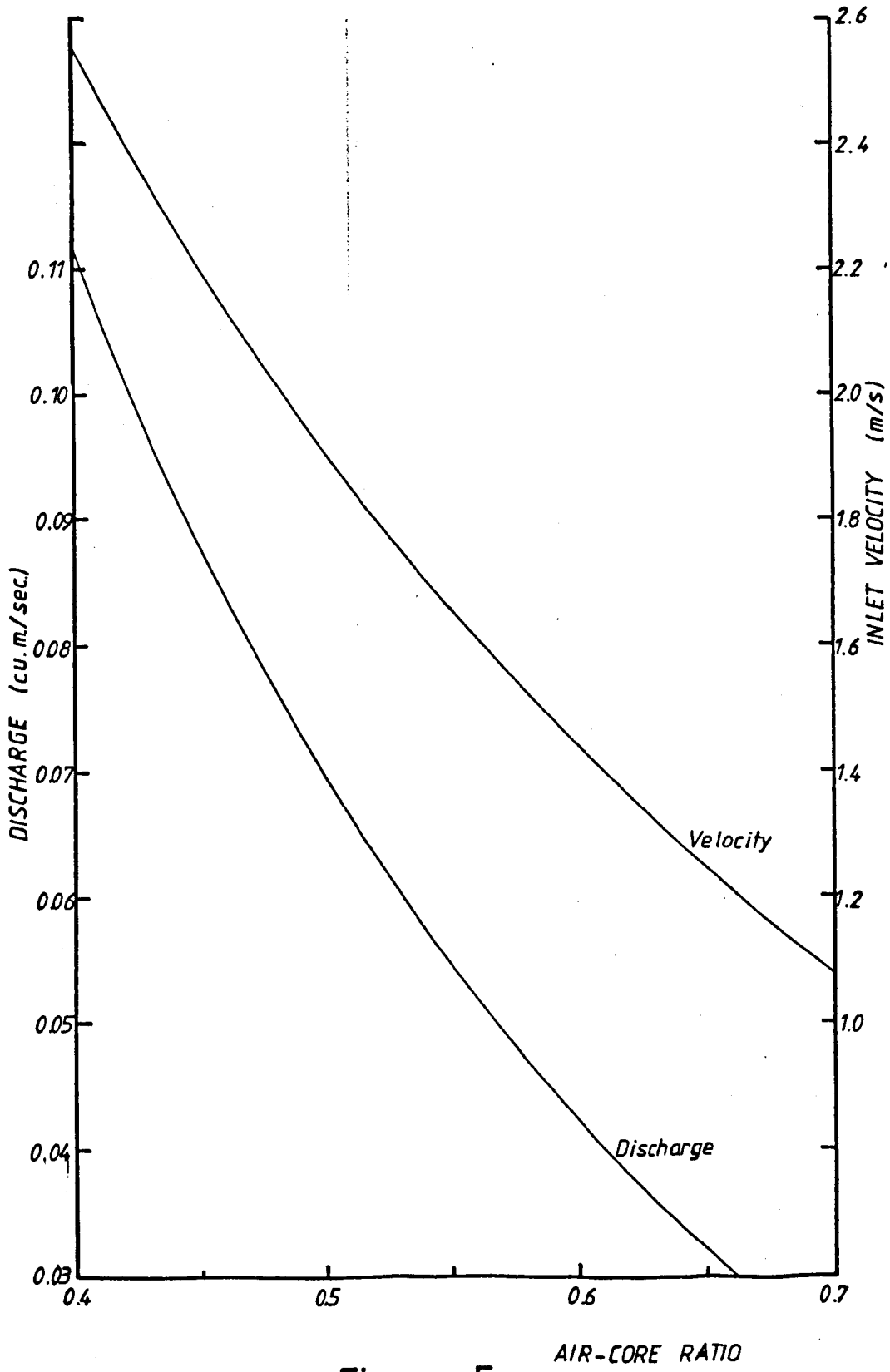


Figure E

Relationship between Discharge and Velocity

1:20 Scale Model (H.R.S.)

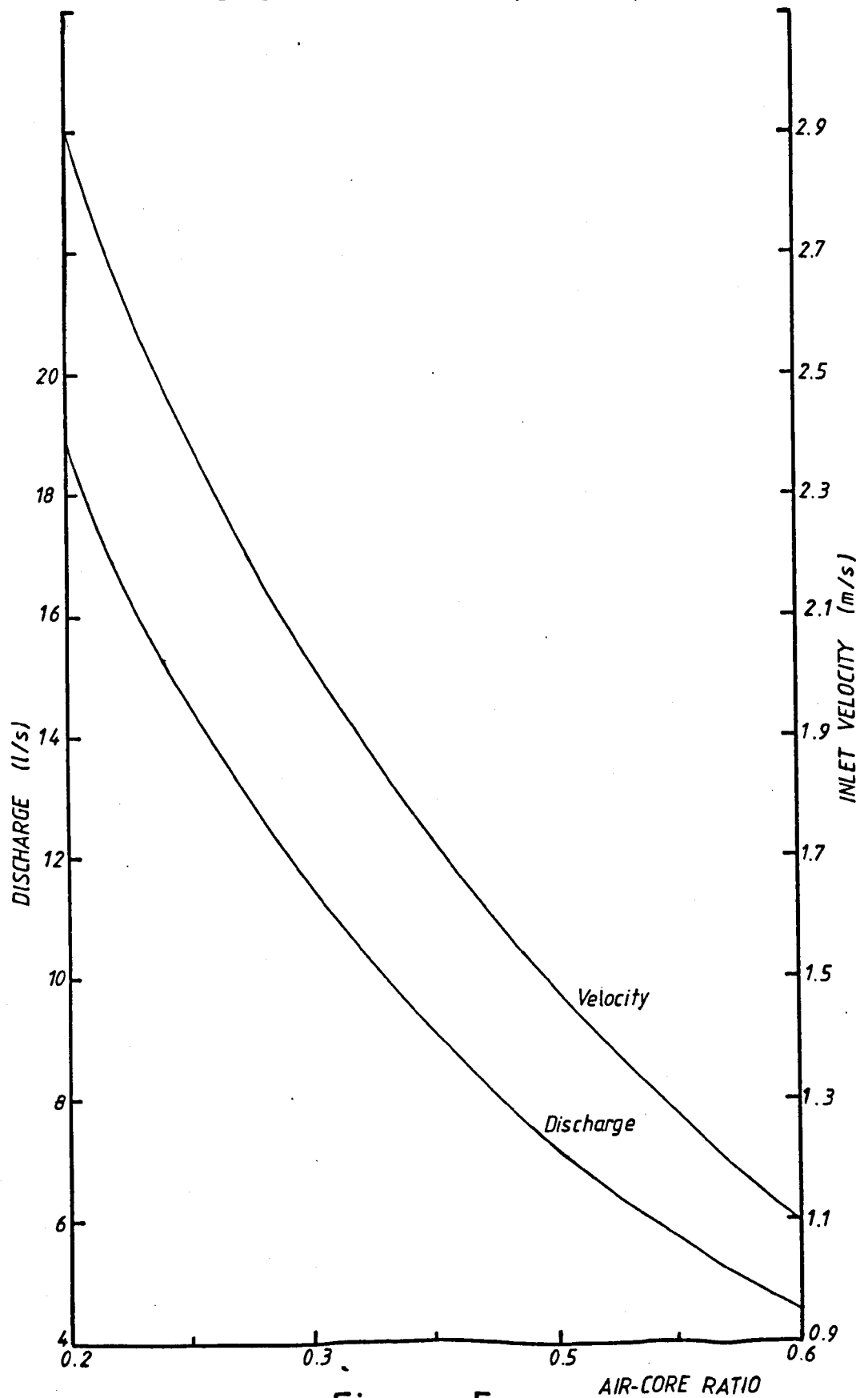


Figure F

Relationship between Discharge and Velocity 1:30 Scale Model (H.R.S.)

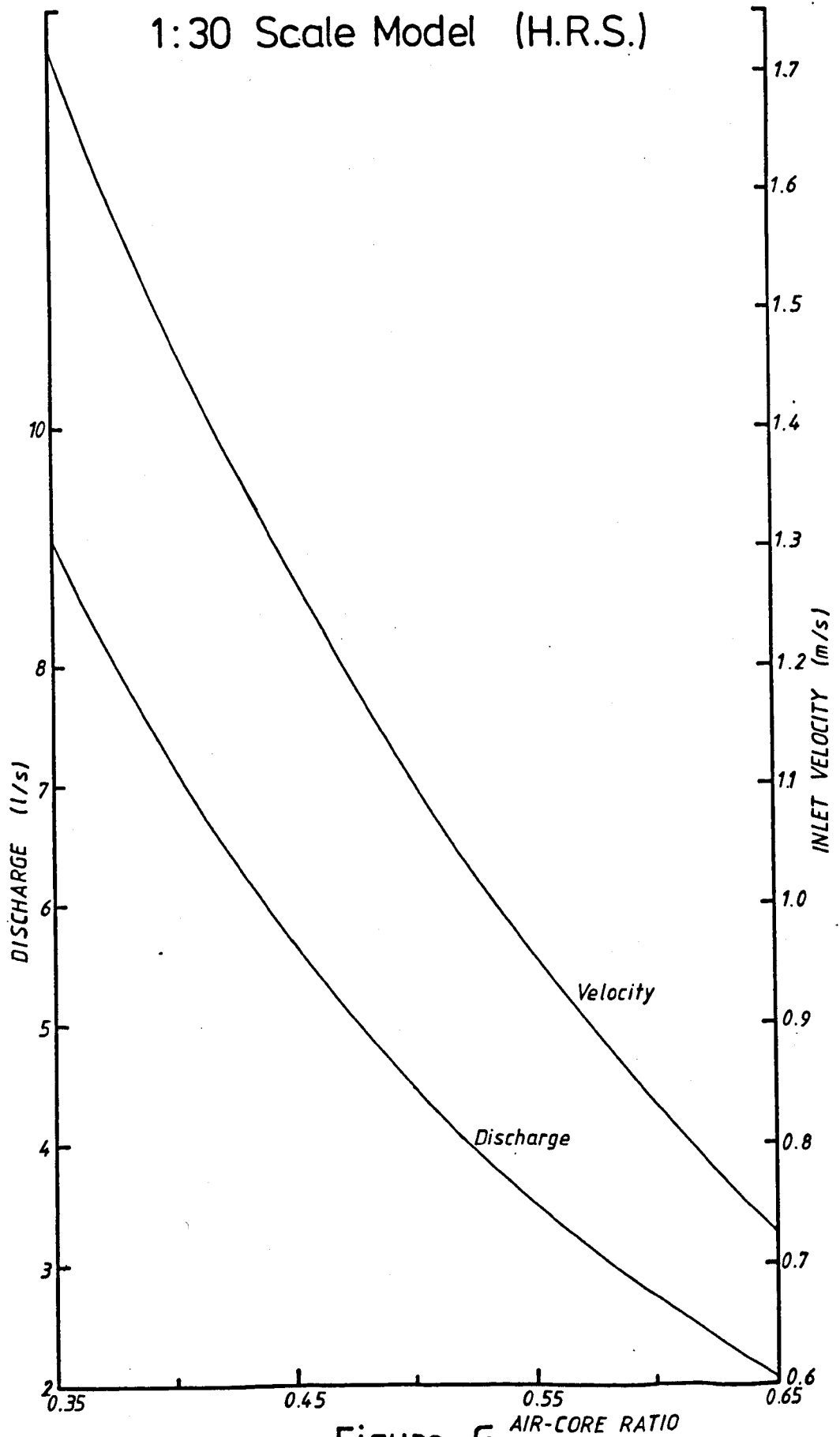


Figure G

APPENDIX C

Solution of Equation 4.1.18

$$\frac{\partial (\gamma^{5/4})}{\partial z} + \frac{4.107g}{W^2} \gamma^{5/4} = 0.296 \gamma^{1/4} \cdot W^{-1/4}$$

By Integrating Factor Method

$$\frac{\partial (D)}{\partial z} + \frac{A(D)}{W^2} = B \cdot W^{-1/4}$$

where

$$D = \gamma^{5/4}$$

$$A = 4.107g$$

$$B = 0.296 \gamma^{1/4}$$

$$W = (W_0^2 + 2gz)^{0.5}$$

$$\begin{aligned} I &= \int A \cdot W^{-2} \partial z = A \int (W_0^2 + 2gz)^{-1} \partial z \\ &= \frac{A \cdot \text{Ln}(W_0^2 + 2gz)}{2g} \\ &= (W_0^2 + 2gz)^{A/2g} \\ &= W^{A/g} \end{aligned}$$

$$\begin{aligned} \text{So } D \cdot W^{A/g} &= \int B W^{-1/4} W^{A/g} \partial z = B \int W^{(A/g - 1/4)} \partial z \\ &= B \int (W_0^2 + 2gz)^{(A/2g - 1/8)} \partial z \\ &= \frac{B \cdot 8g}{4A + 7g} \cdot (W_0^2 + 2gz)^{\left(\frac{4A + 7g}{8g}\right)} \cdot \frac{1}{2g} + C \\ &= \frac{B \cdot 4g}{g(4A + 7g)} \cdot (W_0^2 + 2gz)^{\left(\frac{A}{2g} + \frac{7}{8}\right)} + C \end{aligned}$$

$$\gamma = D = 0 \text{ when } z = 0$$

$$C = -\frac{4 \cdot B \cdot g}{g(4A + 7g)} \cdot W_0^{\left(\frac{A}{g} + \frac{7}{4}\right)}$$

Hence

$$DW^{\frac{A}{9}} = \frac{4Bg}{(4A+7g)g} \cdot W^{\left(\frac{A}{9} + \frac{7}{4}\right)} - \frac{4Bg}{(4A+7g)g} \cdot W_0^{\left(\frac{A}{9} + \frac{7}{4}\right)}$$

$$D = \frac{4Bg}{(4A+7g)g} \left(W^{\left(\frac{A}{9} + \frac{7}{4}\right)} - W_0^{\left(\frac{A}{9} + \frac{7}{4}\right)} \right) W^{-\frac{A}{9}}$$

$$\chi^{\frac{5}{4}} = \frac{0.0016727}{g} \left(W^{5.857} - W_0^{5.857} \right) W^{-4.107}$$

APPENDIX D

Data for Non-Dimensional Groups - Circular Shafts

Q_w (1/s)	Q_a/Q_w	j_w/u_c	$\frac{q_w}{D^{1.5}g^{0.5}}$	$\frac{L - z_t}{D}$
51 mm dia. L'pool Poly				
0.62	0.058	1.10	0.1073	5.812
	0.074			9.773
0.75	0.048	1.24	0.1297	3.694
	0.071			5.655
	0.107			9.576
	0.120			13.498
0.91	0.048	1.35	0.1575	3.50
	0.071			5.461
	0.110			9.382
	0.132			13.304
0.98	0.049	1.37	0.1697	3.418
	0.069			5.378
	0.102			8.320
	0.131			13.222
1.06	0.054	1.40	0.1835	3.320
	0.071			5.280
	0.104			8.22
	0.123			14.104
1.19	0.053	1.43	0.2060	3.165
	0.071			5.125
	0.105			8.067
	0.118			14.929
1.33	0.071	1.44	0.2301	4.951
	0.086			6.912
	0.106			10.833
	0.120			16.716
1.51	0.076	1.43	0.2610	4.755
	0.086			6.716
	0.099			10.637
	0.113			16.520
	0.119			20.441
1.69	0.095	1.41	0.2924	8.461
	0.104			12.382
	0.114			18.265
	0.118			24.145
1.84	0.098	1.38	0.3180	10.241
	0.106			14.163
	0.114			20.045
	0.120			25.927

Q_w (1/s)	Q_a/Q_w	j_w/u_c	$\frac{q_w}{D^{1.5}g^{0.5}}$	$\frac{L - z_t}{D}$
101 mm dia. L'pool Poly				
2.028	0.049	0.98	0.0636	2.637
	0.074			5.805
	0.099			7.938
	0.111			9.567
2.633	0.038	1.16	0.0825	2.82
	0.076			4.80
	0.114			6.978
	0.152			10.345
3.261	0.061	1.29	0.1022	2.896
	0.092			4.183
	0.123			6.163
	0.153			9.629
3.512	0.085	1.33	0.1101	3.601
	0.114			5.284
	0.142			7.264
	0.171			10.037
3.916	0.102	1.38	0.1227	4.441
	0.128			5.827
	0.153			8.005
	0.179			12.658
4.156	0.096	1.40	0.1303	4.348
	0.120			5.338
	0.144			6.828
	0.168			9.793
	0.180			13.753
4.476	0.112	1.42	0.1403	4.628
	0.134			6.311
	0.156			9.677
	0.179			15.618
4.835	0.124	1.43	0.1516	5.576
	0.145			7.556
	0.165			10.527
	0.186			15.477
5.193	0.135	1.44	0.1628	7.423
	0.154			9.898
	0.173			14.353
	0.181			17.324
5.632	0.142	1.44	0.1766	8.25
	0.160			11.221
	0.178			15.181
6.006	0.142	1.43	0.1833	10.086
	0.158			11.571
	0.175			18.997
6.404	0.141	1.42	0.2007	8.95
	0.156			11.92
	0.172			18.85
7.178	0.139	1.38	0.2250	8.651
	0.153			12.612
	0.167			17.562
7.760	0.142	1.35	0.2433	11.417
	0.155			13.892
	0.168			18.843

Q_w (1/s)	Q_a/Q_w	j_w/u_c	$\frac{q_w}{D^{1.5} \cdot g^{0.5}}$	$\frac{L - z_t}{D}$
4" dia. HRS				
2.187	0.0013	1.03	0.0887	6.484
	0.071			10.514
	0.113			13.534
	0.148			17.563
4.019	0.043	1.39	0.1241	7.098
	0.100			10.108
	0.146			13.128
	0.181			16.148
5.168	0.024	1.44	0.1596	3.175
	0.091			8.693
	0.141			11.713
	0.171			14.723
6.316	0.052	1.42	0.1951	5.673
	0.102			8.693
	0.143			11.815
	0.165			15.455
7.465	0.044	1.37	0.2306	4.823
	0.080			6.834
	0.123			9.853
	0.159			12.873
8.613	0.048	1.32	0.2660	4.414
	0.102			7.434
	0.130			9.444
	0.154			11.453

Q_w (1/s)	Q_a/Q_w	j_w/u_c	$\frac{q_w}{D^{1.5}g^{0.5}}$	$\frac{L - z_t}{D}$
6" dia. HRS				
6.329	0.09	1.20	0.0709	8.425
	0.13			11.378
	0.175			15.906
7.911	0.002	1.33	0.0887	3.163
	0.025			4.123
	0.082			7.166
	0.135			10.184
	0.170			13.203
9.494	0.008	1.40	0.1064	2.979
	0.0237			4.816
	0.12			8.425
	0.18			12.034
11.076	0.012	1.44	0.1241	2.751
	0.042			4.816
	0.11			7.279
	0.18			11.806
12.658	0.012	1.44	0.1419	2.881
	0.04			4.783
	0.13			8.392
	0.20			12.592
	0.23			14.442
14.241	0.016	1.42	0.1596	2.697
	0.046			5.387
	0.11			8.077
	0.21			12.867
	0.23			14.442

Q_w (1/s)	Q_a/Q_w	j_w/uc	$\frac{q_w}{D^{1.5} g^{0.5}}$	$\frac{L - z_t}{D}$
12" dia. HRS				
28.86	0.053	1.28	0.053	5.348
	0.088			9.115
	0.140			12.741
	0.176			14.341
35.81	0.066	1.38	0.071	6.40
	0.132			9.898
	0.198			12.197
	0.25			13.495
44.75	0.053	1.44	0.089	3.862
	0.105			7.059
	0.158			9.157
	0.211			10.856
53.69	0.264	1.44	0.1060	12.154
	0.044			3.439
	0.088			4.938
	0.176			8.436
60.12	0.220	1.41	0.119	9.833
	0.264			11.033
	0.039			1.633
	0.078			4.033
71.61	0.157	1.34	0.142	7.131
	0.235			9.528
	0.274			10.630
	0.033			1.010
80.56	0.066	1.29	0.159	3.308
	0.132			6.407
	0.198			8.505
	0.231			9.505
	0.029			0.262
	0.059			2.161
	0.117			4.961
	0.176			7.059
	0.234			8.757

Data for Non-Dimensional Groups
Rectangular Column Results

Q_w (1/s)	Q_a/Q_w	j_w/u_c	$\frac{q_w}{d^{1.5}g^{0.5}}$	$\frac{(L-z_t)}{d}$
Column Width = 38mm				
2.484	0.078	0.92	0.397	8.184
	0.155			16.079
	0.190			34.500
3.332	0.131	1.13	0.532	4.658
	0.185			12.553
	0.220			33.605
2.472	0.090	0.92	0.395	10.105
	0.150			23.264
	0.170			44.316
4.390	0.090	1.30	0.701	3.526
	0.200			8.789
	0.250			21.947
	0.300			48.263
3.341	0.090	1.13	0.533	3.842
	0.160			11.737
	0.240			38.053
2.519	0.070	0.92	0.402	6.816
	0.160			17.342
	0.180			38.395
5.715	0.160	1.40	0.912	2.206
	0.190			7.289
	0.270			33.605
	0.310			46.763
4.403	0.120	1.30	0.703	5.263
	0.200			13.158
	0.250			28.947
	0.290			44.737
3.376	0.090	1.13	0.539	5.842
	0.160			13.737
	0.220			26.895
2.495	0.050	0.92	0.398	6.553
	0.130			17.079
	0.160			38.132
6.962	0.180	1.44	1.112	3.184
	0.230			13.710
	0.280			32.132
	0.310			42.658
5.710	0.180	1.40	0.912	3.842
	0.210			14.368
	0.270			30.158
	0.300			43.316
4.416	0.140	1.30	0.705	4.711
	0.190			9.974
	0.240			23.132
	0.280			44.184
3.35	0.100	1.13	0.535	5.579
	0.180			13.474
	0.230			29.263
2.519	0.070	0.92	0.402	6.263
	0.130			19.421
	0.190			40.473

Q_w (1/s)	Q_a/Q_w	j_w/u_c	$\frac{q_w}{d^{1.5}g^{0.5}}$	$\frac{(L - z_t)}{d}$
----------------	-----------	-----------	------------------------------	-----------------------

Column Width = 45mm

2.519	0.09	0.82	0.312	9.111
	0.13			22.444
	0.095			3.933
	0.15			8.378
2.519	0.20	0.82	0.312	21.711
	0.09			9.622
4.423	0.13	1.20	0.548	26.289
	0.16			2.933
	0.22			11.822
3.358	0.26	1.0	0.416	31.822
	0.10			5.511
	0.15			9.956
2.519	0.21	0.82	0.312	29.956
	0.10			10.244
5.72	0.14	1.35	0.709	30.244
	0.17			1.711
	0.21			8.378
	0.25			19.489
4.423	0.29	1.20	0.548	30.600
	0.13			2.222
	0.19			8.889
3.358	0.25	1.0	0.416	28.889
	0.10			6.067
	0.16			10.511
2.519	0.21	0.82	0.312	27.178
	0.09			9.956
6.958	0.13	1.42	0.862	27.733
	0.17			0.467
	0.20			4.911
	0.25			16.022
5.725	0.30	1.35	0.709	40.467
	0.17			3.267
	0.22			7.711
	0.26			17.711
4.423	0.29	1.20	0.548	32.156
	0.13			2.867
	0.19			8.422
3.358	0.27	1.0	0.416	32.867
	0.10			6.744
	0.18			11.289
2.495	0.22	0.82	0.309	26.844
	0.09			9.711
	0.12			20.822

Q_w	Q_a/Q_w	j_w/u_c	$\frac{q_w}{d^{1.5}g^{0.5}}$	$\frac{(L - zt)}{d}$
-------	-----------	-----------	------------------------------	----------------------

(1/s)

Column Width = 50mm

2.159	0.05	0.75	0.266	8.20
	0.09			18.20
3.350	0.10	0.94	0.354	3.52
	0.14			7.52
	0.17			13.52
2.530	0.05	0.75	0.268	8.66
	0.09			19.66
4.383	0.13	1.13	0.463	2.68
	0.18			6.68
	0.23			22.68
3.350	0.10	0.94	0.354	3.96
	0.14			8.96
	0.18			16.96
2.519	0.05	0.75	0.266	9.22
	0.10			21.22
	0.15	1.29	0.605	1.54
	0.18			4.54
	0.22			11.54
	0.28			31.54
4.410	0.12	1.13	0.466	4.02
	0.18			7.02
	0.24			22.02
3.385	0.10	0.94	0.358	4.44
	0.14			8.44
	0.17			16.44
2.507	0.05	0.75	0.265	7.96
	0.10			20.96
6.953	0.16	1.39	0.735	0.44
	0.20			5.44
	0.25			16.44
	0.30			43.22
5.715	0.15	1.29	0.605	2.94
	0.19			6.94
	0.23			14.94
	0.28			28.94
4.423	0.12	1.13	0.468	3.58
	0.20			9.58
	0.24			23.58
3.358	0.10	0.94	0.355	5.20
	0.14			9.20
	0.19			19.20
2.530	0.06	0.75	0.268	8.74
	0.10			20.74